ABSTRACT

BRASWELL, ELIZABETH SLOAN. Laboratory Aging of Modern Mixtures to Simulate Field Aging. (Under the direction of Dr. Cassandra Castorena).

Significant research has been devoted to understanding and modeling the aging of asphalt binder. The accurate characterization of asphalt mixture properties in terms of the service life of a pavement is becoming more important as more powerful pavement design and performance prediction methods are implemented. The accuracy of an aging model to represent the long-term aging of asphalt mixtures at different depths of in-service pavements is critical to a model's ability to predict critical pavement distresses. The current laboratory mixture aging procedure, AASHTO R 30 only considers a single aging time and temperature to reflect all mixtures. This was calibrated before the prevalent use of reclaimed materials, modifiers, and warm-mix asphalt (WMA). In this research, a laboratory aging procedure is calibrated using modern mixtures WMA, mixtures containing reclaimed asphalt pavement (RAP), and other unconventional mixtures, as well as adding field core replicates to the existing database. The materials used for this have a variety of air void contents, asphalt contents, and climatic conditions. The aging procedure is calibrated using laboratory aging experiments coupled with field cores obtained from in-service pavements throughout the United States and Canada to relate laboratory aging conditions to climate and depth. In addition, the effects of asphalt mixture morphology on aging is studied through analysis of field cores with systematic changes in air void content and binder content. The final outcomes of this project include the recalibration of the loose mixture aging procedure and the field calibration of the pavement aging model applied to the kinetics model as a function of depth with the incorporation of the consideration of asphalt content. This study also investigates the effect of asphalt mixture morphology on pavement aging.

Laboratory Aging of Modern Mixtures to Simulate Field Aging

by
Elizabeth Sloan Braswell

A thesis submitted to the Graduate Faculty of
North Carolina State University
in partial fulfillment of the
requirements for the degree of
Master of Science

Civil Engineering

Raleigh, North Carolina
2019

APPROVED BY:

Dr. Y. Richard Kim	Dr. Benjamin Underwood

Dr. Cassandra Castorena
Committee Chair

DEDICATION

I would like to dedicate my thesis first of all to my family and second to my friends. My family has loved me and supported me throughout my entire collegiate career. To my parents, I cannot begin to thank you for putting me through college. I can’t express how much you guys mean to me. Thank you for believing in me and encouraging me to follow my dreams. To my mother, thank you for pushing me to pursue a graduate degree. To my father, I’ll get you to cheer for the Wolfpack some day! I would like to especially dedicate this to my G. Daddy, who will not be able to see me graduate, but I know is proud of me. Thank you to my friends, who I could not have survived college without. Thank you for laughing and crying with me, supporting me, and challenging me to be the person I am today.

BIOGRAPHY

Elizabeth Sloan Braswell was born and grew up in Asheville, North Carolina. She is the daughter of Michael and Karen Braswell, who also grew up in Asheville. She has a younger brother, Matthew, who attends Clemson University. She graduated as the valedictorian from Clyde A. Erwin High School in 2013. After graduating, she decided to attend North Carolina State University, but was undecided about a major as she entered the First Year College program. During her freshman year, she decided to pursue a Bachelor's degree in Civil Engineering. Elizabeth enjoyed her undergraduate years at NC State. From learning and applying knowledge learned in the classroom to developing a since of belonging and purpose with her surrounding community, Elizabeth fully embraced the culture of NC State and reflects on those years as some of the best times and memories in her life. While pursuing an undergraduate degree, she began assisting graduate students in the transportation lab with Dr. Cassie Castorena as her advisor. She helped with countless hours of sieving component materials and running specific gravity tests. Through around two years of lab work and the advice of Dr. Castorena, she decided to apply to graduate school for a masters in transportation materials. She finished her undergraduate degree in Civil Engineering in the Spring of 2017. Her interests include transportation materials. She has enjoyed her graduate career at North Carolina State University and is excited to start a full time position with the Public Land Development Department as a Project Engineer I at Timmons Group in Raleigh, North Carolina.

ACKNOWLEDGMENTS

I would like to thank my family, friends, and fellow graduate students for their constant love and support throughout my entire academic career at North Carolina State University. To all of my family, thank you for calling me and sending me postcards from four hours away. Thank you for believing in me and loving me even though I chose NC State over UNC (best choice I ever made). To my friends, I have made some of the best memories of my life during my time at NC State that I will forever cherish. From living with the girls of Suite 319 to competing with my teammates and friends in club racquetball, I am so grateful for all of the lasting friendships that have been fundamental to enriching my academic career. To Meredith, thank you for being my civil rock and overall boss lady throughout undergrad. I couldn't have made it through all of the classes we had together without you. To my professors, thank you for all of the hours that you put into teaching material, as well as answering all of the questions that I had. It was by the main influence of Dr. Castorena that I decided to pursue a graduate degree in Civil Engineer. Without her guidance as my undergraduate and graduate advisor, I would not be the student I am today, and I cannot begin to thank her enough for what she has done for me in my career at NC State. To the professors who were the leads on the 9-54 project, Dr. Kim, Dr. Shane, and Dr. Castorena, thank you for your dedication to the project and your expert knowledge to help guide me along the way. Dr. Kim, thank you for always keeping the schedule and timing of things in check and providing helpful suggestions since the start of the project. Thank you for always looking at the big picture, and for being there whenever I encountered an issue. To Dr. Shane, thank you for always giving valuable input during the course of the project, and for helping out so much with the EICM portion of the project. I enjoyed getting to work with you. To Dr. Castorena, thank you for always being available to answer all of my questions, and for being my go-to person. To Noor, thank you for always being there to answer my countless questions about the project. I don’t know what I would have done without you working on this project. Thank you to everyone who has impacted my life during my time at NC State. This experience has helped me grow in ways that I could not have imagined, and I will be forever grateful for the opportunities that I have gotten to participate in. Go Wolfpack!

TABLE OF CONTENTS

LIST OF TABLES

LIST OF FIGURES

INTRODUCTION

The road network system is a critical part of civil engineering infrastructure that is essential to how society functions every day. Effective roads are crucial in the transportation of people and goods. Roads are constantly monitored to study their structural performance and quality in terms of driver expectations. As roads age and deteriorate, they require maintenance and rehabilitation to restore their structural and functional properties. Oxidative aging in asphalt pavements is a complex process that results in the hardening and embrittlement of asphalt binder, which increases cracking susceptibility and contributes significantly to the deterioration of asphalt pavements. Oxidative aging is affected by a number of factors, including morphological properties of the asphalt concrete, asphalt binder chemistry, and climatic conditions. Several research studies have established that asphalt aging fundamentally occurs in two phases: short-term and long-term. Short-term aging phase occurs during the production and mixing stage at high temperatures, which include the blending, mixing and compaction processes of asphalt binders with aggregates. Both volatilization and oxidation occur during short-term aging. Over the course of the asphalt pavement material service life, the long-term oxidative aging of binders occurs during in-service exposure to temperatures, traffic loading, and other environmental effects (Bell 1989).

Laboratory procedures to simulate long-term oxidation of asphalt mixtures mixture procedures and models to predict the changes in asphalt properties with long-term aging within Mechanistic-Empirical (ME) pavement analyses have been developed. The most prominent practices for laboratory aging of asphalt mixtures and modeling aging within pavements are AASHTO R 30 (AASHTO R30 2002) and the Global Aging System (GAS) model (Mirza and Witczak 1995), respectively.

AASHTO R 30 describes the laboratory aging procedures for both short-term and long-term aging of asphalt mixtures. A major shortcoming of the AASHTO R 30 standard is that the procedure prescribes a single laboratory temperature and duration (85°C for 5 days) of compacted specimen conditioning for simulating the long-term aging of asphalt mixtures despite that it is well known that aging is a strong function of climatic conditions. In addition, the oven conditioning of compacted specimens can lead to the development of an oxidation gradient and consequently heterogeneous properties in aged specimens, which is problematic for performance testing and prediction (Kim et al. 2018).

The GAS Model is an empirical model that allows for prediction of the change in binder viscosity as a function of pavement age, given a specific depth and mean annual air temperature (MAAT). One of the major shortcomings of the GAS Model is that it does not account for aging deeper than 1.5 inches below the pavement surface and that the MAAT is a relatively crude representation of temperature effects (Mirza and Witczak 1995). Another disadvantage of the GAS model is that it does not directly account for differences in asphalt binder kinetics among different binder types, and a limited data set that was used to draw conclusions regarding pavement aging sensitivity to air void content.

The recent National Cooperative Highway Research Program (NCHRP) 09-54 project sought to develop an improved calibrated and validated procedure to simulate long-term oxidative aging of asphalt mixtures for performance testing and prediction to provide better representation to actual field aging levels (Kim at al. 2018). Loose mixture oven aging at 95°C was selected to improve laboratory aging efficiency and avoid the development of an oxidation gradient in performance test specimens. A Climatic Aging Index (CAI) was derived from the simplification of an oxidation kinetics model to prescribe laboratory aging durations as a function of hourly pavement temperature history and depth. The initial NCHRP 09-54 project also sought to develop an oxidation kinetics model for the prediction of pavement aging. This kinetics model was incorporated with pavement temperatures from the Enhanced Integrated Climatic Model (EICM) to predict field aging levels as a function of depth within the pavement. The kinetics model includes a material-specific parameter that can be obtained using loose mixture or Universal Simple Aging Test (USAT) binder experiments conducted at 95°C. A depth-dependent field calibration function was developed to improve field aging predictability (Kim et al. 2018).

There are several shortcomings of the NCHRP 09-54 long-term aging research project. The aging procedure was calibrated primarily using unmodified or conventional mixtures, when warm-mixture asphalt (WMA), reclaimed asphalt pavements (RAP), and modified binders are commonly used in pavement construction today. Another shortcoming of the aging model is that it is kinetics based. It does not consider diffusion through the asphalt pavement and the corresponding influence of the asphalt mixture morphology, such as air void content and asphalt content. The pavement aging model and laboratory aging procedure were primarily developed using the analysis of a single field core for each project location. The incorporation of replicates could greatly improve the reliability of the developed procedure and model. The last shortcoming of the aging model is that climatic data system, Modern-Era Retrospective Analysis for Research and Applications (MERRA), was used. An updated version is available and could improve the accuracy of pavement temperature histories used in analyses. To improve upon the NCHRP 09-54 project, the MERRA2-HCD files were used for hourly temperature to ensure that the most accurate information is being used. This thesis sought to address these shortcomings conducted.

Objectives

The objectives of this study were to:

1) Recalibrate the loose mixture aging procedure proposed in the NCHRP 09-54 project by incorporating additional field projects and field core replicates.
2) Evaluate the effect of asphalt mixture morphology on the long-term aging of pavements.
3) Recalibrate and extend the NCHRP 09-54 pavement aging model by incorporating additional field projects and field core replicates.

LITERATURE REVIEW

Asphalt Aging Mechanisms

Asphalt durability, or age hardening, is a measure of how the physical properties of asphalt binder change as the asphalt ages. As asphalt binder ages, the viscosity increases and it becomes stiffer and more brittle. Pavement aging is the result of many factors, including oxidation, volatilization, air void content, asphalt content, and binder modification.

Oxidation

When oxygen reacts with the asphalt binder, it makes it stiffer and more brittle. This happens primarily at the asphalt surface of the pavement. The rate of oxygen absorption not only depends on the chemical nature of the asphalt, but also on the physical transport of oxygen from the atmosphere to the material interior, thus resulting in an oxidation gradient as the depth of the pavement layer increases. The transport of oxygen affects the aging phenomena of the asphalt pavement (Oort et al. 1956).

Volatilzation

As the temperature increases, the lighter constituents (volatile oils) of asphalt binder evaporate. This changes the chemistry of the asphalt binder, and subsequently affects the aging of the pavement. This mainly occurs during HMA (Hot Mix Asphalt) production. Volatilization mainly affects the short-term aging stage, and in situ field aging is caused by oxidation (Luo et al. 2015).

Material Factors that Affect Pavement Aging

Air Void Content

As the air void content increases, the amount of aging also increases. A higher air void content allows air and moisture to permeate through the pavement down to the deeper layers, resulting in a decrease in durability and an increase in pavement aging. In a study conducted in Texas, researchers found that tighter air voids result in significantly slower rates of binder aging and hardening, thus delaying the asphalt binder from becoming brittle and stiff (Woo et al. 2008).

Asphalt Content

As the asphalt content in a pavement increases, the aging decreases. This is the result of oxidation occurring at a slower rate because of an increase in binder. Too much of an increase in binder content leads to durability issues in the pavement, so there is a trade off between decreased aging and pavement performance. Increased asphalt content leads to a larger film thickness around the aggregates. Subsequently, oxidation takes longer to occur at a larger film thickness. Asphalt content has a more significant impact on pavement aging than air void content, and it is most significant at the pavement surface, where the largest amount of aging occurs. Kandhal and Chakraborty found that having a higher asphalt film thickness results in a lower complex modulus (G*) value and minimizes the aging of the asphalt binder (Kandhal and Chakraborty 1996).

Binder Modification

It is fairly common to see some sort of modified or enhanced binder in the construction of pavements. This includes using binders with RAP (Recycled Asphalt Pavement), additives such as Advera or Evotherm, as well as using HMA (Hot Mix Asphalt). Banerjee, Smit, and Prozzi found that through the testing of modern additives such as Evothem and other WMA materials, the additives reduce the short-term aging effects of the rheological properties of the binder, as well as slow the rate at which the stiffness occurs over time (Banerjee et al. 2012).

Exposure Factors that Impact Asphalt Aging

Temperature

Factors such as weather patterns vary throughout the seasons and years and have a profound effect on the aging of asphalt pavement. Temperature shifts result in contraction and expansion of the pavement, as well as creating rutting and cracking damage. Moisture can damage a pavement without proper drainage and will cause erosion. As the temperature increases, the rate of oxidation also increases. Temperature can affect the rate of oxidation, the type of binder species that are oxidized, and the nature of the oxidized species that are formed. If the temperature is too high, the asphalt binder could age in a way that results in a fundamentally different binder than aged binder at a lower temperature (Kim et al. 2018). All of these factors contribute to the aging of asphalt pavement. Souza and Castro conducted a study on how these factors affect pavement aging and performance and created a computational finite element model to predict the mechanical response of pavement for temperature shifts and repeated traffic loading patterns (Souza and Castro 2012).

Depth

Asphalt pavement aging is impacted based on depth within the pavement layer. On the surface, oxidation occurs and hardens the surface layers more than the deeper layers. The surface is also where the temperature is the highest. There is also UV exposure at the pavement surface that is not occurring in the deeper layers of the pavement. This contributes to UV oxidation at the pavement surface that affects aging. Another factor is the percolation and diffusion of air deeper within the pavement structure. As the oxygen gradient decreases as the depth increases, the amount of aging decreasing with depth (Hachiya et al. 2003). As the amount of air voids increase within a pavement structure, the diffusion of oxygen is easier and affects the rate of aging of the asphalt pavement (Kim et al. 2018).

AASHTO R30 Long-Term Aging Procedure

This laboratory aging procedure simulates the aging that occurs during construction and service for hot mix asphalt (HMA). AASHTO R30 only applies to loose mixture oven aging. Long-term aging (simulates aging in the field) is followed by the short-term aging procedure (simulates aging due to construction and mixing) of oven aging at 135℃ for four hours. Mixture conditioning for long-term aging occurs at 85℃ in the oven for five days in order to allow for binder absorption during the mix design. This allows the properties and performance characteristics of the HMA to be more accurately predicted (AASHTO R30 2002).

Other Laboratory Mixing Procedures

Laboratory mixture and aging are used to simulate and replicate field aging conditions, primarily the hardening that occurs during the mix (laydown) process (short-term aging). Other laboratory aging procedures are utilized to simulate long-term aging that matches field aging (Airey 2003). Short-term aging is mainly due to the volatilization of the mixture during mixing and construction, while long-term aging is due to oxidation and steric hardening in the field.

Extended heating procedures are used to replicate the short-term aging of asphalt mixtures. The thin film oven test (TFOT) (1940) shows the changes in asphalt properties associated with conventional hot-mixing indicated by viscosity, penetration, and ductility measurements (ASTM D1754/D1754M -09). One drawback of this test is that there is a thick binder film that is stationary. This leads to volatile loss on the surface area of the sample. A modified version of the TFOT is the rolling thin film oven test (RTFOT), which incorporates a thinner asphalt binder film thickness, as well as rotating apparatus that simulates the hardening that occurs during mixture more accurately. An advantage of this test is a shorter run time: seventy-five minutes compared to the five hours it takes to run the TFOT. (Airey 2003). The RTFOT is a better measure of asphalt volatility, which is measured through the change in mass before and after the test is run (ASTM D2872 -12). One disadvantage of the RTFOT is that some binders have a tendency to roll out of the rotating bottles during the test, while some high viscosity binders will not roll inside the rotating bottles. The modified rolling thin film oven test (MRTFOT) incorporates small steel rods inside the rotating bottles to help spread the binder into thin films by creating shear forces (Airey 2003). The volatile loss measured by these laboratory tests is higher than what is experienced in the field, and the oxidation level is significantly lower than what is experienced in the field.

Oxidative procedures combine thin film aging with oxidative aging to simulate the effects of long-term aging. The pressure aging vessel (PAV) uses material from the RTFOT and ages it in a pressurized vessel for twenty hours. The binder is exposed to heat and pressure to simulate field aging of seven to ten years (ASTM D6521 -18). Some temperatures used in the PAV test were perceived to be higher than expected pavement temperature, so the high pressure aging test (HiPAT) was developed as a modification to the PAV procedure to run at lower temperatures for a longer period of time to have conditions more similar to expected pavement temperatures (Airey 2003).

Another method for aging is through ultraviolet and infrared light treatments. Ultraviolet treatment changed the physical and photochemical properties of the asphalt binder more effectively compared to infrared light. The binders were aged in thin film rolling oven containers. Results showed that the asphalt properties differed between the UV/IR treatment and the RTFOT/PAV tests. The researchers concluded that to simulate the long-term aging of asphalt materials, the combination of photochemical techniques and extended heating and oxidative aging procedures is necessary for an accurate representation of aging from the field. (Airey 2003). Other methods include microwave aging, which showed results comparable to RTFOT and PAV aging (Bishara et al. 2000) and steric hardening, which is defined as the molecular structuring that reduces the binding properties of bitumen (Traxler 1963). Steric hardening is reversed by heating, but there may be some permanent damage depending on the bitumen composition (Airey 2003).

GAS Model

The objective of the GAS (Global Aging System) Model was to develop an accurate aging predictive system for short term and long term aging for conventional asphalt cements that has global applicability. This model was developed by Mirza and Witczak in 1995. The GAS model is an empirical model that considers the aging gradient with pavement depth to predict the change in binder viscosity as a function of age. This model is only used for conventional (unmodified) mixes. The simplified GAS Model is shown in Equations 1 and 2 below (Mirza and Witczak 1995).

$$\log\log(\eta_i) = A_i + VTS_t \log T_R \tag{1}$$

$$\log\log(\eta_{orig}) = A_{orig} + VTS_{orig} \log T_R \tag{2}$$

Where: η_i = viscosity in centipoise for condition i, T_R = temperature in degrees Rankine, A_i = regression line intercept, VTS_i = regression line slope (called the Viscosity Susceptibility parameter), η_{orig} = original binder viscosity in centipose at T_R, $\mathrm{A_{orig}}$ = original regression line slope.

Asphalt pavements undergo two distinct hardening phenomena: short term hardening (occurs during mix production and construction, simulated by RTFO), and in-situ field aging (simulated by PAV). This is a complex phenomena because of many different factors: mixing time, asphalt content, air void content, temperature of the pavement, chemical composition of the pavement, original asphalt cement, depth within pavement, rate of oxidation, distress damage type and extent, and binder stiffness. Pavement properties were defined in three stages: original properties, mix/laydown properties (t=0), and field aged/ long term properties (t>0). From these properties, three major models were developed to predict short term consistency from the original properties, to predict long term consistency from short term properties, and to predict consistency-depth relationships.

The model developed to relate original viscosity to the mix/laydown viscosity was taken from measurements at three different temperatures (77°F, 140 °F, 275 °F). This was done to characterize the mix/laydown viscosities as a function of temperature. This is shown in Equation (3. The code value, or the hardening ratio, is used to increase the accuracy of the model and is the ratio of log-log mix/laydown viscosity to the log-log original viscosity. This code value is best selected with local experience with asphalt cement types.

$$\log\log\eta_{t=0} = a(0) + a(1)\log\log\eta_{orig} \tag{3}$$

Where: $a(0) = 0.054405 + 0.004082 \cdot code$, $a(1) = 0.972035 + 0.010886 \cdot code$, $\eta_{t=0}$ = mix (laydown) viscosity in centipoise at Temperature T_R, code = hardening resistance (0 for average).

The model developed to relate mix/laydown viscosity to field aging viscosity was taken from the relationship between viscosity at mix/laydown and aged viscosity. The model form is hyperbolic with time and reflects the significant effect of the site environment (MAAT). The measurements were taken on the field core "surface", which means a depth of 6.3 mm (or 0.25 inches). Four other depths below the pavement surface were also considered and measured to characterize the relationship between depth and viscosity. This is shown in Equation 4.

$$\log\log\eta_{aged} = \frac{\log\log\eta_{t=0} + At}{1+Bt} \tag{4}$$

Where: $A = -0.004166+1.41213*C+C*\log(MAAT)+D*\log\log\eta_{(t=0)}$, $B = 0.197725+0.068384*\log(C)$, $C = 10^{\wedge}(274.4946-193.831*\log(T_R)+33.9366*\log(T_R^2)$, $D = -4.5521+10.47662*\log(T_R)-1.88161*\log(T_R^2)$, η_{aged} = aged viscosity in centipoise, and t = time in months.

Next, the air voids adjustment factor was developed to measure the volumetric/gravimetric properties of the mix, and to see how it influences the rate of aging that occurs in an asphalt pavement. Air void data was not included with the GAS Model because Mirza and Witczak had a very limited database. The adjustment factor (Fv) is based on limited air void information, and was developed to improve the predictability of the general long term aging model. It is summarized by Equations 5 and 6 below.

$$F_v = \frac{1+1.0367*10^{-4}*AV*t}{1+6.1798*10^{-4}*t} \tag{5}$$

$$VA = \frac{VA_{orig}+0.0111*t-2}{1+4.24*10^{-4}*t*MAAT*1.169*10^{-3}*\dfrac{t}{\eta_{orig,77}}} \tag{6}$$

Where: $\eta_{orig,77}$ = viscosity at 77°F in megapoise, VA_{orig} = original (initial) air voids in percentage.

The final form of the GAS model is shown below in Equation 7, which defines the relationship of field aged viscosity at time, t, and depth, z.

$$\eta_{t,z} = \frac{\eta_t(4+E) - E\cdot\eta_{t=0}(1-4z)}{4(1+Ez)} \tag{7}$$

Where: η_t= "surface" (z=0.25 in) aged viscosity, z=depth, and $E = 23.82 \exp(-0.0308 \cdot MAAT)$

The GAS model shows that short term viscosity is influenced by chemical composition and variable mix production factors, which leads to a variability of the short term (mix/laydown) aging of asphalt prediction. The predictive model developed for field aged bitumen is a function of mix/laydown viscosity and the environmental temperature of the paving site. The mix/laydown viscosity can be determined from either the short term aging model or actual measurement (extraction) results. There are several shortcomings for the GAS model. The first is that it does not account for aging 1.5 inches below the pavement surface. This is shown below in Figure 1, which displays the relationship between time and viscosity in different depths within the asphalt pavement structure. As the depth increases, the change in viscosity decreases, suggesting that the with increasing depth, aging occurs at a lower rate than the surface layers. Figure 2 shows the change in viscosity with depth at three time intervals. It also shows that the greatest change in viscosity occurs only in the top few inches of the asphalt pavement.

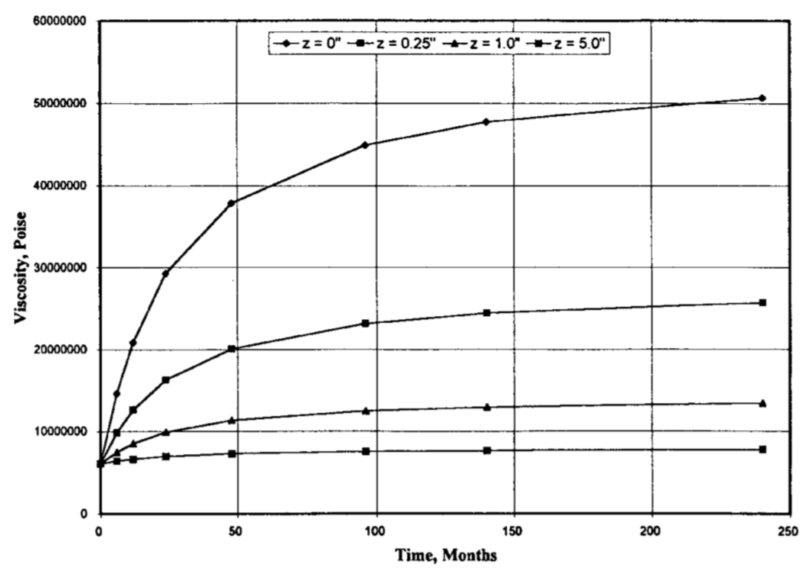

Figure 1. Predicted Viscosity as a Function of Depth for Pennsylvania Study at 77°F

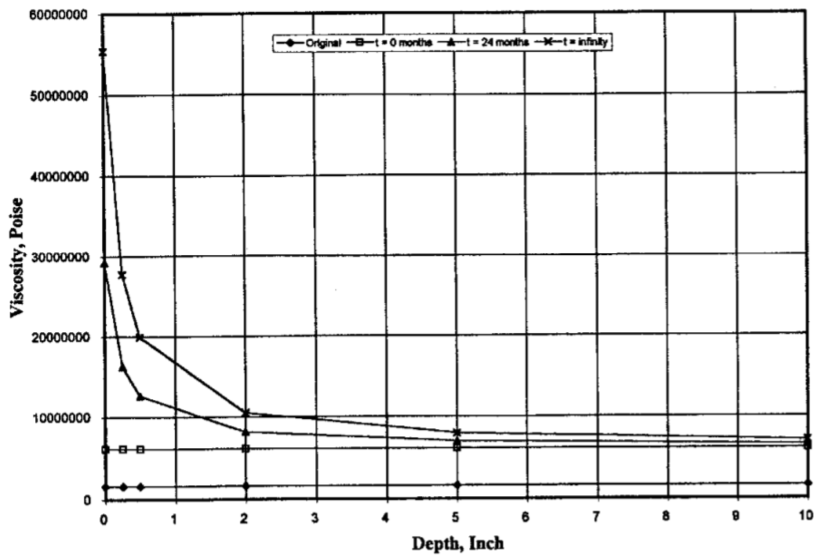

Figure 2. Predicted Viscosity as a Function of Depth for Pennsylvania Study at 77°F

Asphalt does oxidize in lower layers, so the GAS model is not accurate in that sense. A finding of the NCHRP 9-54 Report was a significant oxidation gradient within a field core, with the surface of the field core being more severely oxidized than layers deeper within the pavement. Another setback is that it does not account for differences in asphalt binder kinetics among different binder types. This is important because binder kinetics play a role in asphalt aging behavior. The NCHRP 09-54 kinetics model equation takes into account the mixture specific property of M (how sensitive the mixture is to aging) and the short term aged property of log *G**, which is also mixture specific. Another outcome of the NCHRP 9-54 Report was a validated kinetics model to predict loose mix aging rates at different temperatures using rheology-based AIPs. This model also was paired with hourly pavement temperatures obtained from the Enhanced Integrated Climatic Model (EICM) to predict field aging levels as a function of pavement depth. This model gives a more detailed pavement temperature history than the GAS model, because the GAS model only considers the MAAT (Mean Annual Air Temperature). The next shortcoming is that the method used to account for air void content was based off of a small set of conditions and a limited database, so the predictability of the long term aging model might not be extremely accurate. The GAS Model is only applicable for conventional mixtures, so it would have to be updated if it were to be used for modified mixtures, such as mixtures that contain WMA, RAP, and other unconventional additives. The last shortcoming is that Mirza and Witczak did not record a recovery method used to obtain binder from the field, so those samples could contain solvent and skew the results (Elwardany 2017).

NCHRP 09-54 Aging Procedure and Model

The goals for the NCHRP 09-54 project were to develop a long-term laboratory aging procedure for asphalt mixtures and an asphalt pavement aging model for ME design and analysis (Kim et al. 2018).

First, an aging procedure had to be selected. Factors that were considered were loose mix versus compacted aging, oven aging versus pressurized aging, and an aging temperature of 95°C versus 135°C. Loose mixture aging was chosen over compacted specimen aging because it yielded a higher oxidation rate and homogeneous aging. Oven aging was chosen over pressure aging because a larger amount of material can be aged at one time, and specialized equipment is not necessary. The specimen integrity of specimens that are compacted following long-term oven aging is not maintained based on a comparative study of the dynamic modulus and cyclic fatigue performance of specimen aged in a loose mixture and compacted specimen state. A long-term aging temperature of 95°C was chosen because temperatures exceeding 100°C can change the chemistry of the oxidized binder in a way that is not expected to occur in the field, while a lower temperature would not allow for as efficient of aging. Based on these conclusions, loose mixture oven aging at 95°C was recommended for the fabrication of asphalt mixture performance test specimens.

The project-specific aging durations and pavement aging model proposed in the NCHRP 09-54 project were derived from a rheology-based kinetics model and calibrated using field core measurements of extracted and recovered asphalt binder rheology at varying depths. The NCHRP 09-54 kinetics model was derived using an existing chemistry-based kinetics model that was initially developed for binder aging and adapted to loose mixture aging. The model predicts the log of the dynamic shear modulus (G^*) of the binder at 64°C and 10 rad/s frequency as a function of aging temperature and duration. The log G^* at 64°C and 10 rad/s frequency was used as the Aging Index Property (AIP) in the NCHRP 09-54 project.

AIPs are the binder properties used to measure the extent of oxidation in a pavement. There are two categories of AIPs: chemical and rheological. Chemical AIPs are indicators of oxygen uptake and are measured using Fourier Transform Infrared (FTIR) spectroscopy techniques. Rheological AIPs are used more often than chemical AIPs because they can be directly related to the mechanical properties of an asphalt mixture that relate to pavement distresses. The rheological AIP chosen for this study is the log G^* (dynamic modulus) at 64°C and 10 rad/s frequency because it relates most directly to mixture performance. The kinetics model was based on an existing chemistry-based kinetics model and AIP measurements attained from field cores and laboratory oven-aged loose mixtures. Equations 8 through 10 comprise the kinetics model used in the NCHRP 09-54 project.

$$\log G^* = \log G^*_o + M\left(1 - \frac{k_c}{k_f}\right)(1 - \exp(-k_f t)) + k_c M t \tag{8}$$

$$k_f = A_f \exp\left(\frac{-E_{af}}{RT}\right) \tag{9}$$

$$k_c = A_c \exp\left(\frac{-E_{ac}}{RT}\right) \tag{10}$$

Where: G^* = long-term aged binder shear modulus at 64°C and 10 rad/s (kPa), G^*_o = short-term aged binder shear modulus at 64°C and 10 rad/s (kPa), k = rate of reaction, k_f = rate of fast reaction, k_c = rate of constant reaction, M = material-dependent constant, t = reaction time (days), A = reaction frequency factor, A_f = fast reaction frequency factor, A_c = constant reaction frequency factor, E_a = reaction activation energy, E_{af} = fast reaction activation energy, E_{ac} = constant reaction activation energy, R = universal gas constant, or ideal gas constant, and T = reaction temperature (Kelvin).

The parameter M in Equation 8 must be determined for each specific mixture using isothermal aging experiments conducted at 95°C and optimizing the M value to yield the best relationship between measured and predicted log G^*. The k_f and k_c parameters are universal parameters that were obtained from the least mean square error optimization of Equation 8 to match the values of log G^* at 64°C and 10 rad/s obtained from binders that were extracted and recovered after different durations of laboratory aging at 95°C, 85°C, and 70°C using five mixtures and verified using an additional five mixtures. They are shown below in Table 1.

Table 1. CAI Parameters

k_f	k_c
0.409	0.055

The climatic aging index (CAI) given in Equation 11 was developed based on a simplification of the rigorous kinetics model and was used to prescribe the required laboratory aging durations to match the field aging of a pavement at any depth and location within the pavement structure.

$$t_{oven} = CAI = \sum_{i=1}^{N} DA\exp(-E_a / RT_i) / 24 \qquad (11)$$

Where t_{oven} = required oven aging duration at 95℃ to reflect field aging (day), CAI = climatic aging index, E_a = fitting parameter, D = depth correction factor, T_i = pavement temperature obtained from EICM at the depth of interest at the hour of interest, i (K).

This equation was used to calculate laboratory aging duration as a function of time, climate, and depth. The depth correction factor is shown below in Figure 3 and Equation 12. The CAI was primarily calibrated using unmodified hot-mix asphalt mixtures without RAP. Thus, the CAI should be recalibrated using a broad range of mixtures, including RAP, WMA, and PMA. In addition, a single field core was analyzed for each project location during the initial NCHRP 09-54 project. Thus, the addition of replicate field core testing could improve the reliability of the CAI.

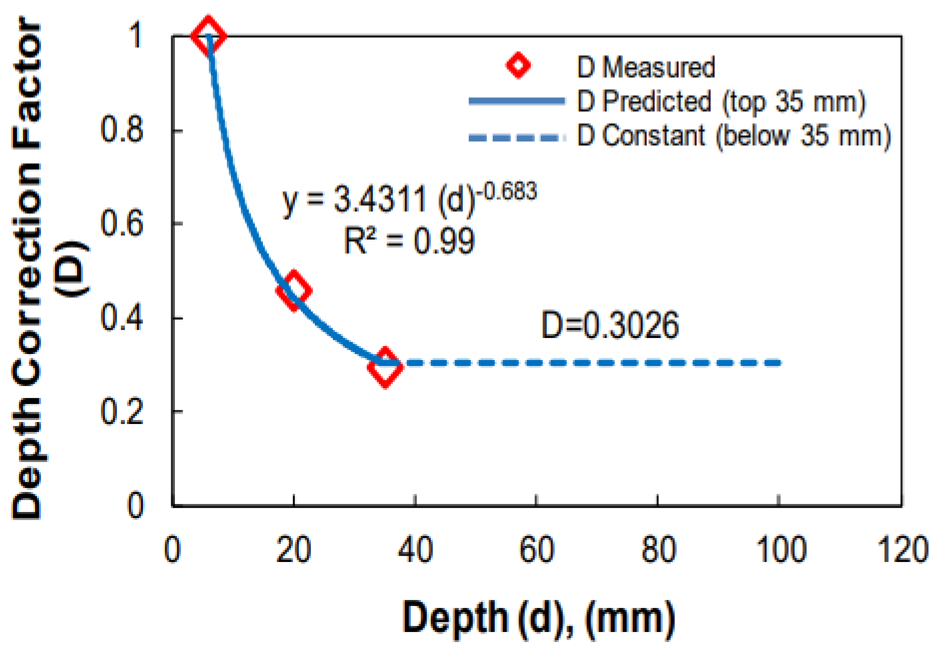

Figure 3. Depth Correction Function

$$C_2 = \begin{cases} 3.4311 \times d^{-0.683}, 6mm \le d \le 35mm \\ 0.3026 \qquad\qquad\quad , d \ge 35mm \end{cases} \tag{12}$$

Note that Equation 11 does not include the material-specific parameter, *M*, given in Equation 8, which means that the required laboratory aging duration required to match a given field condition is independent of material-specific oxidation kinetics. Project-specific loose mixture aging durations at 95°C required to match field age levels were determined for a broad set of materials by comparing the binder log G* of extracted and recovered binders from field cores to those extracted and recovered from laboratory-aged loose mixture conditioning in the oven at 95°C for varying durations. The results were used to calibrate the E_a, *A*, and *D* parameters in Equation 8. In the calibration, the pavement temperature as a function of depth was predicted using the Enhanced Integrated Climatic Model (EICM) data. The pavement temperature data, collected hourly, was downloaded through MERRA-HCD files.

The kinetics model given in Equations (**8** to 10 was also used to calibrate a pavement aging model to predict the field log *G** as a function of depth and time using the material-specific kinetics model parameter M and hourly pavement temperature history. The pavement aging model is given in Equations 13 through 16. The vision was that this model could be modified and extended to replace the Global Aging System (GAS) model to improve the prediction of the changes in asphalt binder properties within ME analyses. The model was calibrated by comparing predictions of log *G** using M values calibrated using loose mixture aging trials conducted at 95°C and measurements of log *G** of binder and extracted from field cores at varying depths.

$$\log G^*_{field\_Predicted} = \log G^*_{o,\mathrm{field}} + M\left[\left(1-\frac{k_c}{k_f}\right)(1-\exp(-k_f t)) + k_c t\right]_{field} \tag{13}$$

$$\log G^*_{field\_measured} = C_1 + C_2 \times \log G^*_{\mathrm{field\_predicted}} \tag{14}$$

$$C_1 = \begin{cases} 1.5855 \times d^{-0.377}, 6mm \le d \le 35mm \\ 0.415 \qquad\qquad\quad, d \ge 35mm \end{cases} \tag{15}$$

$$C_2 = \begin{cases} 0.7636 \times d^{-0.095}, 6mm \le d \le 35mm \\ 0.5447 \qquad\qquad\quad, d \ge 35mm \end{cases} \tag{16}$$

Where: C_1, C_2 = calibration factors.

This equation is not expected to give accurate predictions of field aging because of the diffusion that takes place in the field, which affects field reaction rates significantly. The partial pressure of oxygen that is available to the binder and interacts with it varies with depth and asphalt mixture morphology. Therefore, future research was suggested to incorporate a diffusion model to improve the prediction of the pavement aging (Kim et al. 2018). In addition, a single field core was analyzed for each project location during the initial NCHRP 09-54 project. Thus, the addition of replicate field core testing could improve the reliability of the field calibration of the kinetics model.

METHODOLOGY AND EXPERIMENTAL PLAN

In order to accomplish the goals of this thesis, materials from seven different locations where both component materials and field cores extracted from in-service pavements were available were tested. Field locations included the United States, Brazil, and Canada. The materials varied in morphological properties, climatic conditions, and pavement design. Table 2 below summarizes the materials tested in order to finalize the pavement aging model for M-E analysis and to refine the laboratory aging procedure. It also summarizes which sections had WMA, RAP, or any type of binder modification. It also included which sections included the addition of replicate testing of field cores that were tested in NCHRP 09-54 project.

Projects

Materials and corresponding field cores were evaluated from the following projects:

- Brazil: Sections from Fundao, Brazil were used for the systematic study of morphology.
- FHWA-ALF: Federal Highway Administration Accelerated Load Facility. The FHWA-ALF is an accelerated loading facility in McClean, Virginia. The sections were evaluated based on a study that investigated the effects of asphalt binder modification and pavement structure on pavement performance.
- MIT: Manitoba. The sections evaluated from Manitoba, Canada involve the study of additives such as Advera and Evotherm, as well as sections containing different RAP contents and additives such as foaming and Evotherm.
- NCAT: National Center for Asphalt Technology. The NCAT test track is located in Opelika, Alabama and the sections analyzed in this study include sections with different RAP contents.

- LTPP: Long-Term Pavement Performance Program. The materials used from the LTPP program come from a variety of states and include sections that have a variety of binder types and climatic conditions.
- MNROAD: Minnesota. These sections from the Minnesota test road have different PG grades. These field cores are from a low volume road adjacent to I-94.
- WesTrack: Materials from Reno, Nevada were used for the systematic study of morphology.

Table 2 provides a summary of the materials analyzed. The table indicates which sections correspond to unconventional mixtures (WMA, RAP, or PMA) and which sections correspond to those studied in the original NCHRP 09-54 project for which replicate field cores were analyzed in this study.

Table 2. Summary of Test Sections

Project ID	Location	Age of Field Cores	Section	Number of Cores Tested	Loose Mix Tested	PG Grade	WMA	Modified Binder	Contains RAP	Replicate from Previous Data
FHWA-ALF	*Virginia*	*8 years*	*Control*	*1*		*PG 70-22*				*X*
			SBS-LG	*1*		*PG 70-28*		*X*		*X*
			CR-TB	*2*		*PG 76-28*		*X*		*X*
			Terpolymer	*2*		*PG 70-28*		*X*		*X*
MIT	*Manitoba, Canada*	*4 years*	*Control*	*1*		*AC 150/200*				*X*
			Advera	*1*	*95°C*	*AC 150/200*	*X*			
			Evotherm	*1*	*95°C*	*AC 150/200*	*X*			
			15% RAP	*3*	*95°C*	*AC 150/200*			*X*	
			50% RAP	*2*	*95°C*	*AC 150/200*			*X*	
NCAT	*Alabama*	*4 years*	*(S9) Control*	*1*		*PG 76-22*				
			(S8) 15% RAP	*2*	*95°C*	*PG 76-22*			*X*	
			(N10) 50% RAP	*1*		*PG 67-22*			*X*	
			(S11) Evotherm	*1*	*95°C*	*PG 76-22*	*X*			
			(N11) 50% RAP with Foam	*2*	*95°C*	*PG 67-22*	*X*		*X*	
			(S10) Foam	*1*	*95°C*	*PG 76-22*	*X*			
LTPP	*California*	*8 years*	*California*	*1*		*AR-40*				*X*
	New Mexico	*10 years*	*New Mexico*	*1*		*AC-20*				*X*
	Texas	*11 years*	*Texas*	*1*		*AC-20*				*X*
	Washington	*11 years*	*Washington*	*1*		*AR-20*				*X*
	Wisconsin	*8 years*	*Wisconsin*	*1*		-				*X*
	South Dakota	*14 years*	*South Dakota*	*1*		*AC 120-150 pen*				*X*
WesTrack	*Nevada*	*19 years*	*(S4) Fine, Opt. ac%, L AV% (WTFOL)*	*2*		*PG 64-22*				*X*
			(S2) Fine, Low ac%, M AV% (WTFLM)	*2*						*X*
			(S1) Fine, Opt. ac%, M AV% (WTFOM)	*2*						*X*
			(S14) Fine, High ac%, M AV% (WTFHM)	*2*						*X*
			(S17) Fine, Opt. ac%, H AV% (WTFOH)	*2*						*X*
			(S18) Fine, High ac%, LAV% (WTFHL)	*2*						*X*
			(S3) Fine, Low ac%, HAV% (WTFLH)	*2*						*X*
		17 years	*(S39) Coarse, Opt. ac%, L AV% (WTCOL)*	*1*						*X*
			(S36) Coarse, Opt. ac%, H AV% (WTCOH)	*1*						*X*
Brazil	*Brazil*	*8 years*	*GALP*	*6*		*PG 64-16*				
			LUBNOR	*5*		*PG 70-22*				
			REPAR	*6*		*PG 64-16*				
			REPLAN	*6*		*PG 64-22*				

Significance of Projects

Each section chosen for this study incorporates pavement structures that have a variety of climatic conditions, morphological properties, and unconventional additives that improve pavement performance. FHWA-ALF contains sections that have modified binders, including SBS, CR-TB, and Terapolymer binders. ALF sections were also tested to provide replicates for the existing database. LTPP sections were also tested to provide replicates, as well as to add different field core ages to the existing database. Field cores from Manitoba and NCAT contain sections that include warm-mix asphalt (WMA) and mixtures containing different percentages of reclaimed asphalt pavement (RAP). Field cores from WesTrack and Brazil were used for the systematic study of morphology. WesTrack materials were studied in the original NCHRP 09-54 project; replicate field cores were tested herein to strengthen the existing database.

Field Core Preparation and Binder Extraction and Recovery

Field cores obtained from in-service pavements were first sliced in half, as shown in Figure 4 in order to be able to place the core under a saw and slice into thin layers corresponding to different pavements depths. From the half cores, 11 mm deep slices were cut. A total of 4 slices were obtained from the cores in order to investigate the effects of depth on aging within the asphalt pavement. For cores that had a chip seal or tack coat in between layers, those areas were removed and not included in the analysis, with the change in depth of any slices due to the interlayer noted. After all of the slices were obtained, they were broken up with a hammer into pieces and placed into a jar with a solvent solution comprised of 85 percent toluene and 15 percent ethanol. The solvent dissolves the asphalt binder contained within the asphalt mixture to allow for recovery. After soaking the samples for at least twenty-four hours, the samples were centrifuged, and the binder solution was extracted and placed into the rotary evaporator for recovery at a series of increasing temperatures and time intervals starting from fifteen minutes at 85°C and increasing to ninety minutes at 170°C inside a rotating flask. After the process was complete, the binder was placed into a tin, as shown in Figure 5, and subjected to DSR testing after ensuring that any remaining solvent was absent.

Figure 4. Sample Field Core

Figure 5. Extracted and Recovered Binder

Before DSR testing, it is important to test for the presence of remaining solvent from the extraction and recovery process. To be consistent with previous research, all samples were placed in the oven at 90°C for ten minutes to help evaporate any remaining solvent. The absence of solvent in the samples is very important, because if there is any solvent present, it affects the properties of the binder measured in the DSR. After oven conditioning, the samples were tested using the Fourier-Transform Infrared Spectroscopy (FTIR), shown in Figure 6, which uses infrared to obtain a spectrum of the absorption or emission of a solid, liquid, or gas. The infrared absorption wavenumber 694 (1/cm) corresponds to the solvent used. If there is remaining solvent in the sample, there will be an absorption peak at a wavelength of 694 (1/cm), and the sample will have to undergo extra measures to remove residual solvent. If there is no remaining solvent, there will be a downward sloping line displayed in the wavelength output, and the sample is ready to be DSR tested. The difference between the two outputs are shown in Figure 7 below.

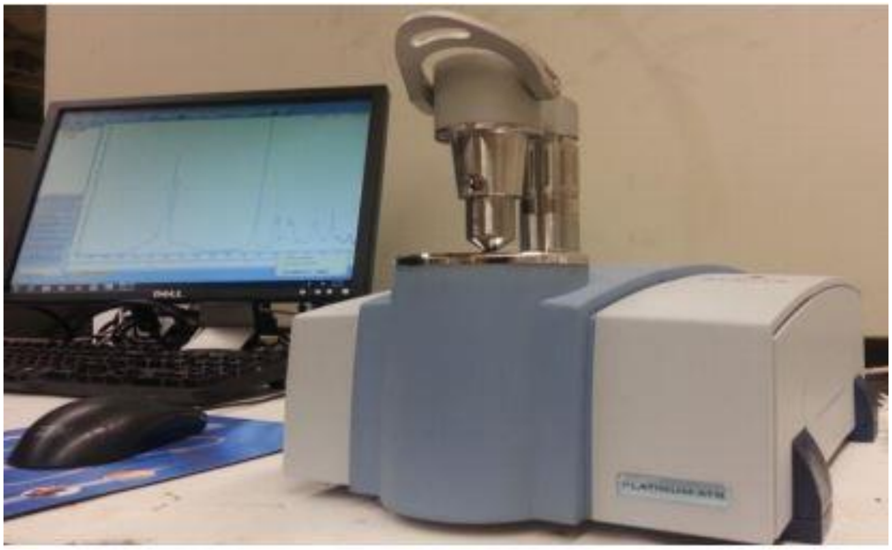

Figure 6. FTIR Machine

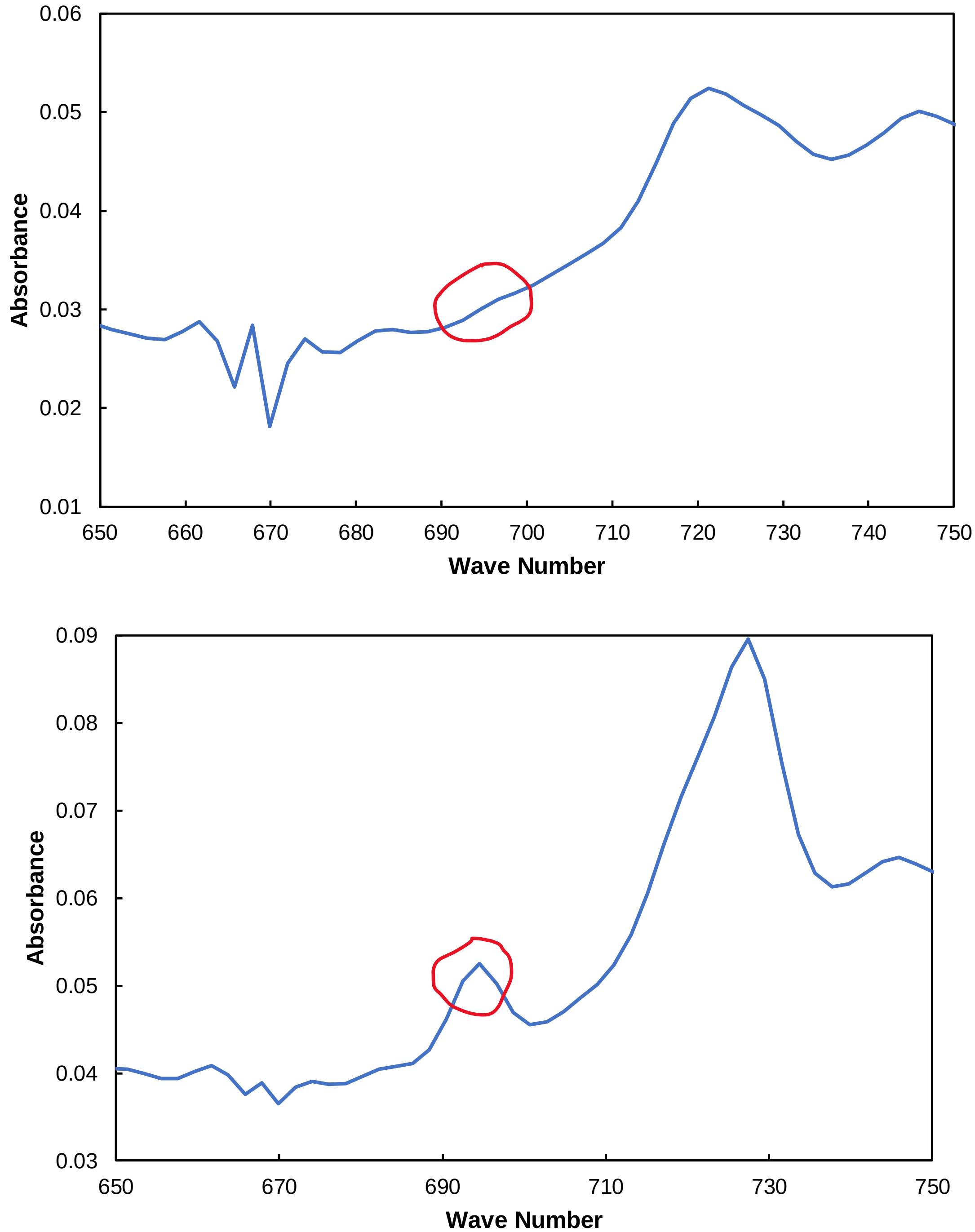

Figure 7. FTIR Output

Samples containing residual solvent were subjected to further conditioning in a reaction vessel, which is shown in Figure 8. The samples were placed on the metal rack shown in the middle of the picture, and then placed into the glass chamber inside the heating vessel. Nitrogen was purged through the system while the pressure was vacuumed out of the chamber to prevent any oxidation and remove residual solvent. The rod on the left was connected to the temperature calibration system, which ensured that the temperature was maintained at 110°C The relatively low temperature and the nitrogen flowing through the system did not cause any additional aging of the binder sample.

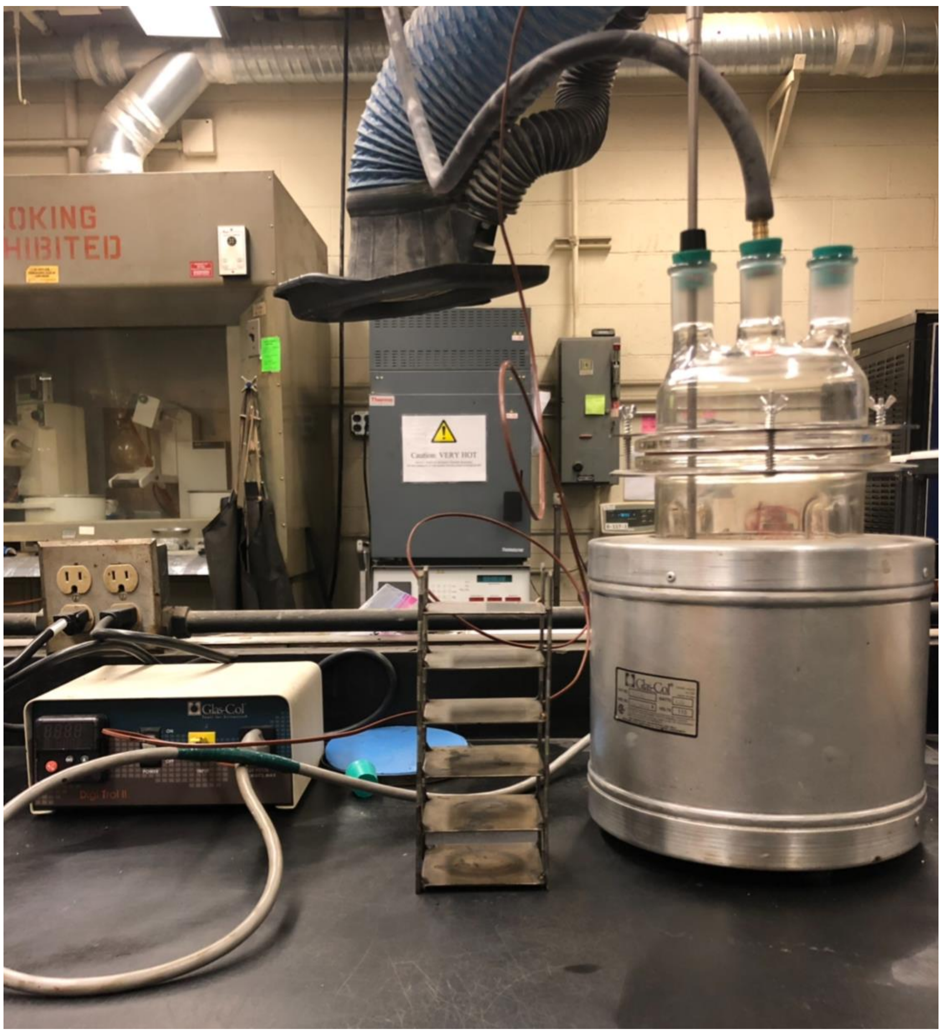

Figure 8. Reaction Vessel

After 50 minutes in the reaction vessel, the samples were taken out and subjected to FTIR testing to check for the presence of solvent again. Ninety percent of the samples showed the absence of solvent after reaction vessel conditioning and were then DSR tested. The samples that still had solvent remaining were put back in the reaction vessel for a second round of conditioning and FTIR was subsequently used to confirm that all of the solvent was removed prior to DSR testing.

Loose Mixture Preparation and Aging

Original component materials were acquired from their respective field sections. Aggregates were sieved according to individual sizes, and then batched according to the available Job Mix Formula (JMF) for each mixture. The aggregates were heated for five hours and the asphalt binder was heated for two hours at the appropriate mixing temperature, also acquired from the JMF. The aggregate and binder were then mixed together in a bucket mixer until the proper mixing was achieved. All of the mixtures were then short-term aged at 135°C for four hours according to the American Association of State Highway and Transportation Officials (AASHTO) R30. After short-term aging, the mixtures were placed in ovens set to either 95°C or 70°C for long-term aging. Samples were taken out of the short-term aged mixture, as well as the long-term aged mixture at four, eight, and sixteen days. These were chosen in order to get a picture of how the mixture aged over time due to the kinetics model. During long -term aging, the pans were rotated systematically in the oven to help minimize any effects of an oven temperature gradient or draft on the degree of aging on the mixtures. The loose mixtures were subject to the same treatment in the rotary evaporator for recovery, as well as subsequent FTIR testing to ensure the absence of solvent before DSR testing.

Dynamic Shear Rheometer (DSR) Testing

Temperature-frequency sweep tests were performed using an Anton Paar MCR 302 DSR, shown below in Figure 9 to measure the rheological properties of the extracted binders. The dynamic shear modulus, G*, was the aging index property (AIP) that was used in analysis. The loading frequencies of the DSR ranged from 0.1 Hz to 30 Hz. All extracted binders were measured at 64°C on an 8 mm parallel plate inset with a strain amplitude of 1 percent. The temperature of 64°C was chosen to be consistent with previous research. 8 mm plates were used instead of the 25 mm plates because of the limited mass of the extracted binder that was available. Two replicates of each binder sample were tested to ensure consistent results.

Figure 9. Dynamic Shear Rheometer (DSR)

Enhanced Integrated Climatic Model (EICM) Analysis

The climatic aging index (CAI) determines the required laboratory aging duration that best reflects the aging in the field at a location of interest and a depth of interest by using the

Enhanced Integrated Climatic Model (EICM) hourly pavement temperature data. MERRA2-HCD pavement temperature files that store hourly pavement temperature data from the years 1980 to 2017 were used in the EICM analysis to determine the laboratory aging duration (Toven) for a section and depth of interest. Temperatures below 20°C were not included in the analysis. According to the results found in the NCHRP 09-54 Report, it is safe to assume that binders do not experience any aging when pavement temperatures fall below 20°C. This was tested on two binders with significantly different aging susceptibilities, and both did not experience any aging when the temperature was less than 20°C for a prolonged period of time (Kim et al. 2018). This is shown in the results in Figure 10. The CAI is a simplified form of the kinetics model and is shown by Equation 11.

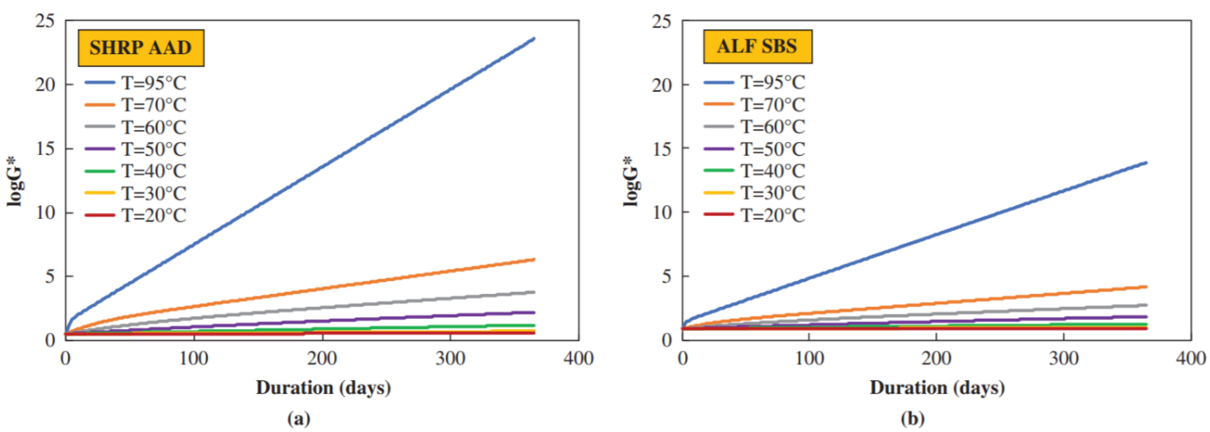

Figure 10. Predictions of log G* Under Different Isothermal Loadings for Prolonged Periods of Time for: (a) SHRP AAD Binder and (b)ALF-SBS-Modified Binder (Kim et al. 2018)

MERRA is a source of climate data that became available in 2012. MERRA data provides a continuous record of hourly values for all inputs to current advanced infrastructure models. MERRA is a physics-based reanalysis model that combines computed model fields like atmospheric temperatures with ground, ocean, atmospheric, and satellite-based observations that are distributed irregularly in space and time to accurately represent air temperature history (Schwartz 2015). The original NCHRP 09-54 project used the original MERRA files.

In contrast, this study used the newer MERRRA2-HCD files, which experienced a series of updates. MERRA2 resolves issues encountered in MERRA and includes new capabilities, such as the assimilation of aerosol observations. MERRA2 uses a cubed-sphere grid, while the old MERRA used a latitude-longitude grid (Gelaro 2017).

The MERRA2-HCD stations with coordinates and elevation closest to each project locations were identified and used in the CAI and kinetics model to obtain the most accurate climate information. For example, the MERRA station 142946 was chosen to represent the climatic data for the WesTrack sections in Nevada. After the appropriate stations were chosen, the thirty-seven years of hourly pavement temperature data (1980-2017) was input and analyzed in the Enhanced Integrated Climate Model (EICM) software to obtain hourly pavement temperate history as a function of depth within the pavement structure. The resulting files were then used as inputs to a CAI calculation spreadsheet and kinetics model. The average response (CAI or kinetics model output) of the analysis of the 37 years of data were used in the analyses to provide the most representative results.

The EICM is used to predict or simulate the changes in behavior and characteristics of pavement in conjunction with environmental conditions over many years of service life and was adapted for use in the Mechanistic-Empirical Pavement Design Guide (MEPDG). Prior to generating the climatic data for analyses to recalibrate CAI and the kinetics model, EICM analyses were conducted using one year of hourly temperature data to determine if there was a difference in the output of the analysis with the changing of the asphalt pavement structure. CAI analysis was run on pavement layers 3 inches and 9 inches thick, with nodes that measure temperature every centimeter in depth. The base and subbase layers were equal among the two pavement structures analyzed. The number of elements in the layer equal the thickness of the layer in inches. The pavement structure followed the sub layering guidelines used in MEPDG of the Figure 11 below.

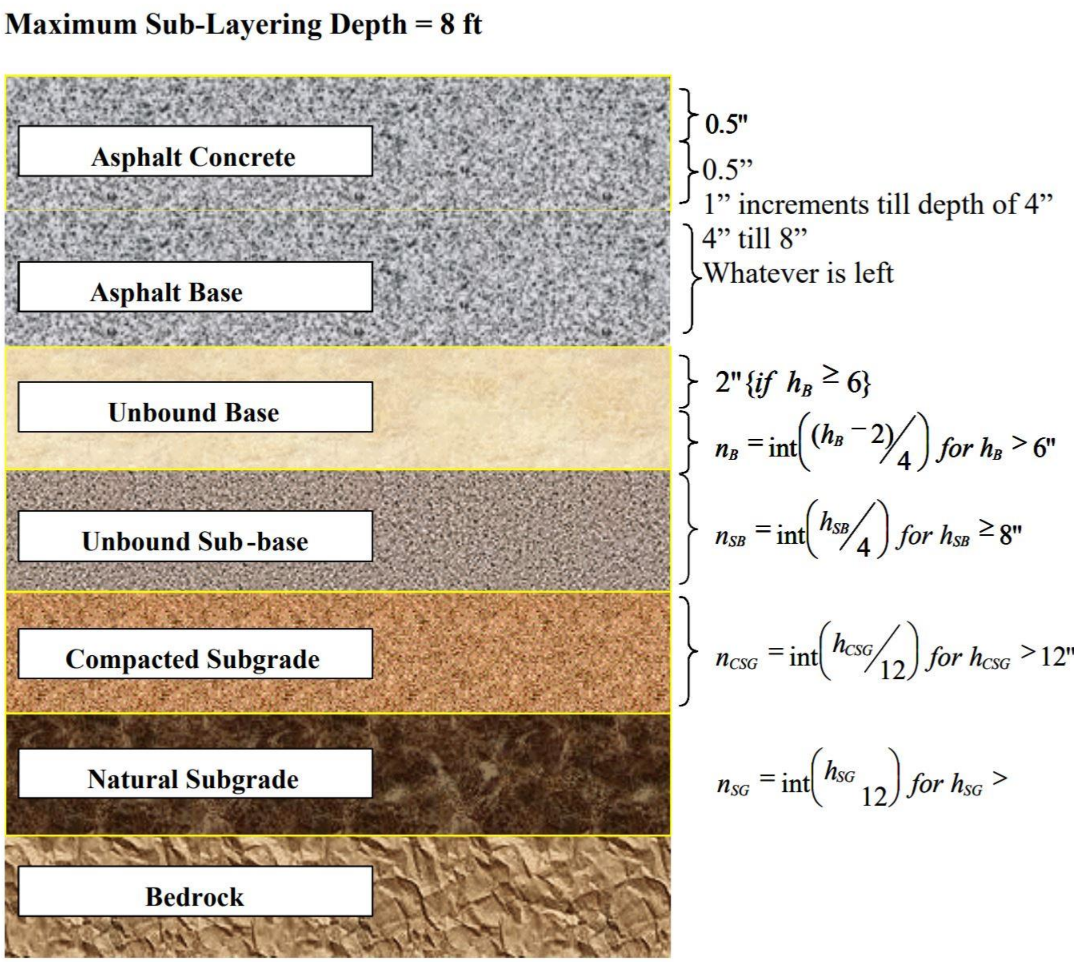

Figure 3.3.9. Layered pavement cross-section for flexible pavement systems (no sub-layering beyond 8 feet).

Figure 11. MEPDG Pavement Structure for EICM Analysis (ARA, Inc. 2000)

Two samples sections were analyzed to see the differences in the CAI output based on the thickness of the asphalt layer. Figure 12 below shows a sample of the EICM interface, and an example of the nine inch thick surface asphalt structure that was tested.

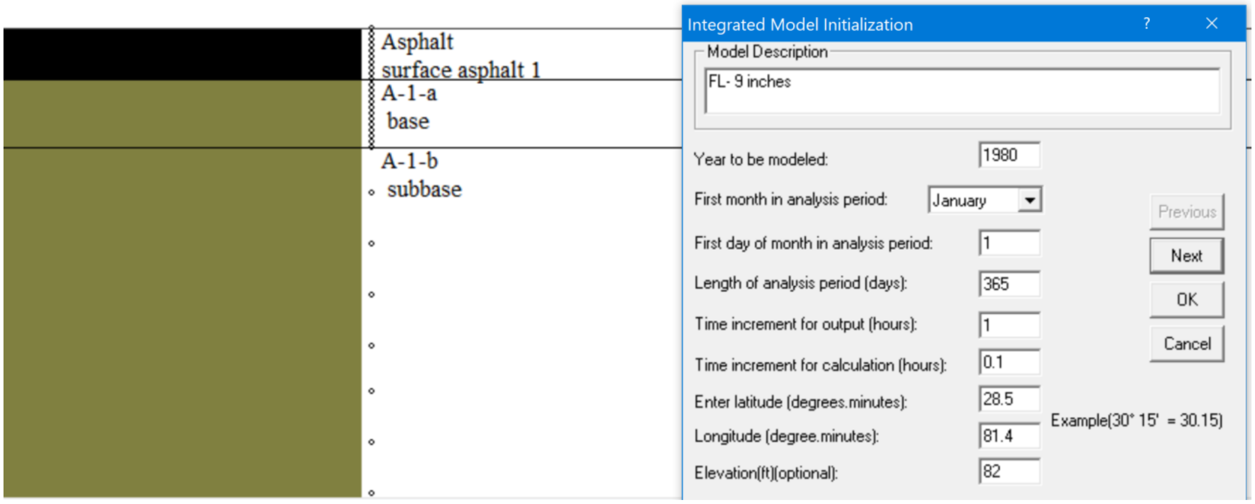

Figure 12. EICM Asphalt Structure

The same analysis was run for a three-inch-thick surface asphalt pavement structure, and the resulting CAI values (using the parameters proposed by Kim et al. (2018)) were compared. EICM and CAI results were compared at two months of the year (January and July) and at two different times of the day (1 pm and 11 pm). Figure 13 (a) shows the results for January at 1 pm, and Figure 13 (b) shows the results for July at 11 pm. The results are shown in Figure 13 and Figure 14 below. The results show that there is not a significant difference between the results of the three inch versus a nine inch structure. The temperatures at increasing depth within the pavement are not significantly different, and the total CAI for sixteen years is not significantly different either. The percent difference in the total CAI calculation for both sections at the tested depths is less than one percent for each node, or location. The asphalt structure chosen for analysis was nine inches thick, because it was more representative of asphalt pavement structures in the field.

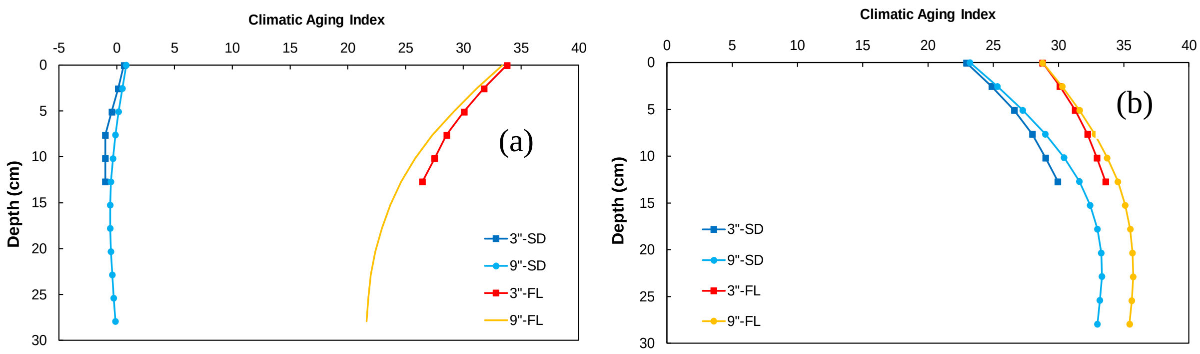

Figure 13. EICM Results (3" vs. 9" Asphalt Layer)

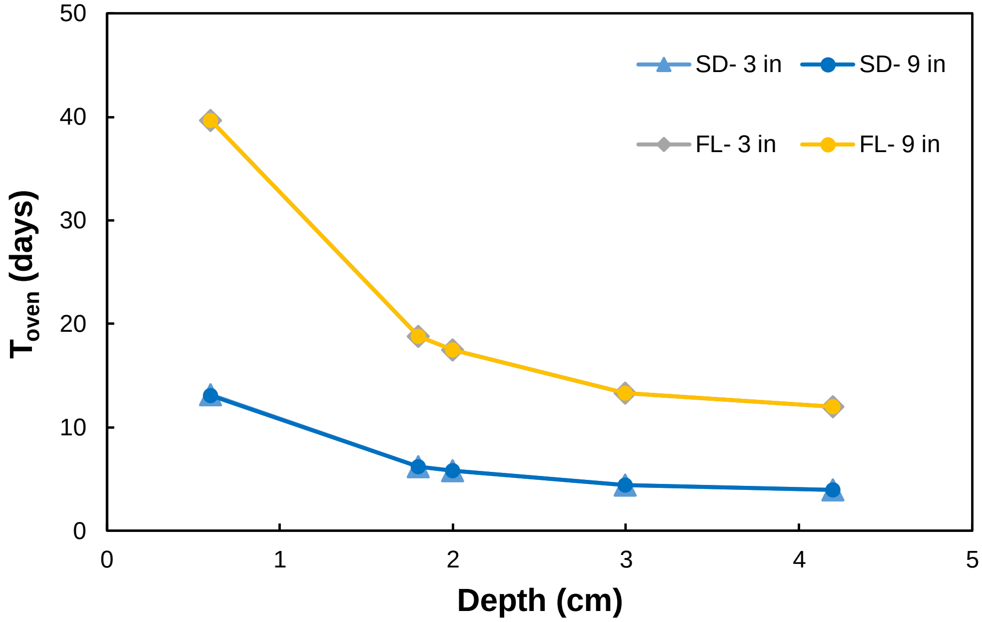

Figure 14. CAI Comparison (3" vs. 9" Asphalt Layer)

To calculate the laboratory loose mixture aging duration at 95°C required to match the aging level of a field core at a given depth (Toven) for use in calibrating the CAI parameters, loose mixture was short-term aged at 135°C for four hours and long-term aged at 95°C for sixteen days. Loose mixture samples were periodically removed from the oven and subjected to extraction and recovery and subsequent measurement of the binder log G* at 64°C and 10 rad/s. The M value to yield the best match between the measured log G* values as a function of aging duration and those predicted using the kinetics model (i.e., Equation 8) was determined.

Subsequently, the average log G* value of the binder extracted and recovered at a given depth from field cores corresponding to an in-service pavement comprised of the same materials used in loose mixture aging was input into Equation 13 and the corresponding time was calculated. This process is shown below in Figure 15**Error! Reference source not found.**.

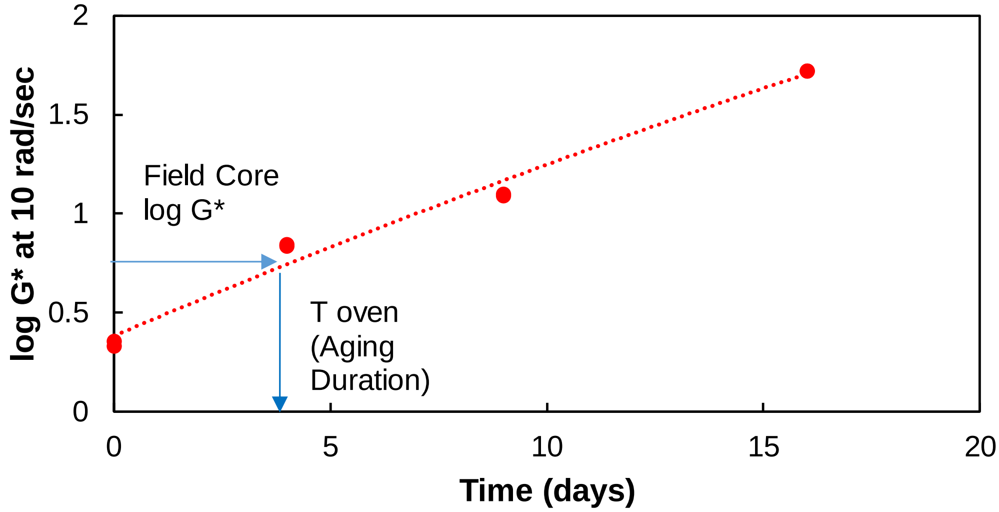

Figure 15. Calculating Toven Values

RESULTS

Recalibration of the Loose Mixture Laboratory Aging Durations with the Addition of Unconventional Mixtures and Field Core Replicates

One of the shortcomings of the NCHRP 09-54 long-term aging research project is that the aging procedure was calibrated primarily using unmodified hot-mix asphalt mixtures without RAP. However, unconventional mixtures such as warm-mixture asphalt (WMA), reclaimed asphalt pavements (RAP), and polymer modified asphalts (PMA) are commonly used today. Therefore, the CAI was recalibrated with the incorporation of additional projects, including unconventional mixtures. The recalibration of the model was also strengthened by adding replicates of field cores to the existing database established from previous research.

Some limitations were encountered with the WMA, RAP, and PMA sections that were evaluated. First, there were a limited number of these sections to test and study compared to the other conventional mixtures. In addition, the RAP and WMA projects (NCAT and MIT) field cores were only four years old. For some of these sections, it was found that the laboratory short-term aged material exceeded the age level of the field cores based on log G^* values of extracted and recovered binder at 64°C and 10 rad/s. This finding could suggest that the short-term aging laboratory procedure included in AASHTO R 30, consisting of loose mixture conditioning at 135°C for four hours produces more aging than occurs during asphalt mixture production and placement. The recently completed NCHRP Project 09-52 supports this speculation by recommending that short-term aging be refined to include only two hours of conditioning in a forced-draft at 116°C for WMA, and 135°C for four hours for hot-mix asphalt (Newcomb et al. 2015). CAI was still calculated for these mixtures and they are included in the graphical representations of the CAI results. However, they were not included in the optimization to recalibrate the CAI parameters.

Original CAI Parameters

Prior to recalibrating the CAI parameters, the accuracy of the CAI parameters proposed in the NCHRP 09-54 project were evaluated. The comparison between the measured laboratory oven aging durations and the original CAI values is shown with delineation by project and depth in **Error! Reference source not found.** and Figure 17, respectively. In **Error! Reference source not found.**, the conventional mixtures are shown in blue, the WMA mixtures are shown in red, the mixtures containing RAP are shown in green, and the PMA mixtures are shown in yellow. Each section within those categories is shown as a different shape to help distinguish the individual sections. Replicate field core testing and unconventional mixtures have been added to the original NCHRP 09-54 database to calculate the measured laboratory oven aging durations. In addition, MERRA 2 climate data was used to calculate hourly pavement temperature history herein whereas the original MERRA climate data was used in the initial calibration of CAI. **Error! Reference source not found.** demonstrates that the majority of the data falls below the line of equality, suggesting the original CAI parameters often underestimates the required laboratory aging duration. Figure 17 shows that the data corresponding to a depth of 6 cm generally fall above the line of equality, suggesting over prediction of the required laboratory aging duration using the original CAI parameters. The data corresponding to deeper depths generally fall below the line of equality, suggesting under estimation of the required laboratory aging duration. Furthermore, the results demonstrate high scatter in the data and generally better prediction at depths of 1.85 to 3.15 cm than 0.6 cm or 4.45 cm. The high scatter in the data at a depth of 0.6 cm is not surprising because the surface conditions may be impacted by Ultraviolet

(UV) oxidation and other surface wear mechanisms that are not accounted for in the CAI calculation. As the depth increases, however, the effect of diffusion may become more significant which is driven by asphalt mixture morphology. Thus, it is also somewhat intuitive that there would also be high scatter at the deepest depth analyzed compared to the intermediate depths. The scatter also reflects the large variability in data measurements taken from the field cores. The WMA and RAP projects are clustered near the low aging levels (corresponding to small CAI values and measured laboratory aging durations), which makes it difficult to determine whether trends differ from that of conventional mixtures; this reflects that the field cores corresponding to these field sections were only 4 years old whereas the other projects contained field cores from greater durations of in-service aging. All PMA sections correspond to the FHWA ALF project. The FHWA ALF cores were extracted from sections that were subjected to high temperatures for rutting experiments. In these cases, the pavements were subjected to temperatures up to 74°C for up to two months (Gibson 2012). The locations and thermal history during the ALF experiments were identified for each field core and incorporated into the CAI calculation. However, these harsh conditions may lead to a bias in the relationship between laboratory and field aging.

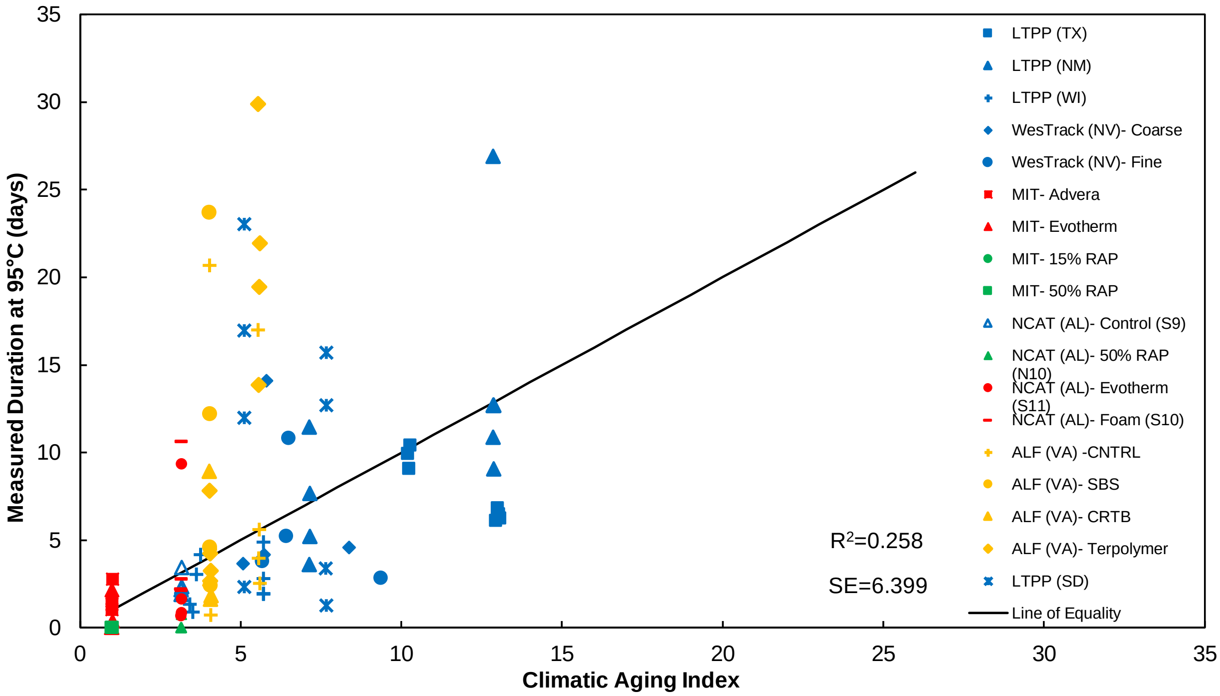

Figure 16. Comparison of Measured Laboratory Aging Durations at 95°C and the Original CAI with Delineation by Project

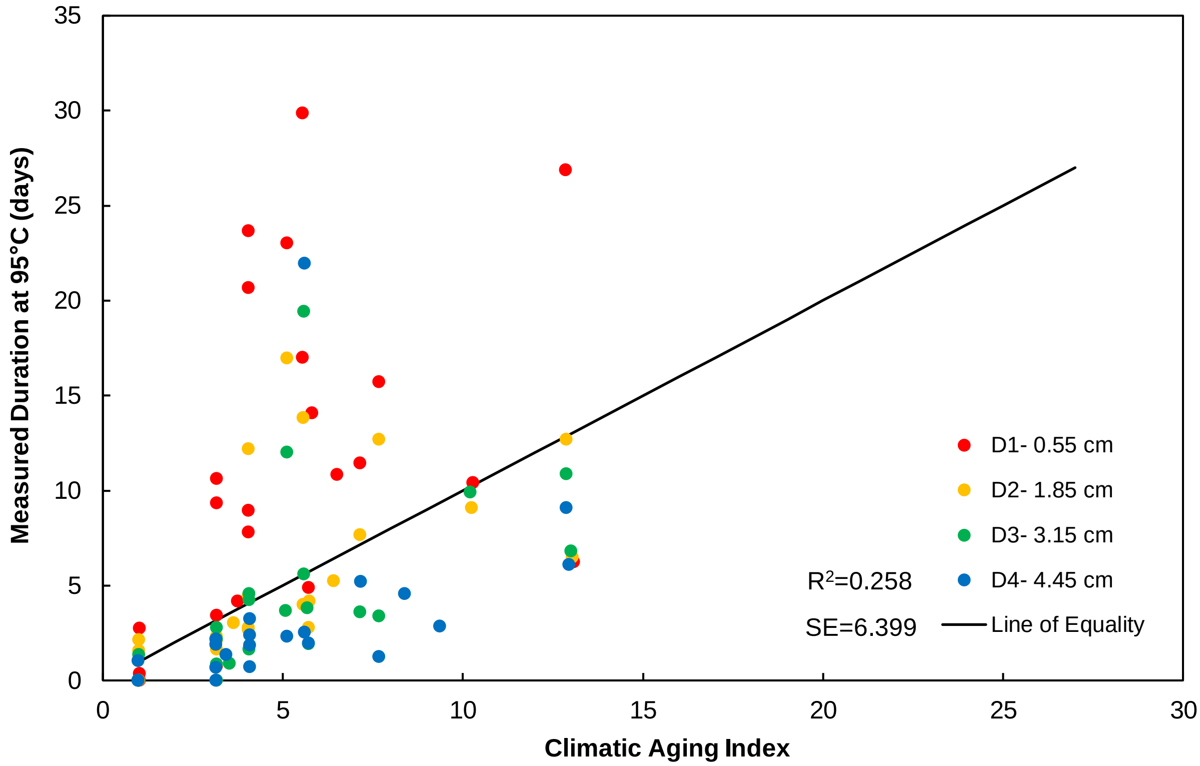

Figure 17. Comparison of Measured Laboratory Aging Durations at 95°C and the Original CAI with Delineation by Depth

Recalibration Effort

The CAI in Equation 11 was simplified and recalibrated by conducting a least squares optimization to minimize the error between the measured laboratory aging durations. The simplified form is shown in Equation 17.

$$t_{oven} = CAI = \sum_{i=1}^{N} C_1 d^{C_2} e^{\frac{C_3}{T_i}} \tag{17}$$

Where: C_1, C_2, and C_3 are fitting parameters and d is depth in cm.

The function D and parameter A in Equation 11 were combined into a single function, ($C_1 d^{C2}$) termed the 'depth factor' herein and the division by 24 was removed and smeared into the optimization. The E_a parameter in Equation 11 was divided by R and renamed C_3 to further simplify the CAI expression. The value of E_a in Equation 11 was not changed. A limited set of E_a values were tried but changing E_a did not appear to lead to significant improvement in the accuracy of CAI and it was very cumbersome to iteratively update E_a due to the large amount of data analyzed (i.e., 37 years of climate data for each section). Optimizations were performed at each depth to determine the depth factor at each depth. Then, the parameters C_1 and C_2 were determined by optimizing the relationship between the factor and depth. It was found that a power law represented the data well and provided reasonable results (i.e., does not decay below zero for very deep conditions).

Initial Recalibration

The results of the recalibration of CAI using all projects (except those where the laboratory STA condition exceeded the age level of the corresponding field cores) are shown in Figure 18 and Figure 19. The conventional mixtures are shown in blue, the WMA mixtures are shown in red, the mixtures containing RAP are shown in green, and the PMA mixtures are shown in yellow. Figure 18 and Figure 19 demonstrate an improvement in the accuracy of the CAI compared to the original parameters based on R2 (0.564 versus 0.258) and standard error (SE) (5.598 versus 6.399). The conventional, or unmodified, mixtures encompass a broader range of locations, binder type, and climatic conditions, and age levels than the unconventional.

The WMA sections appear to align with the conventional mixtures but it is difficult to draw conclusions due to the limited aging of the field cores from these sections. The RAP sections all fall under the line of equality, suggesting future research with additional materials and higher field aging levels is necessary to investigate the relationship between both laboratory short-term and long-term aging with field aging for RAP mixtures.

Approximately half of the PMA sections, denoted as ALF, are outliers for this data set because they stray significantly from the line of equality, shown in black. These sections correspond to the Terpolymer modified binder section (11 years old), control (unmodified) binder section (8 years old), and the SBS modified binder section. The outlier behavior of these ALF sections could be due to the unrealistically harsh temperatures used in the ALF experiments or may suggest that polymer modification can affect the relationship between laboratory and field aging. Since three of the six ALF sections were outliers and the ALF experiment included unrealistic thermal history, the recalibration of the CAI parameters was conducted a second time with the removal of the ALF sections.

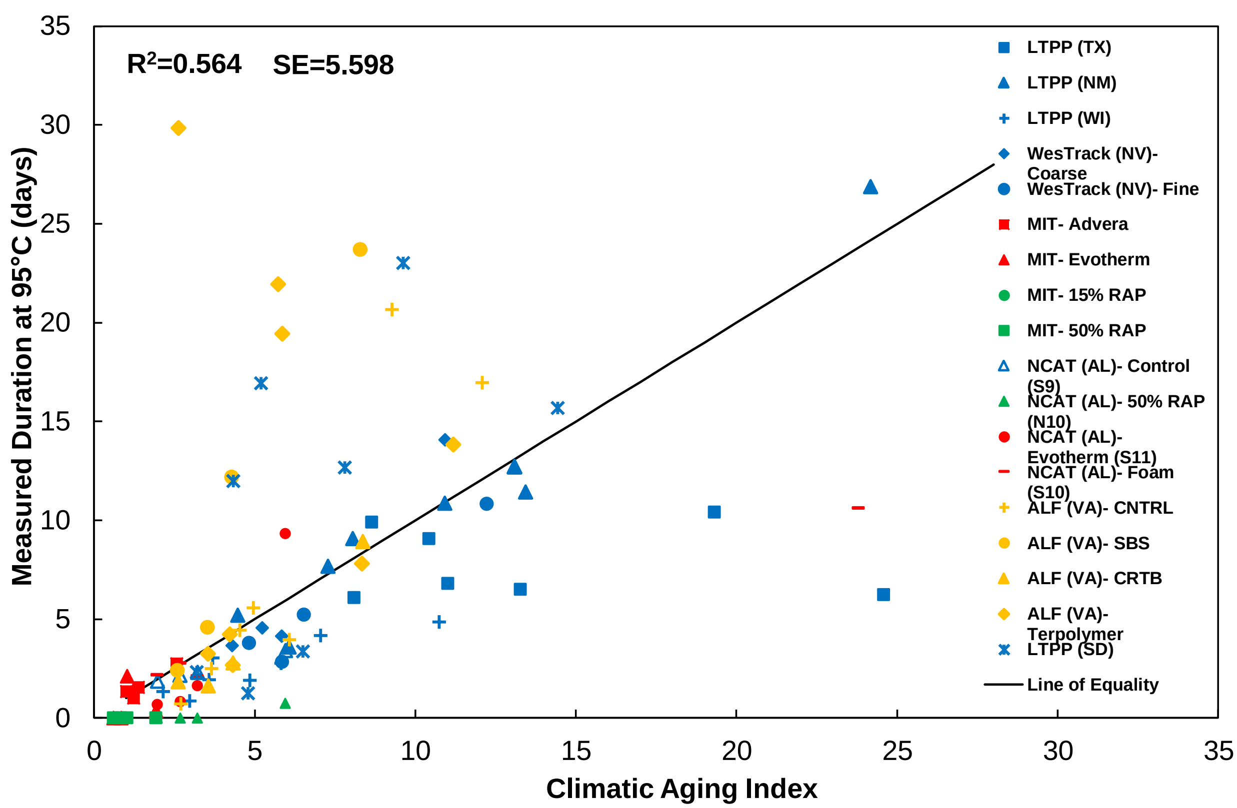

Figure 18. Comparison of Measured Laboratory Aging Durations at 95°C and the Initial Recalibration of CAI with Delineation by Project

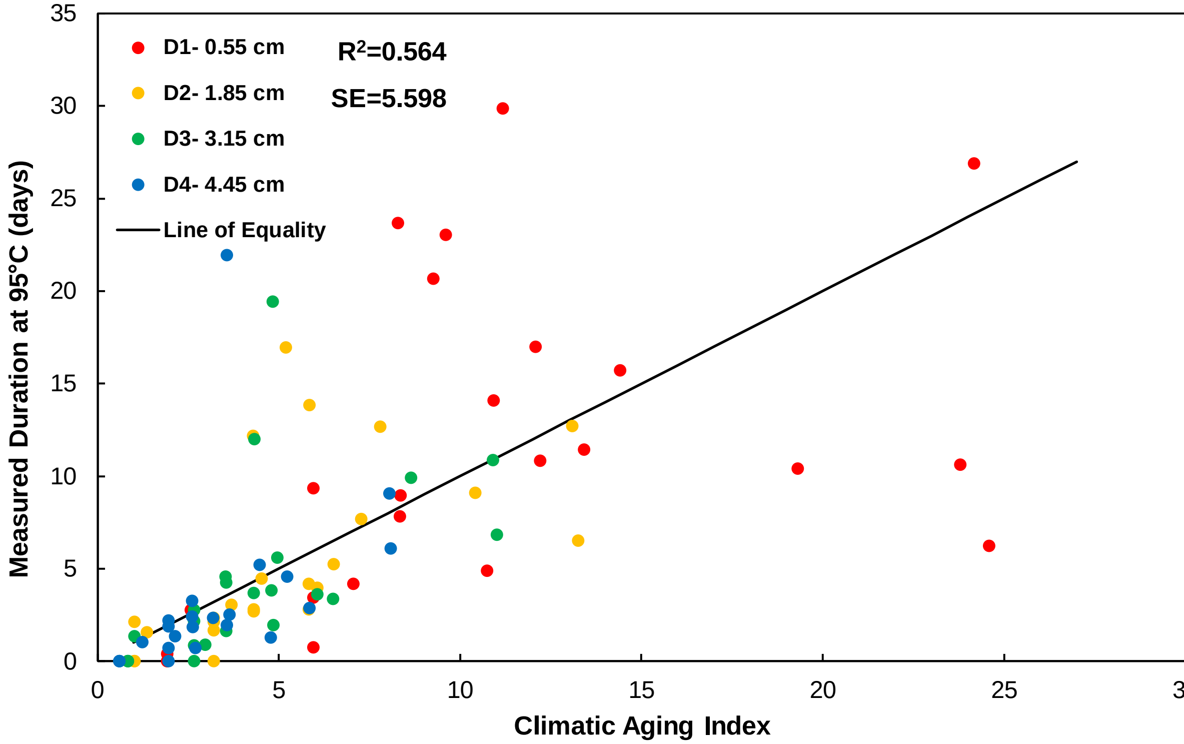

Figure 19. **Comparison of Measured Laboratory Aging Durations at 95°C and the Initial Recalibration of CAI with Delineation by Depth**

Recalibration Without ALF

The results of the recalibration of CAI with the exclusion of the ALF sections are shown in Figure 20 and Figure 21. The conventional mixtures are shown in blue, the WMA mixtures are shown in red, the mixtures containing RAP are shown in green, and the PMA mixtures are shown in gray. The PMA sections are shown in gray because they were not used in the recalibration. A ninety percent confidence interval, shown in gray above and below the line of equality is included in Figure 20 to show the uncertainty in the CAI recalibration results. The results demonstrate that the recalibration with the exclusion of ALF better represents the majority of the sections. The R^2 value was higher than the optimization including the ALF sections (0.783 versus 0.564) and the standard error was lower (3.05 versus 5.598). It should be noted that half of the PMA sections fall within this confidence interval, while the other half fall outside of the bounds. The good agreement between the line of equality and results of ALF sections that are not outliers suggests that the relationship between lab and field aging may not be impacted by polymer modification. However, the relationship between field and laboratory aging of polymer modified materials under realistic climate conditions merits further investigation in future work. The WMA sections fall closely to those of the HMA sections suggesting that the recalibrated CAI is applicable to WMA mixtures.

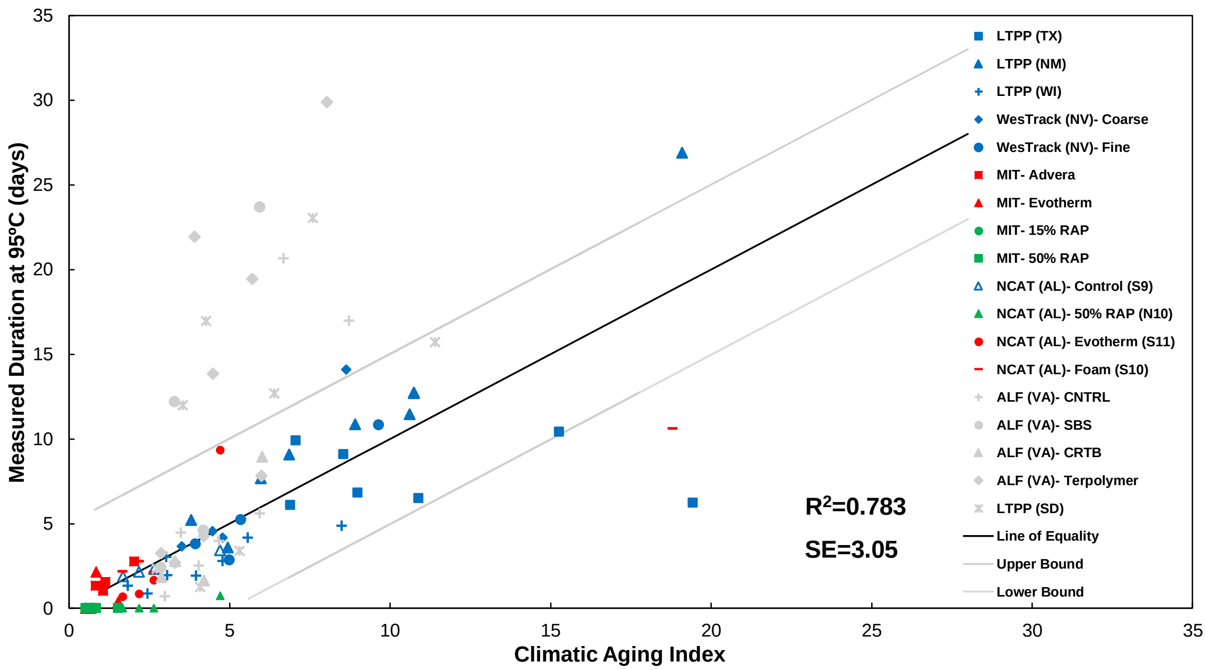

Figure 20. Comparison of Measured Laboratory Aging Durations at 95°C and the Final Recalibration of CAI with Delineation by Project

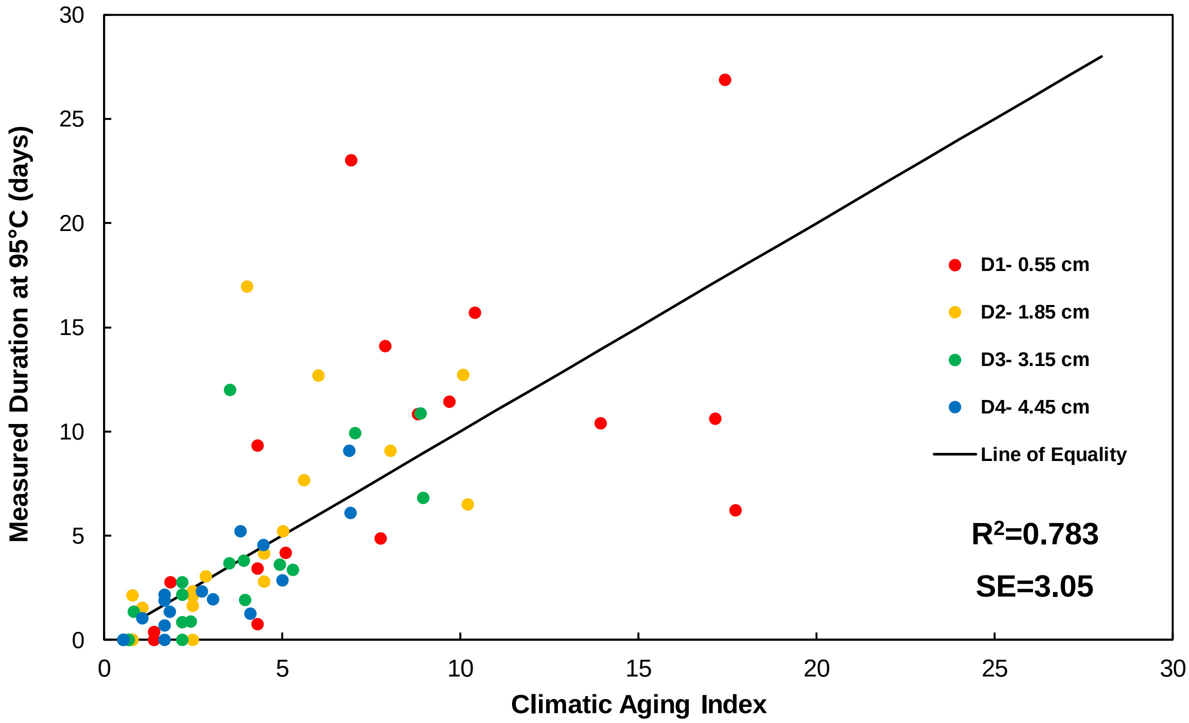

Figure 21. Comparison of Measured Laboratory Aging Durations at 95°C and the Final Recalibration of CAI with Delineation by Depth

Figure 22 shows the depth factor function for the recalibrated parameters. An power law was used to represent the relationship between the depth factor and the depth within the pavement. Table 3 presents a summary of the depth factors and the corresponding depth within the pavement.

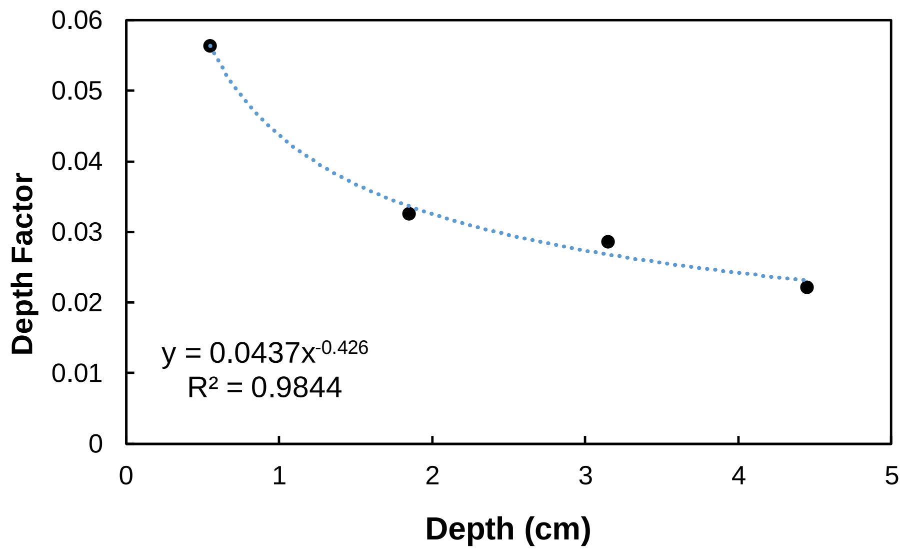

Figure 22. Depth Factor versus Depth

Table 3. Depth Factors From Recalibrated Parameters

Depth (cm)	D (Depth Factor)
0.55	0.056
1.85	0.033
3.15	0.029
4.45	0.022

The values of the C_1, C_2, and C_3 included in the simplified form of CAI given in Equation 17 along with the relationship between C_1 and C_2 to the original CAI expression given in Equation 11 are shown below. The final form of the recalibrated CAI equation with input of the coefficient values shown in Equation 18 through Equation 20 is given in Equation 21.

$$C_1 = \frac{D \cdot A}{24} = 0.0437 \tag{18}$$

$$C_2 = -0.426 \tag{19}$$

$$C_3 = \frac{E_a}{R} = 1{,}601.167 \tag{20}$$

$$t_{oven} = CAI = \sum_{i=1}^{N} 0.0437 d^{-0.426} e^{\frac{1{,}601.167}{T_i}} \tag{21}$$

Figure 23 below shows the CAI calculated for 0 to 20 years for two depths of a section from Texas. The 90 percent confidence intervals for both depths were calculated and are shown to convey the uncertainty in the CAI. It can be seen that the uncertainty in the estimated laboratory aging duration to match field aging can be relatively high (roughly five days).

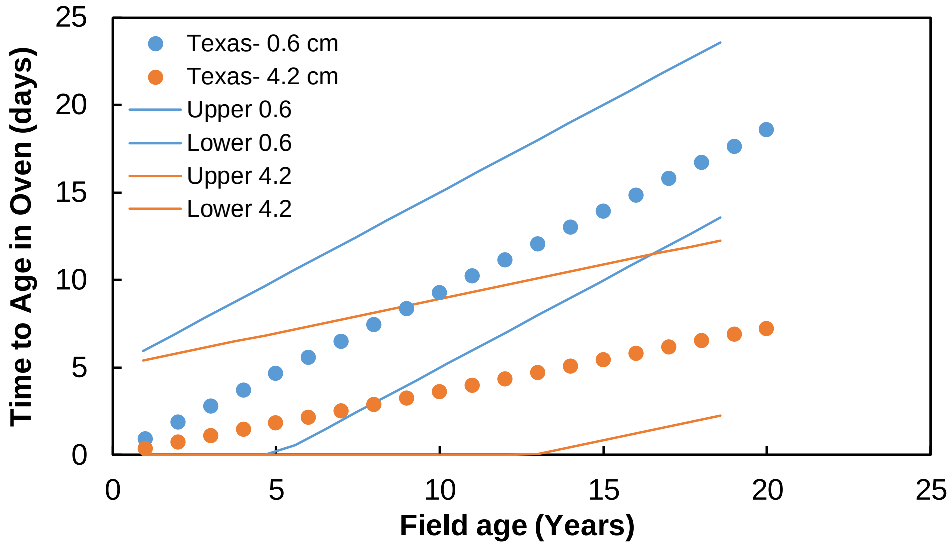

Figure 23. CAI Confidence Intervals

Recalibrated Laboratory Aging During Maps

The following maps within the United States were generated in ArcGIS given the latitude and longitude of the MERRA2 station of the section of interest and the recalibrated CAI value for that section. The maps are grouped by number of years aged, and then by depth within the pavement. These are shown in Figure 24 through Figure 32.

Figure 24. Required Oven Aging Duration at 95°C to Match 4 Years of Field Aging at 6 mm Below Pavement Surface (Days)

Figure 25. Required Oven Aging Duration at 95°C to Match 8 Years of Field Aging at 6 mm Below Pavement Surface (Days)

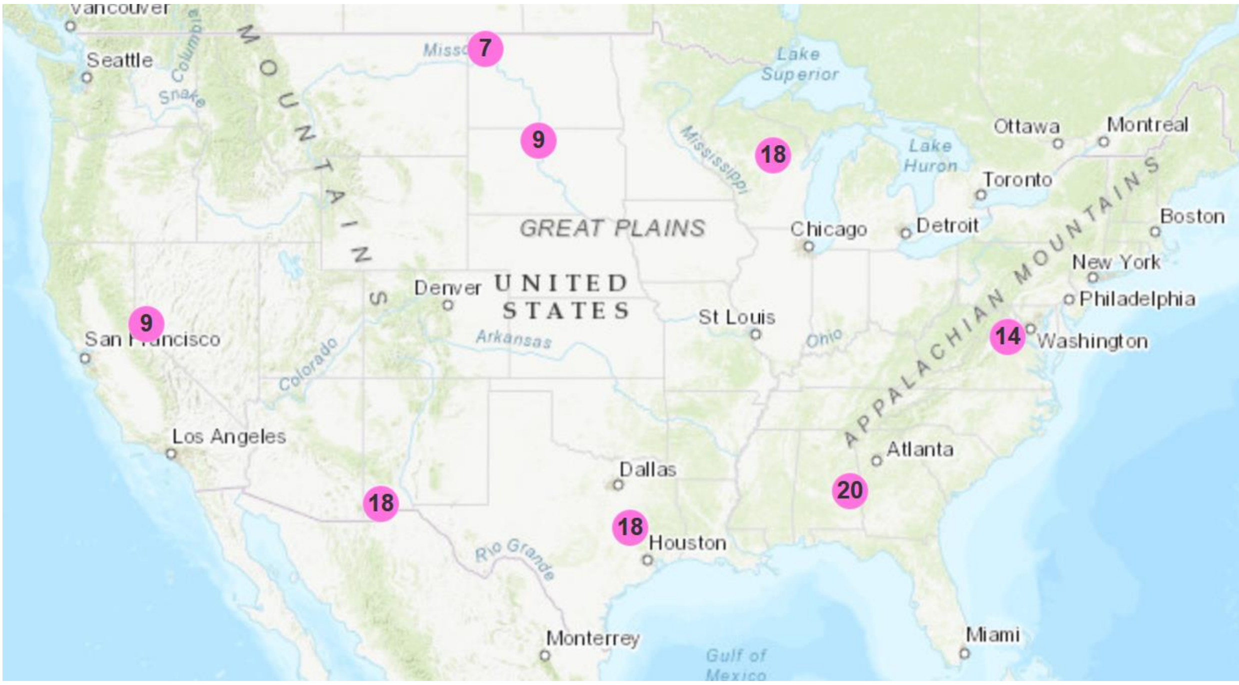

Figure 26. Required Oven Aging Duration at 95°C to Match 16 Years of Field Aging at 6 mm Below Pavement Surface (Days)

Figure 27. Required Oven Aging Duration at 95°C to Match 4 Years of Field Aging at 20 mm Below Pavement Surface (Days)

Figure 28. Required Oven Aging Duration at 95°C to Match 8 Years of Field Aging at 20 mm Below Pavement Surface (Days)

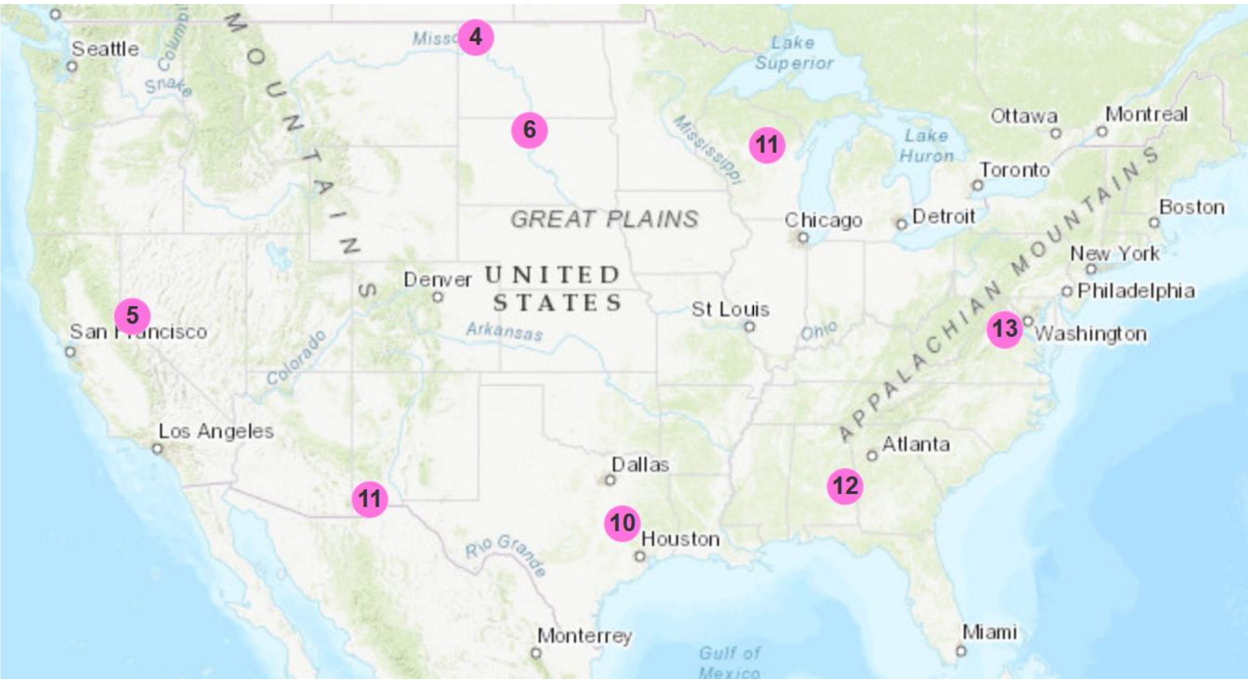

Figure 29. Required Oven Aging Duration at 95°C to Match 16 Years of Field Aging at 20 mm Below Pavement Surface (Days)

Figure 30. Required Oven Aging Duration at 95°C to Match 4 Years of Field Aging at 50 mm Below Pavement Surface (Days)

Figure 31. Required Oven Aging Duration at 95°C to Match 8 Years of Field Aging at 50 mm Below Pavement Surface (Days)

Figure 32. Required Oven Aging Duration at 95°C to Match 16 Years of Field Aging at 50 mm Below Pavement Surface (Days)

Summary

In summary, the CAI proposed by Kim et al. (2018) was simplified and recalibrated using field core replicates that included a wide variety of conventional and unconventional mixtures to yield the required laboratory aging duration as a function of hourly pavement temperature history and depth that yields reasonable accuracy to matching field age levels. The results demonstrated outlier behavior from many of the PMA sections, which could be caused by the unrealistically harsh thermal history of the ALF rutting experiments. However, roughly half of the PMA sections still fall within the 90 percent confidence interval of the recalibrated CAI, suggesting promise for its applicability to PMA materials. The recalibrated CAI results represent WMA materials well, suggesting no bias in the required CAI for WMA materials compared to HMA. The RAP mixtures show evidence of some bias from the virgin mixtures. However, relatively few RAP mixtures were analyzed and the corresponding field cores were just four years old. In some instances, the laboratory short-term aged material prepared according to AASHTO R 30 exceeded the age level of the field cores suggesting refinement of the short-term aging procedure may be necessary prior to investigating the effect of RAP on the relationship between laboratory long-term aging durations and field aging.

Effect of Asphalt Mixture Morphology on Pavement Aging

Brazil Analysis

The Brazil field cores were ideal for analyzing the systematic effect of morphology on pavement aging because they encompass systematic changes in the asphalt content, air voids, and binder source. These cores are 150-mm diameter and 70-mm height gyratory-compacted samples that were inserted in panels and subjected to eight years of field aging (with no traffic loading) in Brazil, as shown in Figure 33. The inner 100 mm of the Brazil cores were extracted and cut into 11-mm slices to study the variation in oxidation levels with depth by extracting and recovering the binder and then testing it to obtain log G^* at 64°C and 10 rad/s. The bulk specific gravity of the Brazil cores was measured before and after coring (150-mm vs. 100-mm diameter cores).

Figure 33. Setting up Gyratory-Compacted Samples in Panels to Subject to Field Aging in Brazil

Table 4 presents the volumetrics of the mixtures obtained from different binder sources. The gradation is the same. The nominal maximum aggregate size is 19.0 mm.

Table 4. Volumetrics for Brazilian Mixtures of Different Binder Sources with the Same Aggregate Gradation

Mixture with Binder Source	G_{mm}	G_{mb}	VFA	VMA
LUBNOR	2.544	2.472	10.3	13.2
REPAR	2.512	2.451	11.2	13.6
GALP	2.532	2.454	11.0	14.0
REPLAN	2.533	2.454	11.1	14.1

The binder content within these field cores ranges from 3.8 percent to 6.0 percent. The four binder sources are GALP (PG 64-12), REPAR (PG 64-12), REPLAN (PG 64-22), and LUBNOR (PG 70-22). Previous studies conducted by Petrobras in Brazil have shown that LUBNOR and REPAR are more susceptible to aging than the other two binders. During those studies, cores were extracted and tested at different age levels for various chemical and rheological properties.

For the purpose of developing a diffusion model, testing included the extraction and recovery of binder from field cores, DSR analysis of the binder, and FTIR testing to determine the absence or presence of solvent in the extracted binders. Results from the Brazil cores have been organized and analyzed. As the depth from the surface increases, the log G* value is expected to decrease, which is the general trend for each binder type. Another factor that was analyzed was the various asphalt contents of the sections within each asphalt binder source. It is expected that the sections with the lowest asphalt contents would have the highest log G* values due to their smaller film thicknesses that create a shorter diffusion path for oxygen to cause oxidation. Conversely, the sections with the highest asphalt contents are expected to have the lowest log G* values. However, this trend is not clearly seen in the data.

GALP

The data from the GALP binder source suggests no sensitivity of log G* to the change in asphalt content from 4.1% to 5.1% with the same air void content of 8% (Figure 34 (c)). Little difference is evident between these two asphalt contents at 4% AV as well, as shown in Figure 34 (a) and (b). According to Figure 35, aging increases as asphalt content increases from 4.1% to 4.6% and then decreases when the asphalt content increases to 5.0% and 5.1%, with a peak at 5.0% for deeper depths (32 mm and below). However, the aging level starts to increase with depth, so this data set must be viewed with caution. Figure 36 shows that an increase in air void content leads to increased aging for a given asphalt content. This finding is most significant at lower asphalt contents and deeper depths within the pavement.

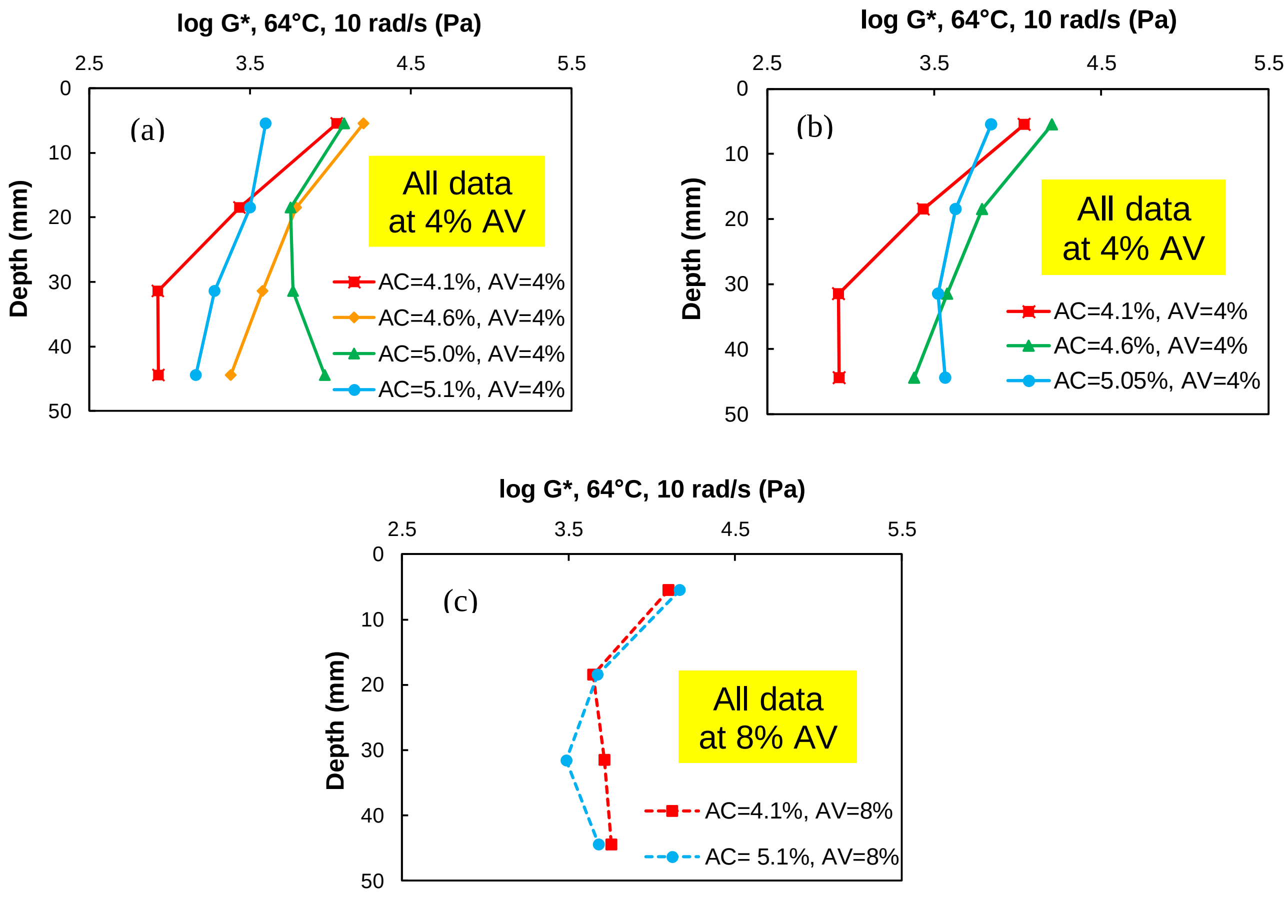

Figure 34. Field measured log G* value trends for binder source GALP (PG 64-12): (a) varying %AC and 4% AV, (b), varying %AC and 4% AV (average) and (c) varying %AC and 8% AV

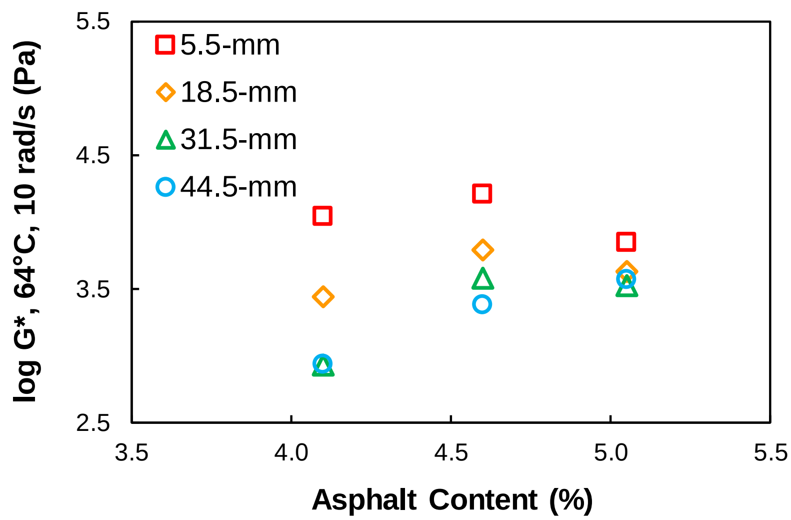

Figure 35. Field measured log G* values for binder source GALP (PG 64-12) versus %AC for different depths

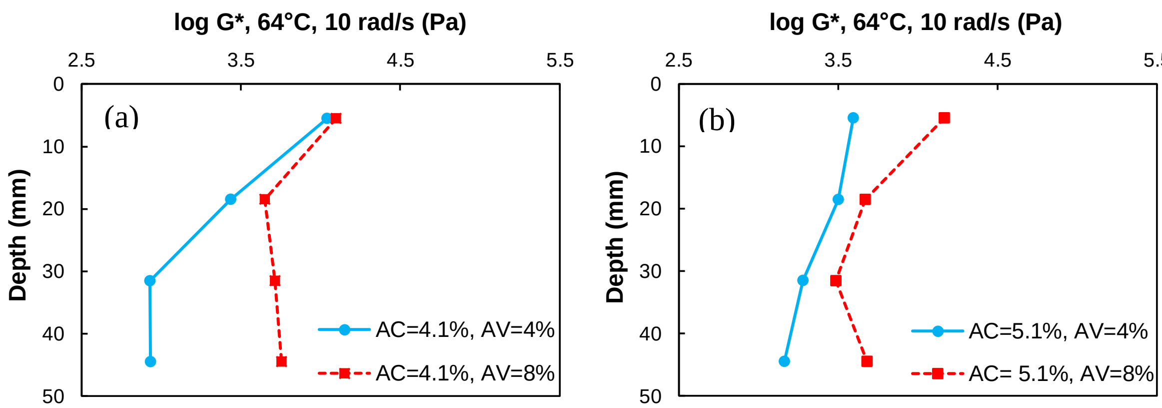

Figure 36. Field measured log G* for binder source GALP (PG 64-12): (a) 4.1% AC content and varying AV content, and (b) 5.1% AC content and varying AV content.

LUBNOR

As shown in Figure 37, LUBNOR seems to have no significant sensitivity to asphalt content when %AV is constant at 8% with only two asphalt contents (3.8% vs. 4.8%). Figure 37 (a) shows a larger difference among the three asphalt contents (3.8%, 4.3%, and 4.8%) at 4% AV. According to Figure 37 and Figure 38, the aging pattern appears to differ at each depth. For 6-mm depth, the aging level decreases as the asphalt content increases from 3.8% to 4.3% and then increases as the asphalt content further increases to 4.8 percent. On the other hand, the aging level at 44.5-mm depth starts high (higher than the aging level at shallower depths) and decreases to a minimum with an increase in the binder content. The trends shown for 4.8% asphalt content are the opposite of the trends shown for 3.8% asphalt content in Figure 39. No clear trends are shown for LUBNOR.

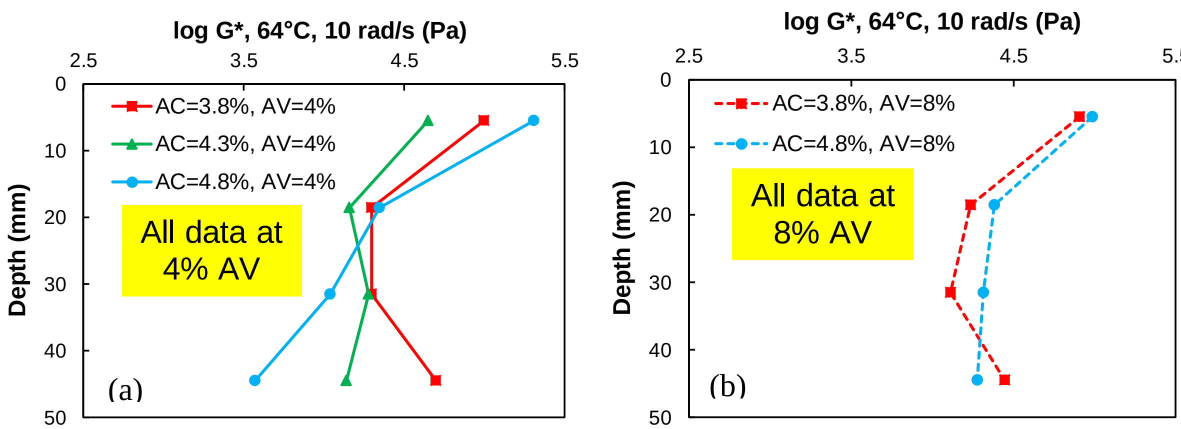

Figure 37. Field measured log G* value trends for binder source LUBNOR (PG 70-22): (a) varying %AC and 4% AV and (b) varying %AC and 8% AV.

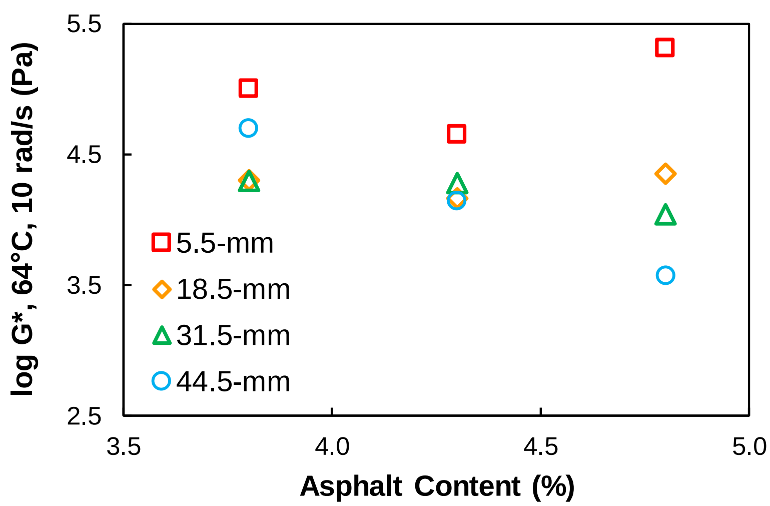

Figure 38. Field measured log G* values for binder source LUBNOR (PG 70-22) versus %AC for different depths.

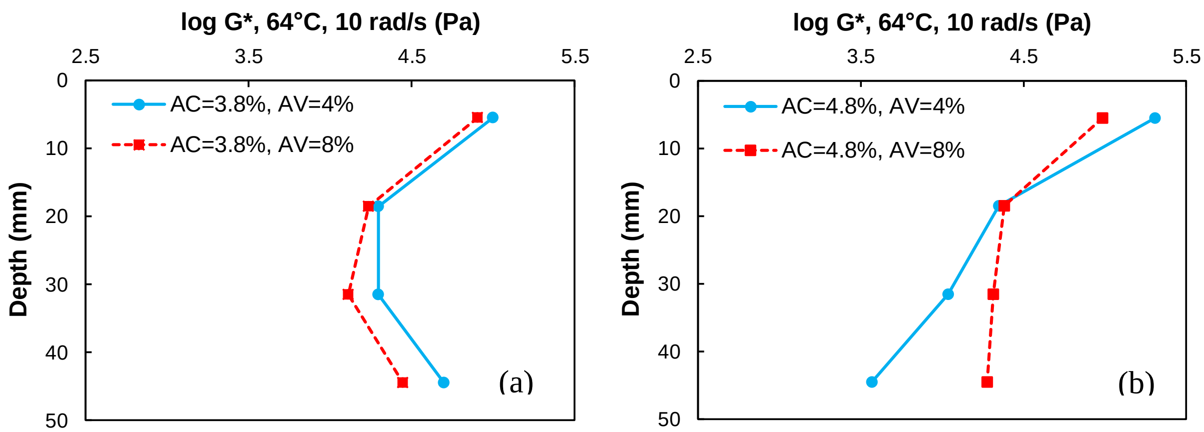

Figure 39. Field measured log G* for binder source LUBNOR (PG 70-22): (a) 3.8% AC content and varying AV content, (b) 4.8% AC content and varying AV content.

REPAR

REPAR shows a moderate sensitivity to asphalt content when AV = 8% with three asphalt contents (4.6%, 5.1%, and 6.0%) and a larger difference in data measurements among these three asphalt contents at 4% AV, as shown in Figure 40. According to Figure 41, aging decreases as the asphalt content increases from 4.6% to 5.1% and then increases when the asphalt content increases from 5.1% to 6.0%, with a minimum log G* value at the 5.1% asphalt content. Figure 42 shows that increasing the air void content leads to increased aging for a given asphalt content. This finding is most significant at a higher asphalt content and at deeper depths within the pavement.

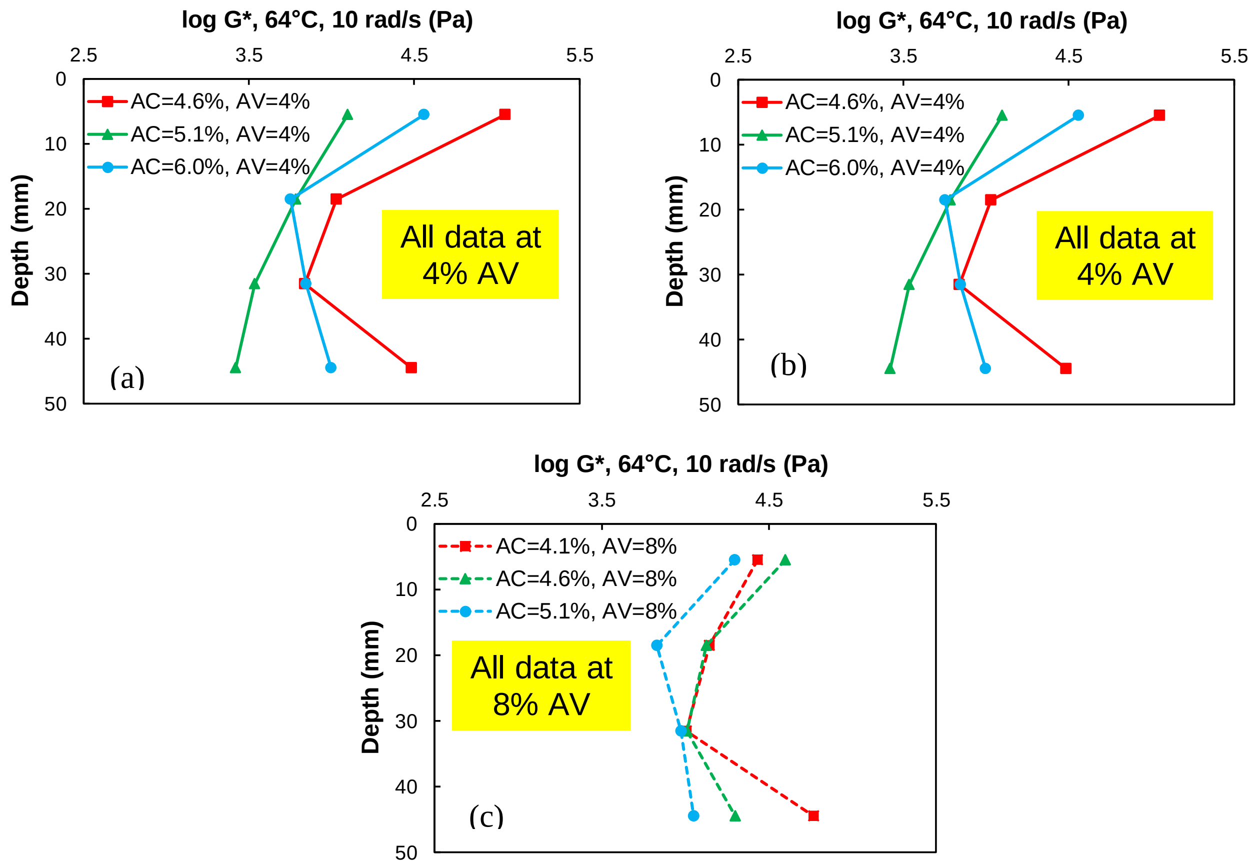

Figure 40. Field measured log G* value trends for binder source REPAR (PG 64-12): (a) varying %AC and 4% AV and (d) varying %AC and 8% AV

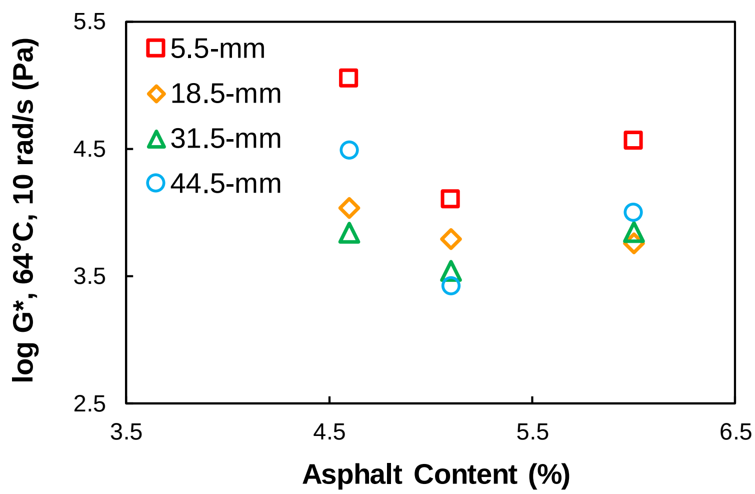

Figure 41. Field measured log G* values for binder source REPAR (PG 64-12) versus %AC for different depths.

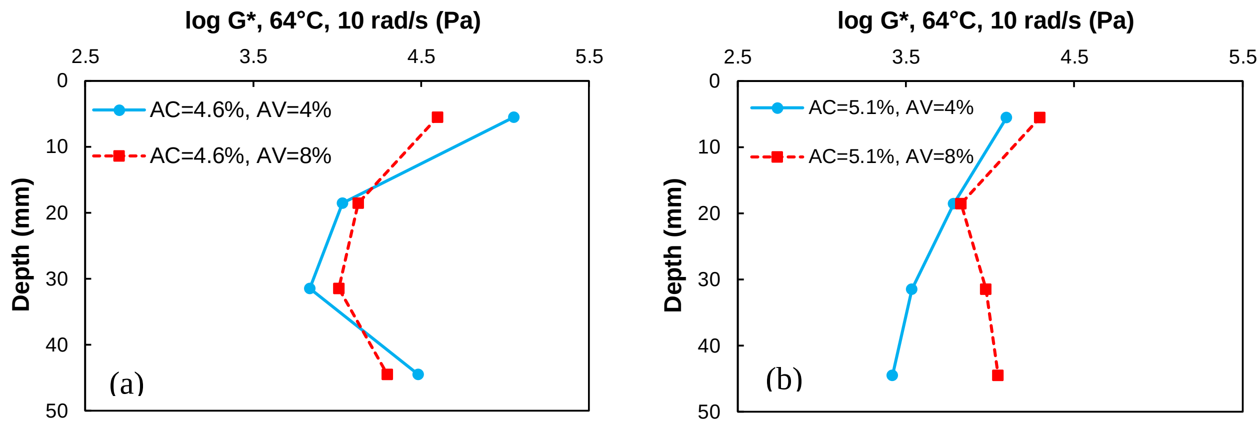

Figure 42. Field measured log G* for binder source REPAR (PG 64-12): (a) 4.6% AC content and varying AV content, (b) 5.1% AC content and varying AV content.

REPLAN

REPLAN shows little sensitivity to asphalt content when AV = 8% with three asphalt contents (4.1%, 4.6%, and 5.1%) and a larger difference among these three asphalt contents at 4% AV, shown in Figure 43. A larger difference in measurements is evident as the depth within the pavement increases. According to Figure 44, the aging trend for the top layer (5.5 mm) differs from all the other layers. For the top layer (5.5-mm), aging increases as asphalt content increases from 4.1% to 4.6%, then decreases as asphalt content increases from 4.6% to 5.1 percent. For all the other layers, aging decreases as asphalt content increases. Figure 45 shows that increasing the air void content leads to increased aging for higher asphalt contents, and increasing the air void content leads to decreased aging for lower asphalt contents. The most significant differences generally occur at deeper depths within the pavement.

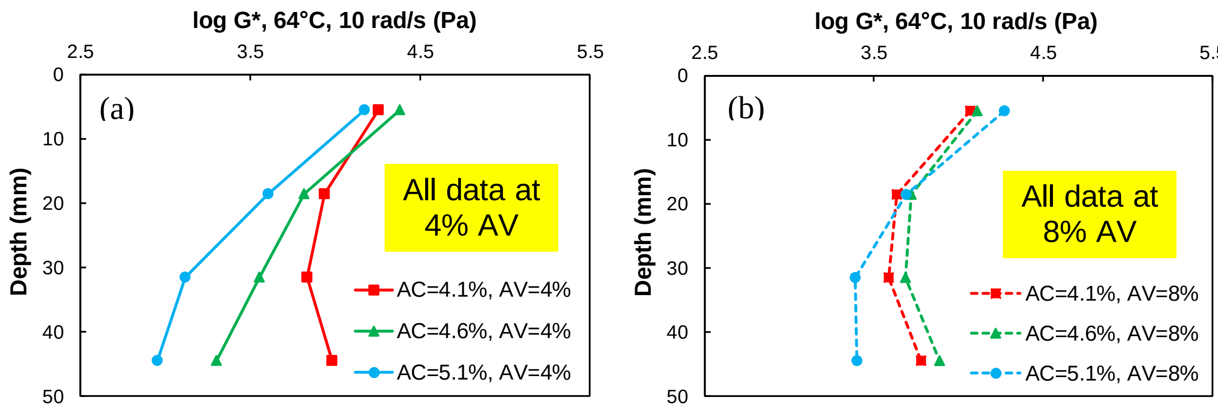

Figure 43. Field measured log G* value trends for binder source REPLAN (PG 64-22): (a) varying AC and 4% AV and (b) varying AC and 8% AV.

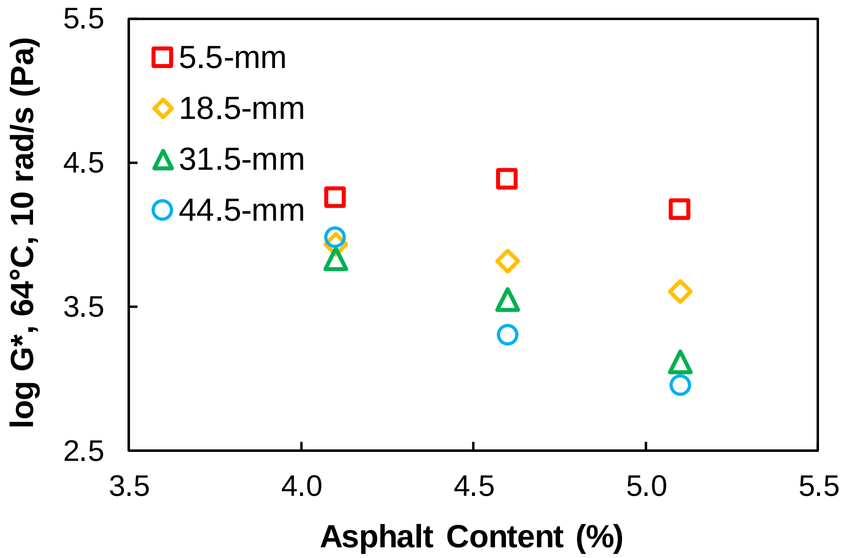

Figure 44. Field measured log G* values for binder source REPLAN (PG 64-22) versus AC for different depths.

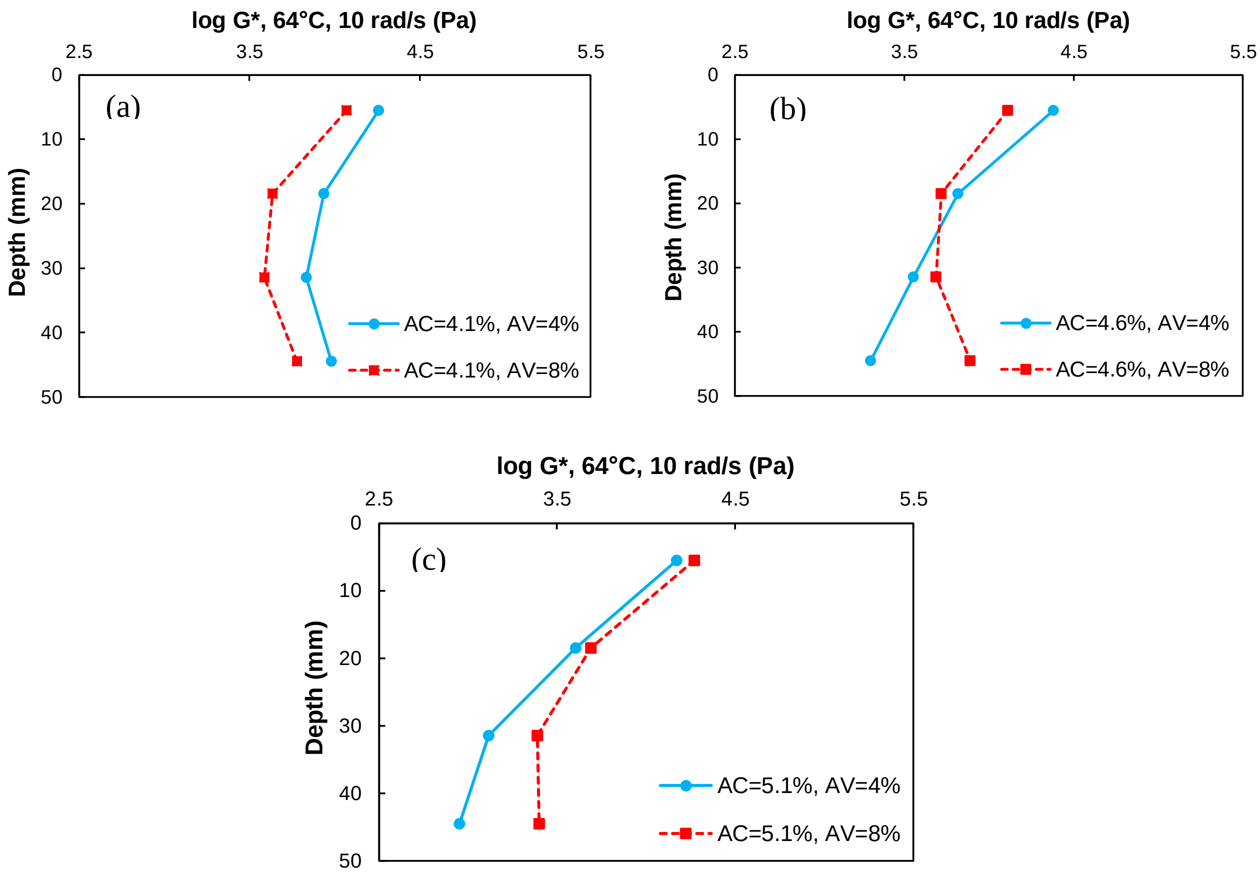

Figure 45. Field measured log G* for binder source REPLAN (PG 64-22): (a) 4.1% AC content and varying AV content, (b) 4.6% AC content and varying AV content, and (c) 5.1% AC content and varying AV.

General Conclusions

It is expected that an increase in asphalt content and/or a decrease in air void content would lead to less aging. The increase in asphalt content increases the asphalt film thickness that surrounds the aggregate particles, consequently increasing the diffusion path for oxygen. A decrease in air void content is expected to increase the distance between air void channels within the asphalt concrete, consequently increasing the diffusion path for oxygen. Generally, the data follow the expected trends in aging level as a function of asphalt content when the asphalt content is increased from the optimum asphalt content to the optimum asphalt content plus 0.5 percent and the air void content is 4 percent. For three out of the four binders evaluated (GALP, REPLAN, REPAR), this general trend holds for the effect of asphalt content when the air void content is 4 percent. At other asphalt contents, however, trends vary among the different binders evaluated and often do not match intuition.

Overall, the aging levels show little sensitivity to asphalt content when the air void content is 8 percent. In most cases, the results show an increase in aging when the air void content increases from 4 percent to 8 percent and the asphalt content is at or above optimum, with the exception of the 6-mm depth in many cases. In many cases, the change in aging level with air void content is marginal. The sensitivity of aging level to air void content appears to increase with asphalt content.

Trends that do not match intuition could possibly be explained by the work of Das, Birgisson, Jelagin, and Kringos. Das et al. (2015) postulated that both the air void content and size of the air voids affect aging susceptibility. Mixtures with the same air void content but smaller air voids will have more surface area for air to come in contact with and therefore will have increased aging susceptibility. A mixture with the same aggregate gradation, binder, and air void content but higher binder content than another mixture would require less compaction. Due to less compaction, the average air void size would be expected to increase with an increase in asphalt content. A mixture with the same binder and air void content but higher binder content and different gradation would require more compaction and have smaller average air voids. In this case, aging would decrease as the asphalt content increases. (However, this outcome does not apply to the Brazil mixtures). In short, some trends that do not match intuition may be due to changes in air void size. It is impossible to measure air void size, so it is not feasible to determine if air void size is the reason for the discrepancy.

WesTrack Analysis

Figure 46 shows the relationship between the average log G* values at different depths (5.5 mm, 18.5 mm, 31.5 mm, and 44.5 mm) for different WesTrack cores. WesTrack cores have three levels of asphalt content: low, optimum, and high, as well as three air void content levels: low, medium, and high. The naming system WTFLM for example, means a WesTrack field core (WTF) with low asphalt content (L) and medium air void content (M). The F-19Y stands for a field core (F) that is 19 years old. Overall trends show that there is a larger difference in measurements when looking at asphalt content as opposed to air void content (Figure 47). Figure 47 and Figure 48 look at asphalt content and air void content respectively.

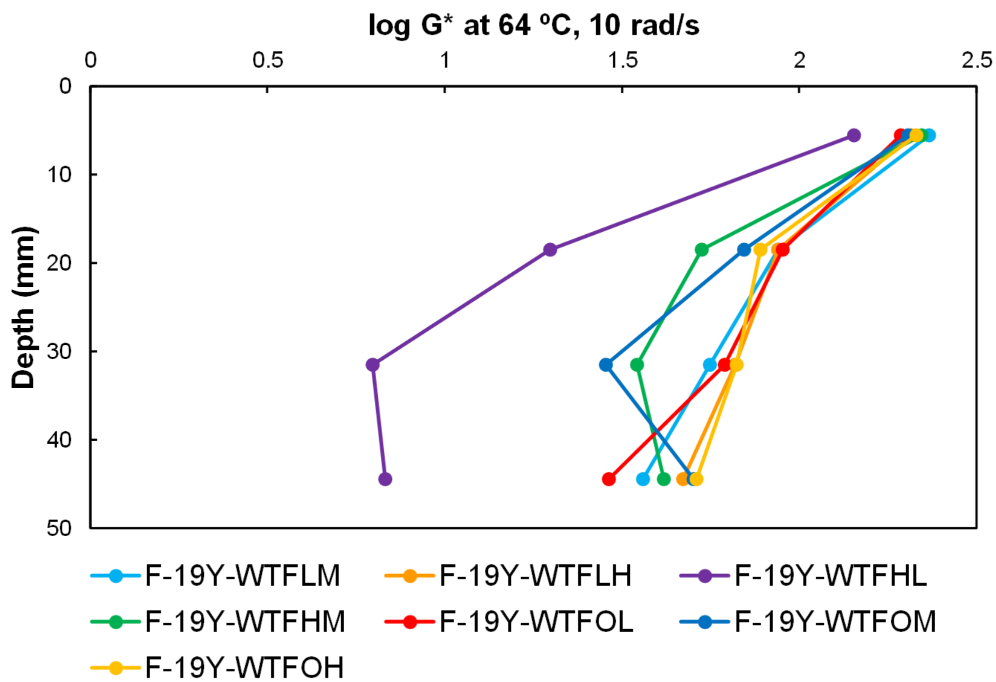

Figure 46. WesTrack Analysis

Figure 47 below shows the results of DSR testing grouped by asphalt content. Low asphalt content is shown in blue, while optimum asphalt content is shown in green and high asphalt content is shown in red. There is not a large difference in the measurements in optimum and low AC. There seems to be a significant difference between high AC and low/optimum AC. As asphalt content increases, the log G* values seem to decrease. This result makes sense because with a larger film thickness, there should be less aging of the material. There is a difference in the log G* values as the AV content increases for the high AC, but it is not significant in the lower/optimum AC. Increasing the air voids has a larger impact on aging at higher asphalt contents.

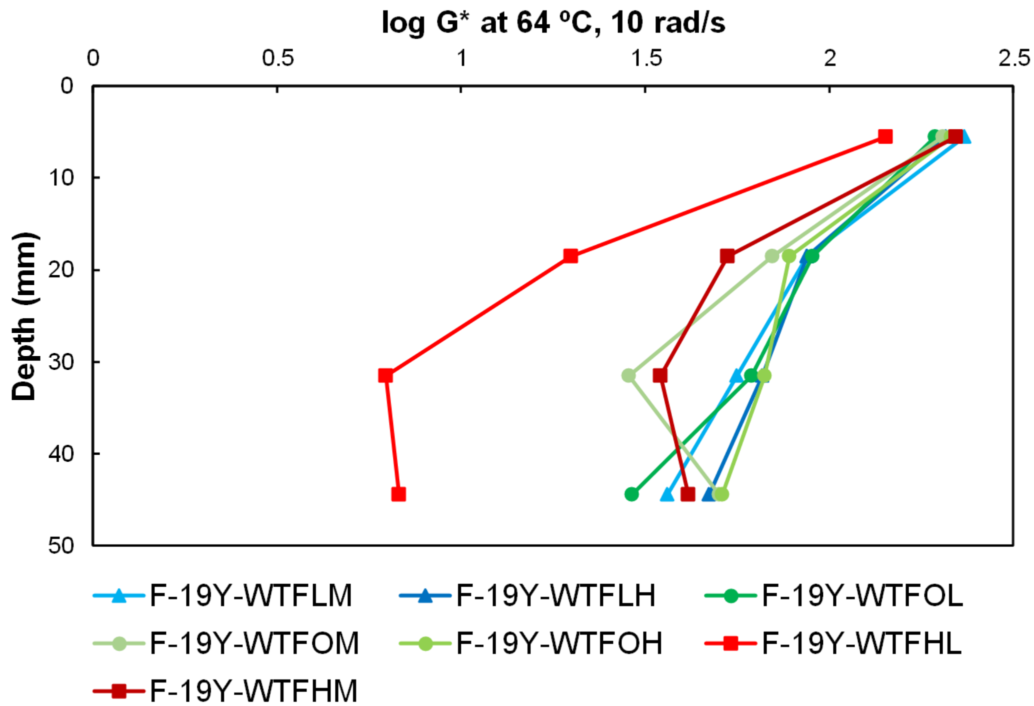

Figure 47. WesTrack Analysis (Asphalt Content)

Figure 48 shows the results of DSR testing grouped by air void content. Low air void content is shown in blue, while medium air void content is shown in green and high air void content is shown in red. As air void (AV) content increases, the log G* values seem to increase as well. This result makes sense, because as more air voids are introduced into the material, more aging occurs. There is a significant difference between the log G* values as asphalt content increases for lower air void contents, but there is not a significant change with medium and high AV content.

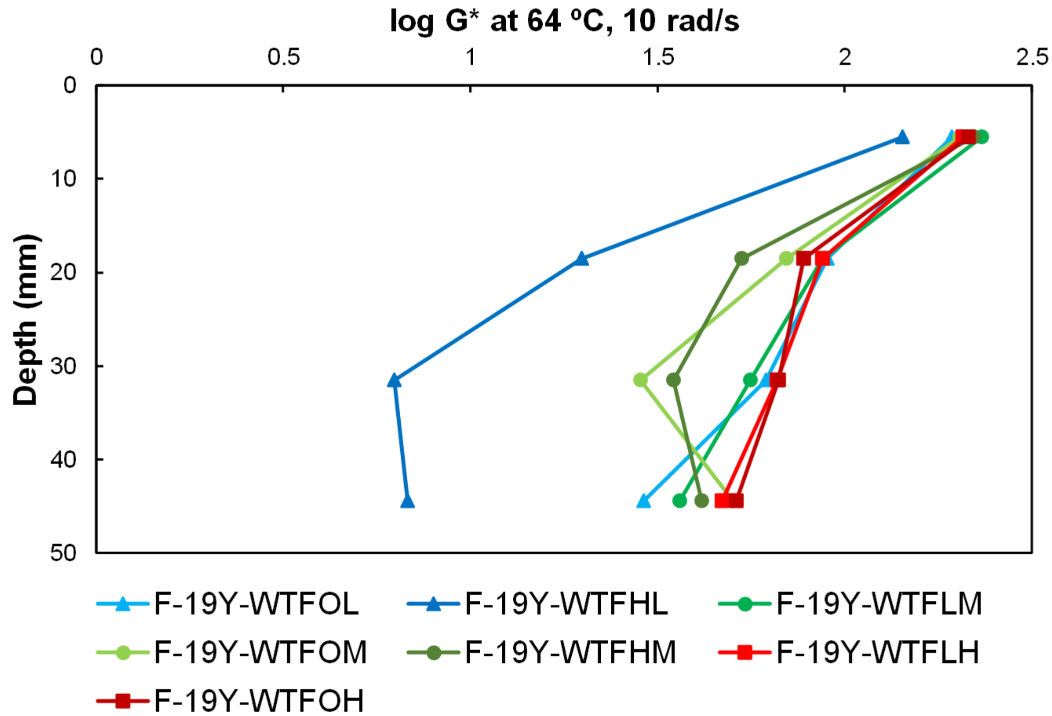

Figure 48. WesTrack Analysis (Air Void Content)

Statistical Analysis

After looking at the initial graphical data, a statistical analysis was performed on the materials from Brazil and WesTrack. For the Brazil materials, analysis was done on type of binder, asphalt content, and air void content. For the WesTrack materials, analysis was done on asphalt content and air void content. These analyses were performed by layer (T1-T4) because each layer corresponds to a different depth (5.5 mm, 18.5 mm, 31.5 mm, and 44.5 mm). The statistical coding software "R" was used to aid in the analysis of the data sets. First, an ANOVA test was run on the set of data for depth T1 (5.5 mm), grouped by binder type. The p-value shown in

Table 5 is an indicator of whether the average log G* values at 64 °C and 10 rad/s are different for different binder types (or asphalt content/air void content). Then, the Tukey HSD (honestly significant difference) test was run to compare specific mean values of different variables against each other. The R program output tells specifically what variables are different from other variables (for example, high AV content vs. low AV content). In Table 5 and Table 6, the variables under the column labeled "Tukey" are the variables that are statistically different from one another. Based on a 0.05 significance level, if the p-value given by the R program from the input data is less than 0.05, one can claim that the values for average log G* are different from one another.

Table 5. Summary of the Statistical Analysis for WesTrack Materials

WT		**P-value**	**Tukey**
Asphalt Content Analysis	T1	0.3734	None
	T2	0.0325	low-high
	T3	0.0053	opt-high low-high
	T4	0.0889	None
Air Void Content Analysis	T1	0.4786	None
	T2	0.2132	None
	T3	0.143	None
	T4	0.0182	low-medium

Table 6. Summary of the Statistical Analysis for Brazil Materials

Brazil		P-value	Tukey
Binder Type Analysis	T1	1.76E-05	REPAR-GALP LUBNOR GALP LUBNOR-REPLAN LUBNOR-REPAR
	T2	1.30E-06	REPAR-GALP LUBNOR GALP LUBNOR-REPLAN LUBNOR-REPAR
	T3	1.27E-04	REPAR-GALP LUBNOR GALP LUBNOR-REPLAN
	T4	0.00952	REPAR-GALP LUBNOR GALP
Asphalt Content Analysis	T1	0.0027	3.8-5.1%, 4.8-5.1%, 4.1-4.8%
	T2	0.0042	3.8-5.1%, 4.8-5.1%, 4.1-4.8%
	T3	0.051	None
	T4	0.362	None
Air Void Content Analysis	T1	0.9007	None
	T2	0.7016	None
	T3	0.3629	None
	T4	0.1213	None

Summary

Brazil

Overall, the LUBNOR binder type seems to be significantly different from the other means more than any other binder type. GALP seems to be significantly different as well, just not as often as LUBNOR. As the depth increases (T1$\rightarrow$T4), there seems to be less binders that are significantly different from one another. These results make sense, because aging affects the surface layers more than the layers deeper into the pavement.

Asphalt content does not play a large role as the depth of the pavement increases (T3 and T4 vs. T1 and T2). There were a larger number of significantly different results in the upper layers of the pavement compared to the deeper layers. This conclusion is the same as that when comparing binder types. The asphalt contents of 3.8%, 4.1%, 5.1%, and 4.8% were significantly different for T1 and T2.

When looking at air void content for each depth level, none of the results were significantly different from one another (4% vs. 8%). As the depth increased, the results did start to deviate from each other a bit more, but the results still were not statistically different from each other. This has been seen in past analysis by simply looking at the graphical results of the DSR data.

WesTrack

There is a more pronounced relationship between asphalt content and depth than air void content and depth. There are a higher number of significantly different relationships between the means of the log G* values when looking at asphalt content than air void content. There were more statistically different results for layers T2 and T3 when looking at asphalt content, and layer T4 when looking at air void content. For both analyses, the significantly different results usually contained the low and/or high AC/AV. This has been seen in past analysis by simply looking at the graphical results of the DSR data.

Field Calibration of the Pavement Aging Model

Overview

Aging is one of the most prominent distresses mechanisms for asphalt pavements and is a complex process. An accurate prediction of asphalt mixture properties in terms of pavement service life and performance is very important. The kinetics model, as described in Equation 8, only accounts for temperature dependence of oxidation, and not for diffusion which becomes especially important below the asphalt pavement surface. In this thesis, there was insufficient data collected to develop a rigorous diffusion model that accounts for asphalt mixture morphology and corresponding depth dependence of oxidation. Therefore, a depth-dependent field calibration of the kinetics model was conducted using all field projects that included asphalt mixtures prepared at the optimum asphalt content. Functions were developed for deviations from the optimum asphalt content using the limited data available from the WesTrack materials. It should be noted that this was a limited data set, and future work should expand upon the results herein to elucidate the effects of morphology on pavement aging.

The hourly pavement temperature history used in the CAI analyses (i.e., output of EICM using MERRA2 climate files) combined with the material-specific kinetics model parameter M and the log G^* of the short-term aged material were used to predict field log G^* values using the kinetics model given in Equation 13. The analysis was conducted using climate data for the years 1980 to 2017 and the average results were used in the analysis. The kinetics model-predicted log G^* values were compared to those of binders extracted and recovered from field cores at different depths. The relationship between the kinetics model predictions and field core measurements were used to develop a depth-dependent field calibration function.

Data Smoothing Prior to Field Calibration

A power law function was fit to represent the relationship between the measured log *G** values versus depth for each section prior to field calibration to account for the inherent variability in the field core results as a function of depth. The power law fit suggests a higher rate of change in log G* with depth near the pavement surface and less change deeper within the pavement structure, which matches expectations. The data smoothing ensured reasonable trends with depth for each section prior to the field calibration. Looking at each individual data set, outliers were identified that clearly did not follow the expected data trend and removed from the data smoothing process to improve the quality and precision of the power function prediction of log *G**. Clear outliers were identified and removed in the MIT 15% RAP and MIT Evotherm sections only; these outliers are shown in grey in Figure 50. The results are shown in Figure 49 through **Error! Reference source not found.** below.

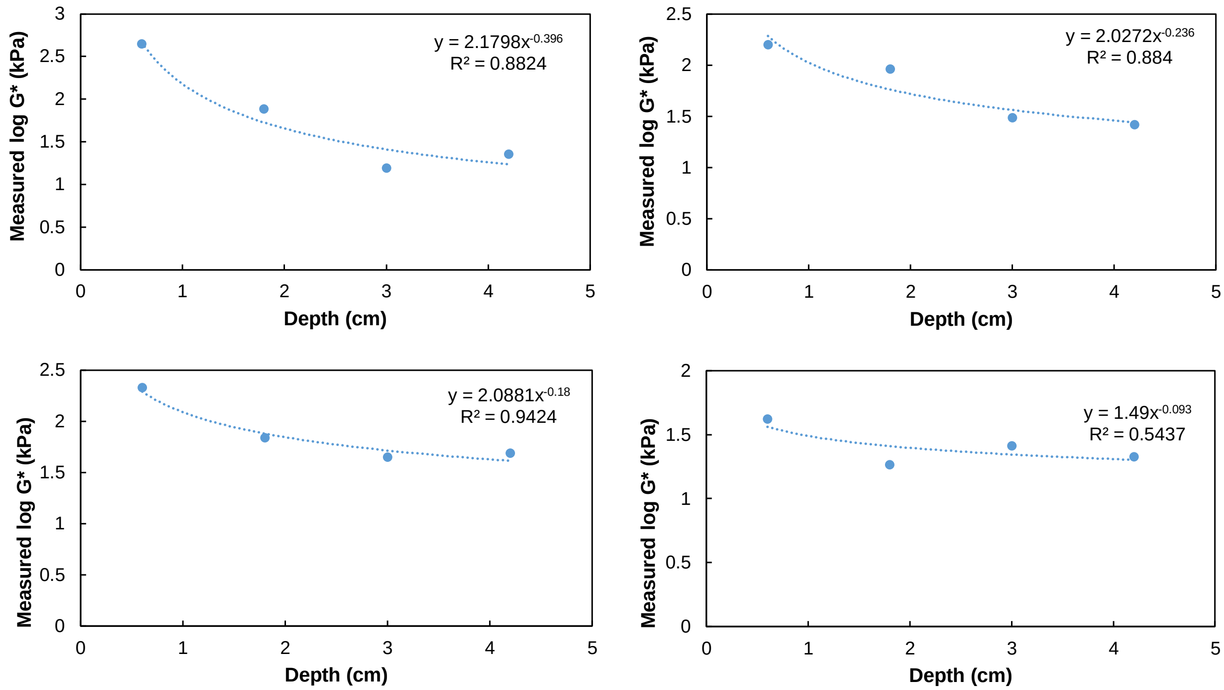

Figure 49. Power Law Fit of log *G versus Depth for (a) ALF CNTRL (b) ALF SBS (c) ALF CRTB and (d) ALF Terpolymer**

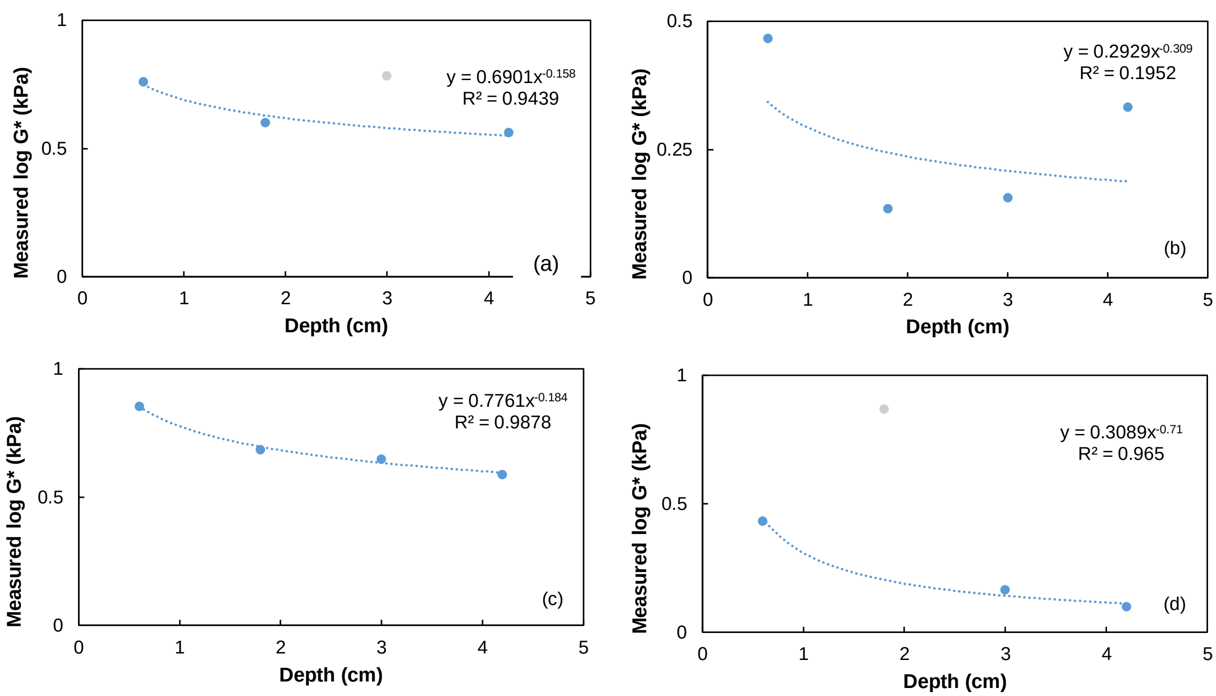

Figure 50. Power Law Fit of log *G versus Depth for (a) MIT 15% RAP (b) MIT 50% RAP (c) MIT Advera and (d) MIT Evotherm**

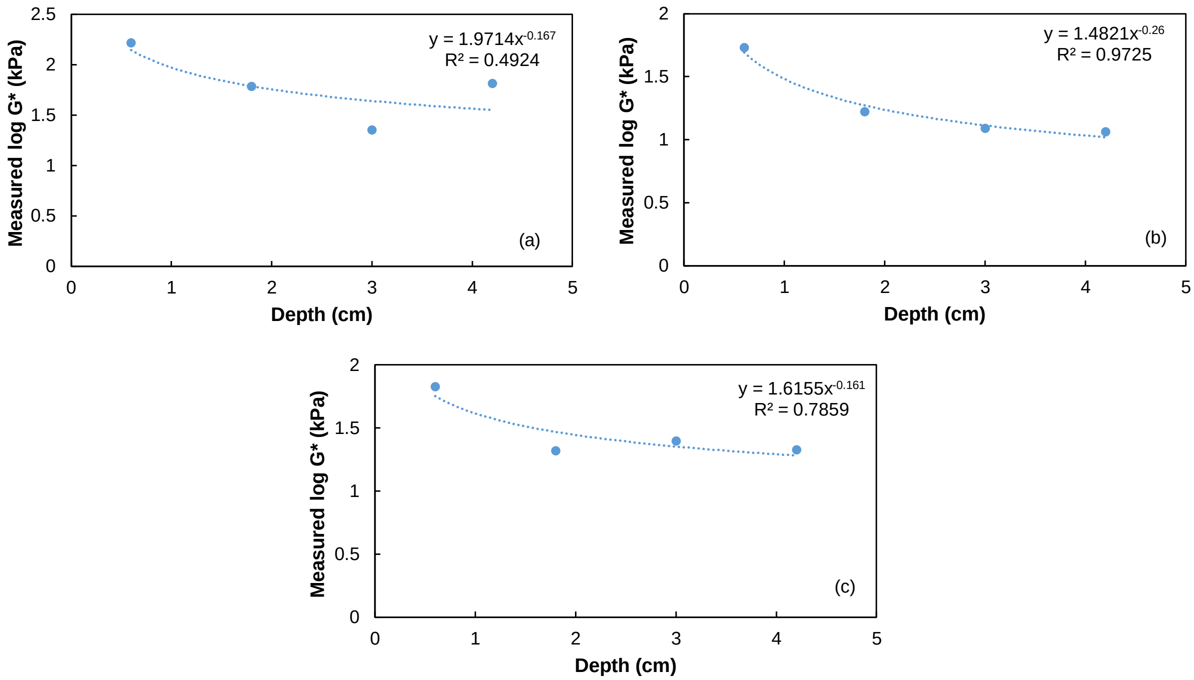

Figure 51. Power Law Fit of log *G versus Depth for (a) NCAT 50% RAP (b) NCAT Evotherm and (c) NCAT Foam**

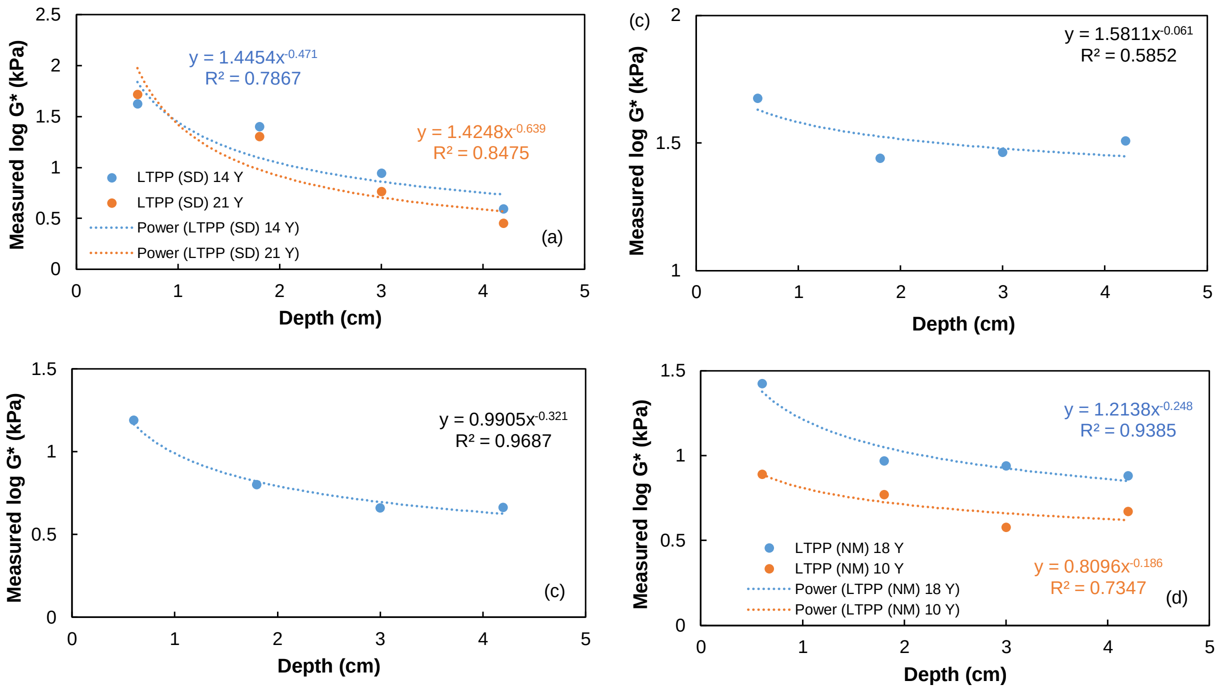

Figure 52. Power Law Fit of log *G versus Depth for (a) South Dakota (b) Texas (c) Wisconsin and (d) New Mexico**

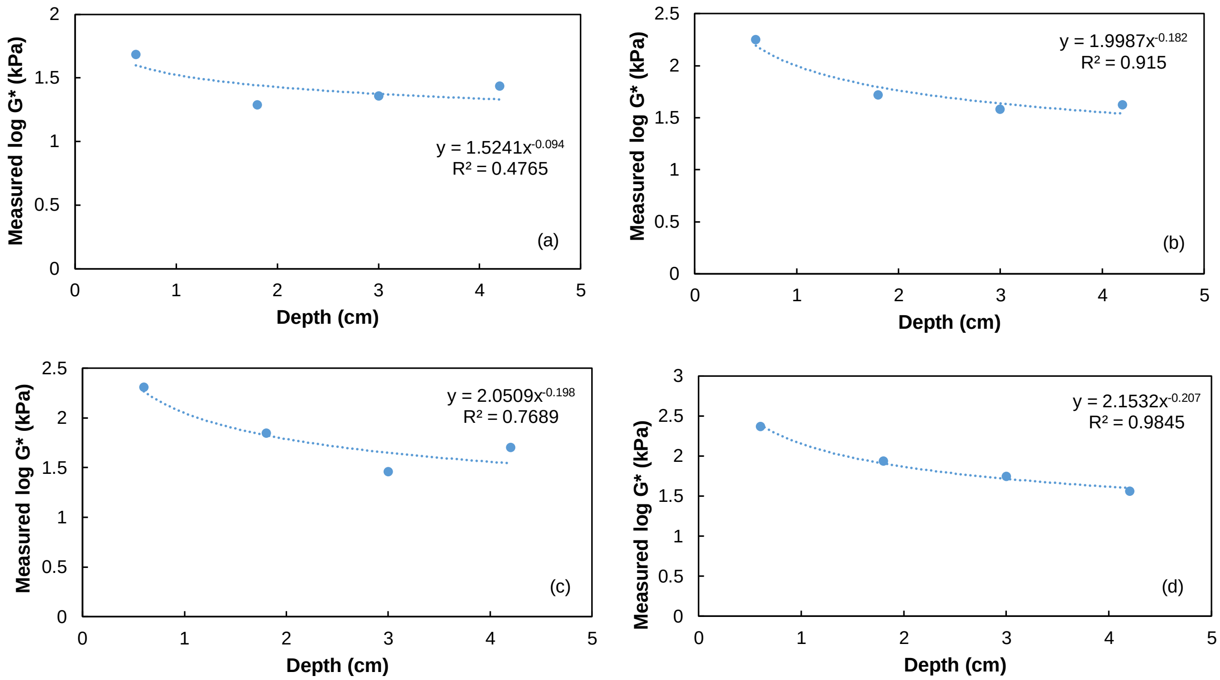

Figure 53. Power Law Fit of log *G versus Depth for (a) WesTrack Coarse (b) WesTrack Fine- High AC (c) WesTrack Fine- Optimum AC and (d) WesTrack Fine- Low AC**

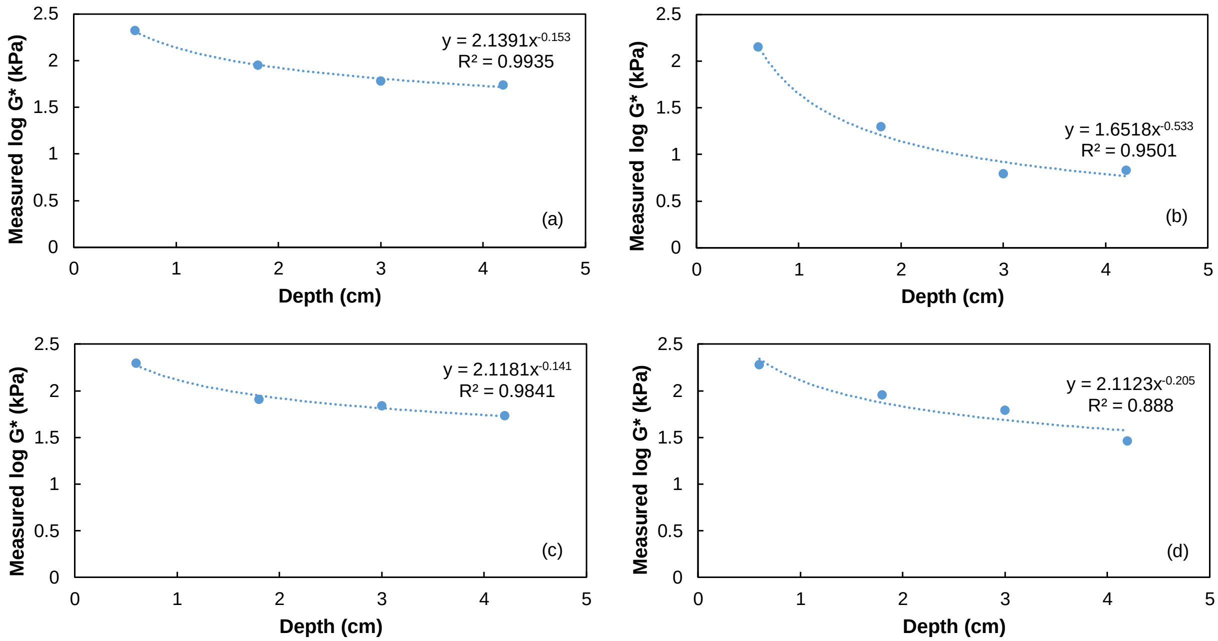

Figure 54. Power Law Fit of log *G versus Depth for (a) WesTrack Fine- Low AC, High AV (b) WesTrack Fine- High AC, Low AV (c) WesTrack Fine- Optimum AC, High AV and (d) WesTrack Fine- Optimum AC, Low AV**

After the data smoothing was performed for each section, the power law equations were used to generated smoothed log G^* values versus depth for each section. The comparison between the smoothed log G^* values and the measured values are shown below in Figure 55. The results generally demonstrate good agreement between the measured and smoothed log G^* values. The smoothed log G^* values were then used in the proceeding field calibration of the pavement aging model.

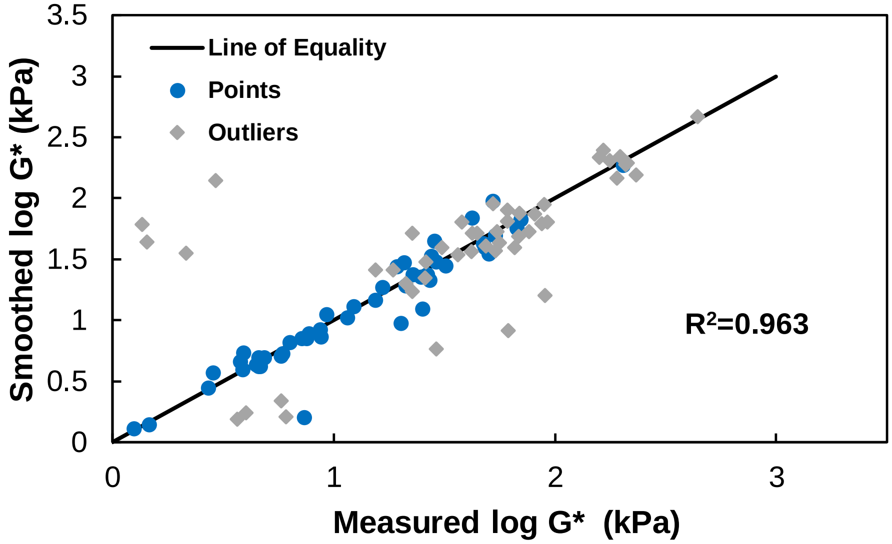

Figure 55. Smoothed versus Measured log *G Values (All Sections)**

Relationship between Kinetics Model Predictions and Smoothed Field Core Measurements

To establish the field calibration function, the relationship between kinetics model-predictions of log *G** and the smoothed field core measurements of log *G** at different depths were evaluated. Figure 56 through Figure 59 show the results of the smoothed log *G** values from field cores and those predicted from the kinetics model at different depths. In each figure, the conventional mixtures are shown in blue, the WMA mixtures are shown in red, and the mixtures containing RAP are shown in green. The PMA sections were not included in the field calibration of the pavement aging model due to the unrealistic thermal history included in the ALF rutting experiment as described in the Recalibration of the Loose Mixture Aging Procedure section. The PMA sections are shown in gray, but were not included in the field calibration analysis. A linear trend line was regressed to the data, similar to the analysis conducted by Kim et al. (2018) to arrive at their field calibration function given in Equation 14. The results show relatively weak correlations between the smoothed field core measured values and kinetics model predicted values of log *G**. However, it is apparent that the MIT 15% RAP, MIT 50% RAP and NCAT 50% RAP sections are outliers; this suggests that RAP contents may affect the relationship between laboratory and field aging and merits consideration in future work. Herein, insufficient data was available to conduct a separate field calibration of the kinetics model for RAP mixtures. Therefore, the MIT 15% RAP, MIT 50% RAP and NCAT 50% RAP sections were excluded from the field calibration of the kinetics model.

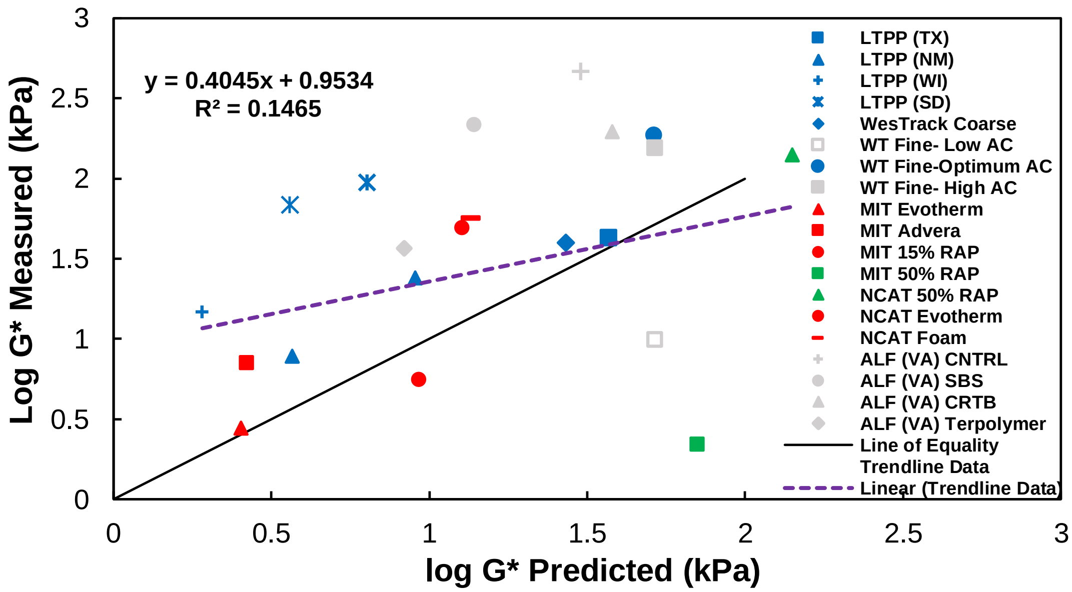

Figure 56. Relationship between Smoothed log *G Values Measured from Field Cores and those Predicted from the Kinetics Model at 0.6 cm Depth**

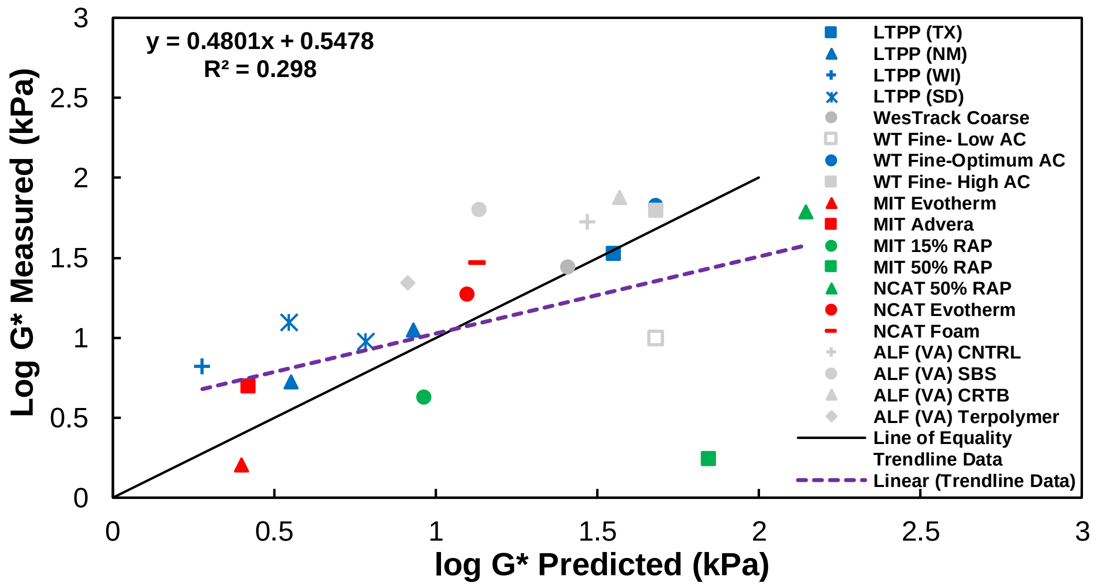

Figure 57. Relationship between Smoothed log *G Values Measured from Field Cores and those Predicted from the Kinetics Model at 1.8 cm Depth**

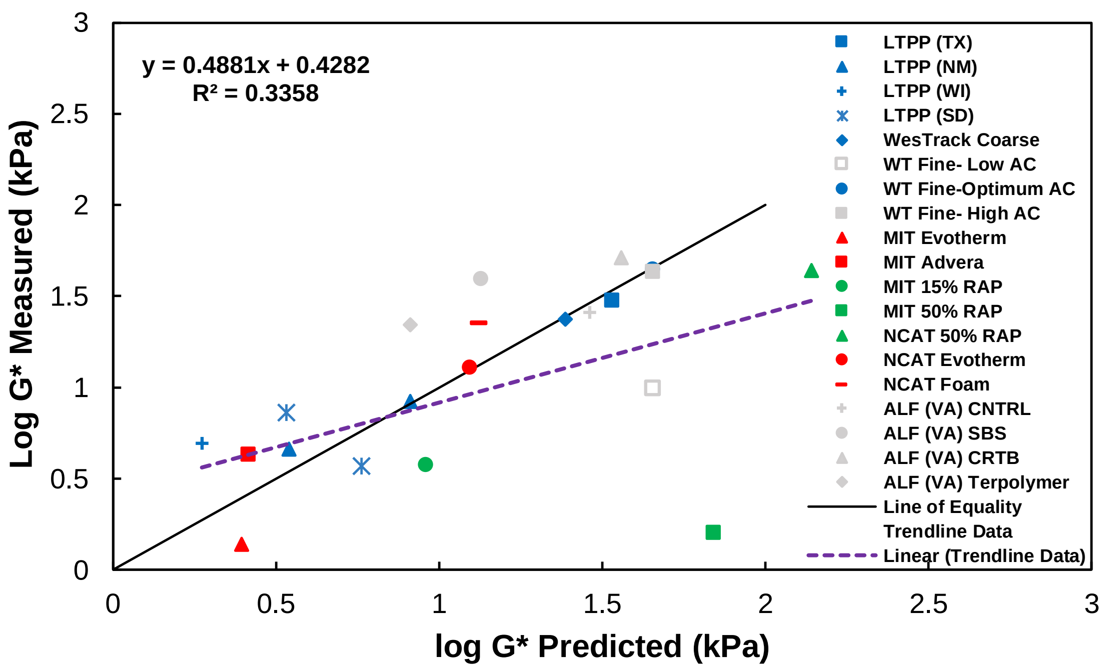

Figure 58. Relationship between Smoothed log *G Values Measured from Field Cores and those Predicted from the Kinetics Model at 3 cm Depth**

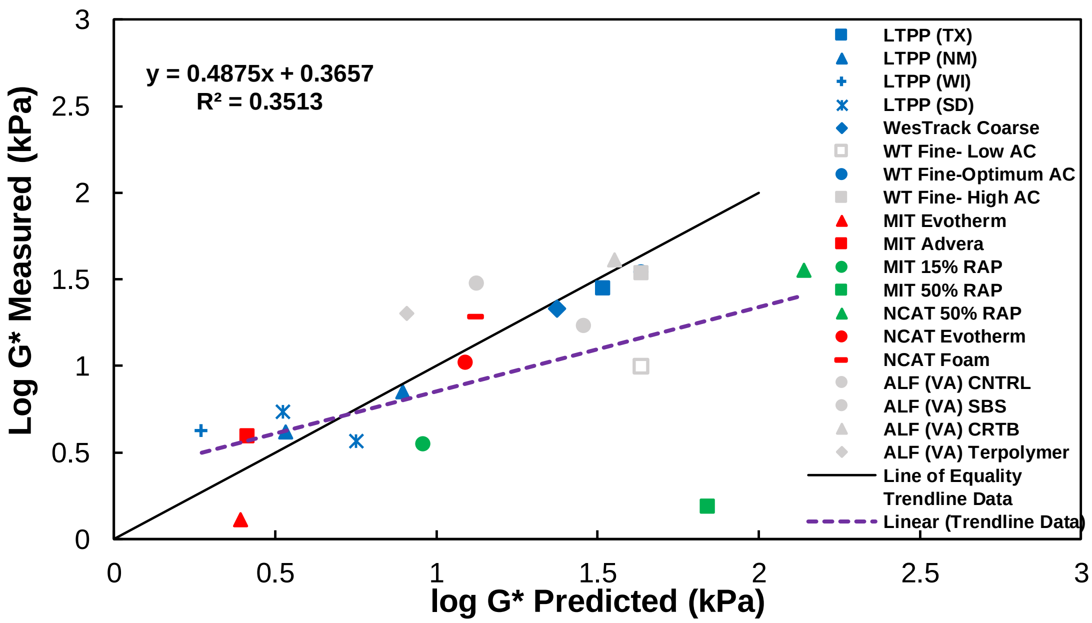

Figure 59. Relationship between Smoothed log *G Values Measured from Field Cores and those Predicted from the Kinetics Model at 4.2 cm Depth**

Figure 60 through Figure 63 show the results of the smoothed log *G** values from field cores and those predicted from the kinetics model at different depths with the trend lines formed with the removal of the MIT 15% RAP, MIT 50% RAP and NCAT 50% RAP sections. The outlier data points are still included in the figure in grey for reference. Removing the outliers greatly improved the R^2 values of the trend lines, suggesting that the kinetics model predictions are related to the smoothed field core measurements. Figure 60 through Figure 63 demonstrates that the scatter in the relationship between smoothed field core measurements and kinetics model predictions is much higher at a depth of 0.6 cm than deeper depths. This suggests that ultraviolet aging and other surface mechanisms that are not accounted for in the kinetics model impact surface aging may be significant. In addition, the results show no bias in the WMA results compared to HMA, suggesting that a separate field calibration of the pavement aging model for WMA is unnecessary. Also, while the PMA sections were not used in the field calibration due to the unrealistic thermal history of the ALF, the PMA results in Figure 60 through Figure 63 generally align with the rest of the data, suggesting that the field calibration conducted herein represents PMA materials reasonably well.

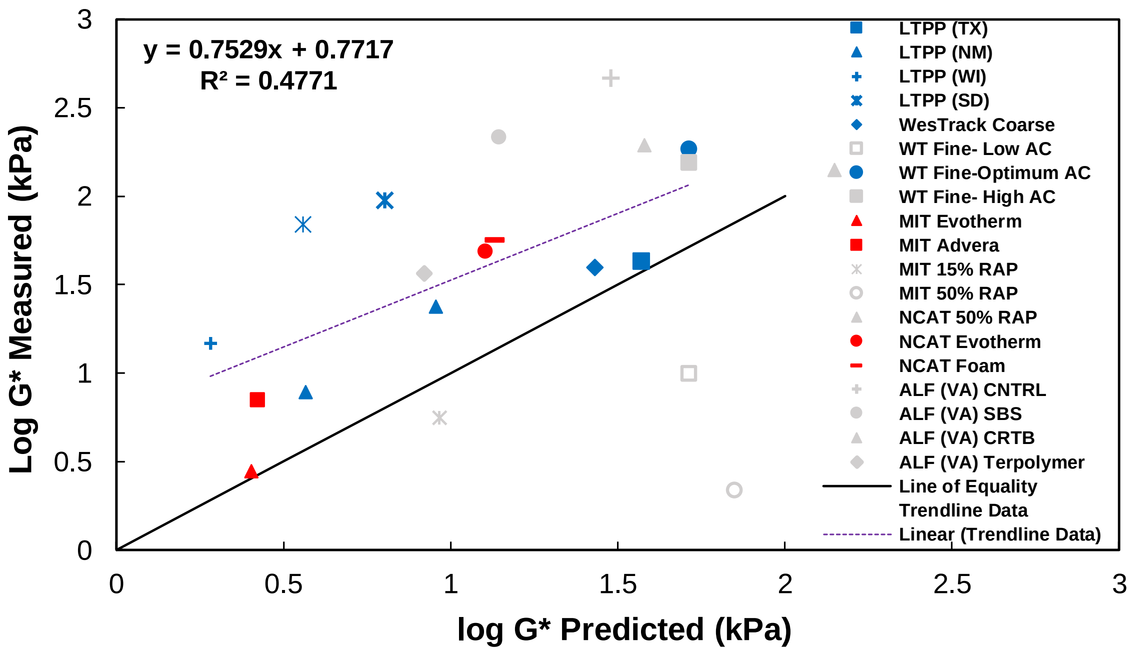

Figure 60. Relationship between Smoothed log *G Values Measured from Field Cores and those Predicted from the Kinetics Model at 0.6 cm Depth (Excluding MIT 15% RAP, MIT 50% RAP and NCAT 50% RAP)**

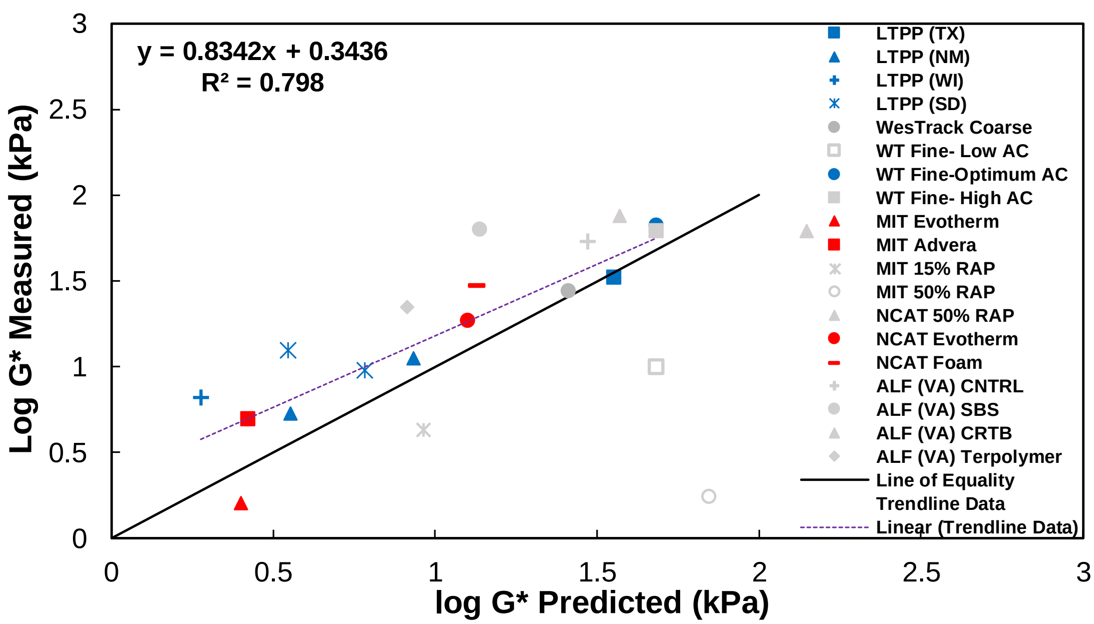

Figure 61. Relationship between Smoothed log *G Values Measured from Field Cores and those Predicted from the Kinetics Model at 1.8 cm Depth (Excluding MIT 15% RAP, MIT 50% RAP and NCAT 50% RAP)**

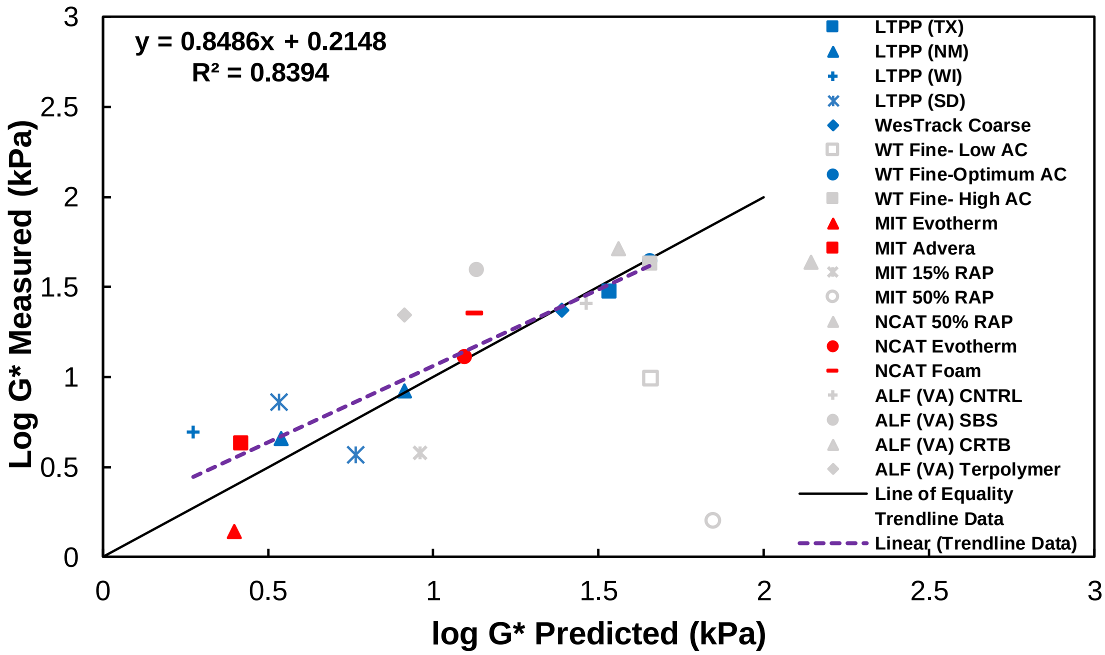

Figure 62. Relationship between Smoothed log *G Values Measured from Field Cores and those Predicted from the Kinetics Model at 3 cm Depth (Excluding MIT 15% RAP, MIT 50% RAP and NCAT 50% RAP)**

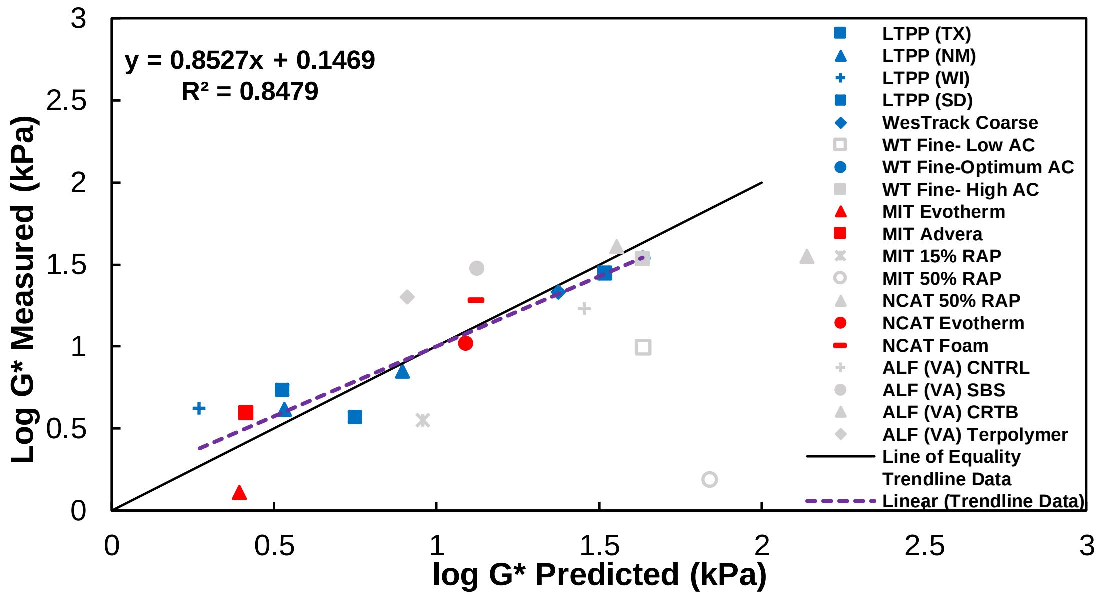

Figure 63. Relationship between Smoothed log *G Values Measured from Field Cores and those Predicted from the Kinetics Model at 4.2 cm Depth (Excluding MIT 15% RAP, MIT 50% RAP and NCAT 50% RAP)**

Field Calibration of the Kinetics Model

The slope and intercept values from the trend lines shown in Figure 60 through Figure 63 were plotted as a function of depth to inform the appropriate form of the field calibration function. The relationship between the slope and intercept parameters with depth are shown below in Figure 64 and Figure 65, respectively. Figure 64 suggests that the slope of the relationship between kinetics model predictions and smooth field core measurements of log G^* at each depth are similar. Therefore, a slope adjustment was included in the recalibration that is not depth-dependent. The intercept, however, exhibits depth dependence. Based on the results shown in Figure 65, a power function was fit to represent the relationship between the intercept and depth. Therefore, a power equation was chosen to represent the intercept calibration parameter function as a function of depth.

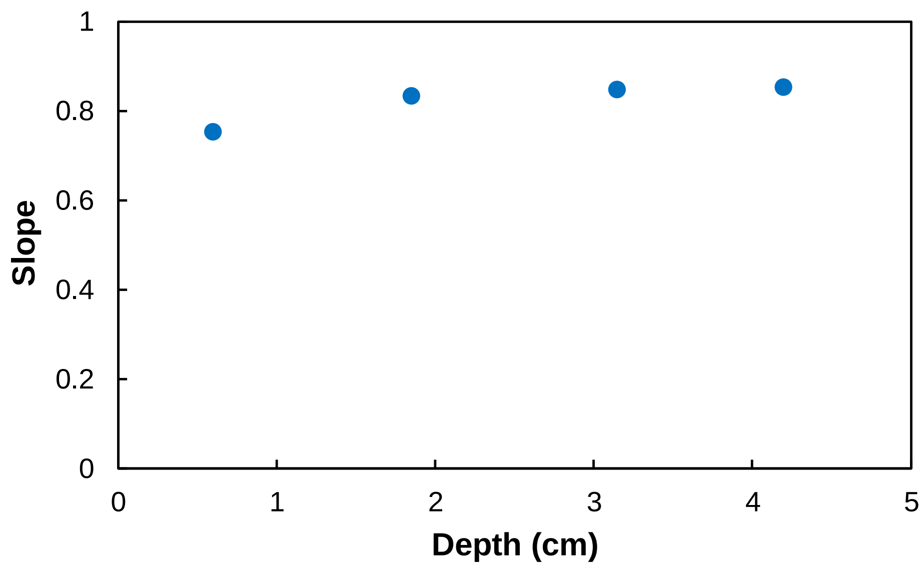

Figure 64. Depth Versus Slope

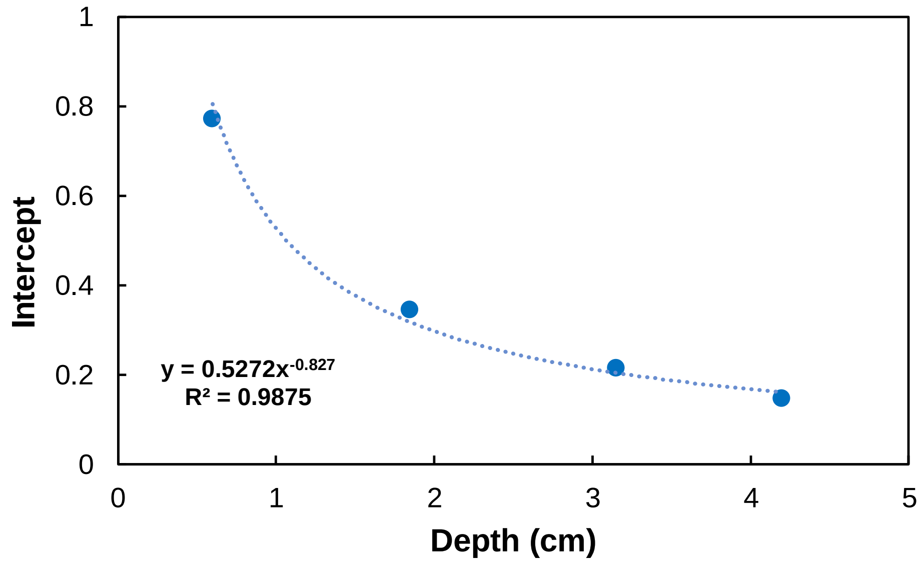

Figure 65. Depth Versus Intercept

Based on the above discussion, the field calibration function proposed is shown below in Equation 22.

$$\log G^*_{field} = a \cdot \log G^*_{kinetics} + b \cdot d^c \tag{22}$$

Where: *a*, *b*, and *c* are optimized coefficients and *d* is depth in cm.

The coefficients *a*, *b*, and *c* were determined by a least squares optimization between the smoothed measured log *G** values from field cores and the log *G** values obtained using Equation 22. The optimized coefficient values are shown in Table 7.

Table 7. Field Calibration Parameters

a	b	c
0.818	0.508	-0.673

Using these optimized parameters, the field calibrated pavement aging model predictions of log *G** values were determined for each project and depth of field core measurements. The relationship between the field calibrated pavement aging model predictions and field core measurements of log *G** are shown as a function of depth in Figure 66 through Figure 69. The conventional mixtures are shown in blue, the WMA mixtures are shown in red, and the mixtures containing RAP are shown in green. The mixtures shown in gray were not used in the calibration but are shown in the graphs for completeness. The results demonstrate relatively poor prediction accuracy at a depth of 0.6 cm but reasonable accuracy at depths of 1.8 cm, 3 cm, and 4.2 cm. The results show that the calibrated pavement aging model predicts the aging of the conventional HMA mixtures, WMA mixtures, and even the ALF PMA mixtures relatively well, suggesting that a separate calibration for WMA and PMA is not needed. However, these findings should be confirmed by analyzing additional PMA and WMA materials in future work.

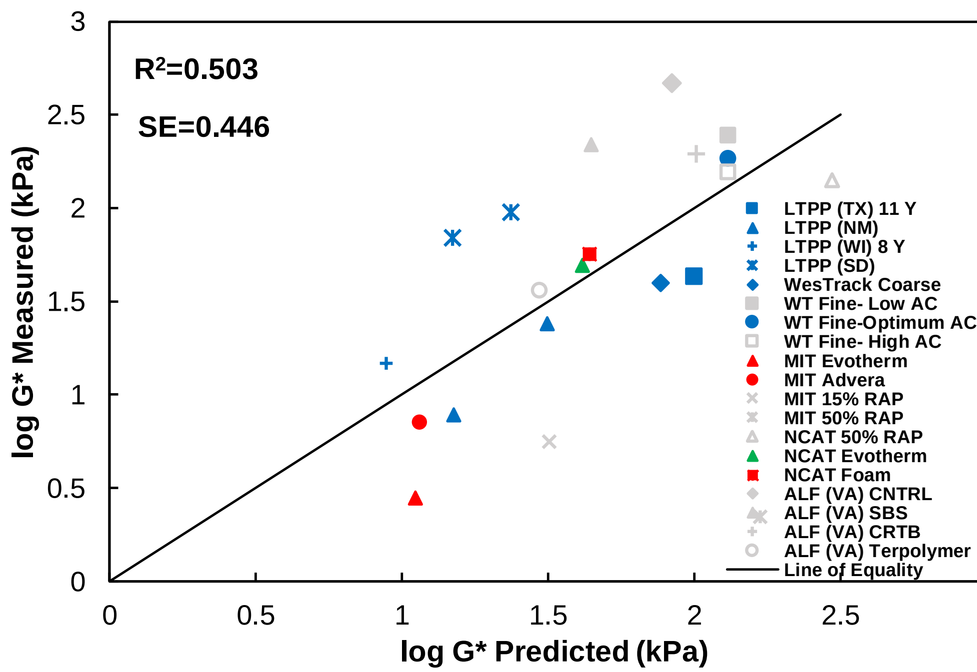

Figure 66. Smoothed Field Core Measurements versus Field Calibrated Kinetics Model Predictions at a Depth of 0.6 cm

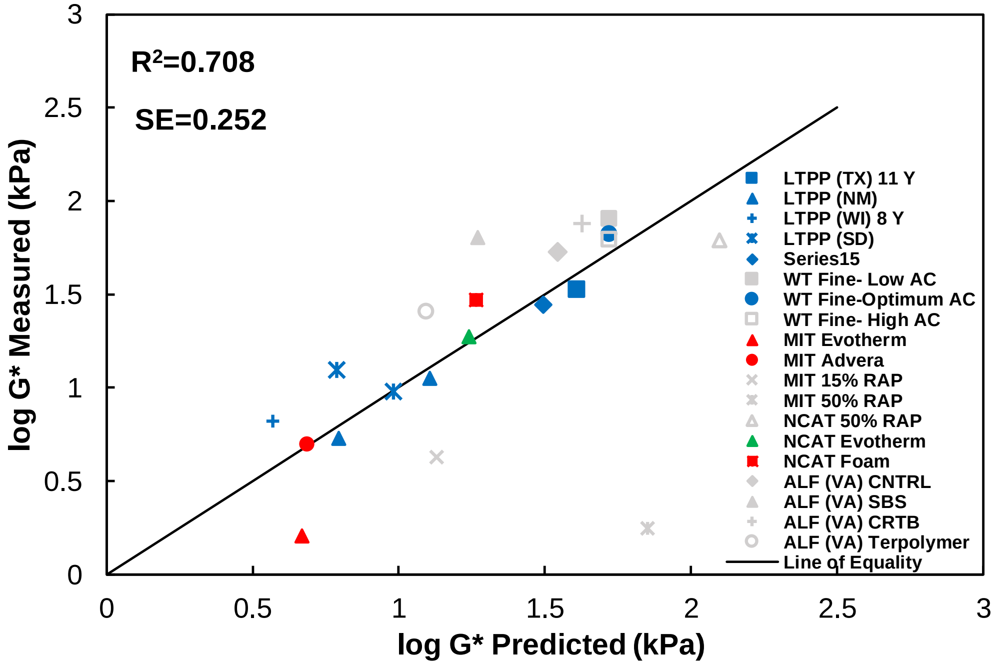

Figure 67. Smoothed Field Core Measurements versus Field Calibrated Kinetics Model Predictions at a Depth of 1.8 cm

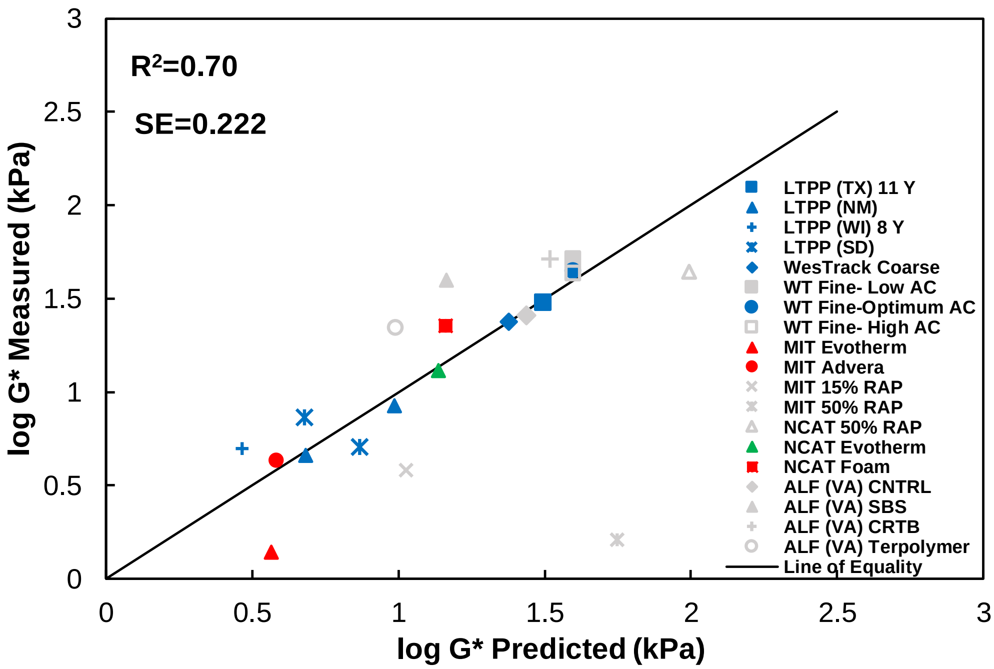

Figure 68. Smoothed Field Core Measurements versus Field Calibrated Kinetics Model Predictions at a Depth of 3 cm

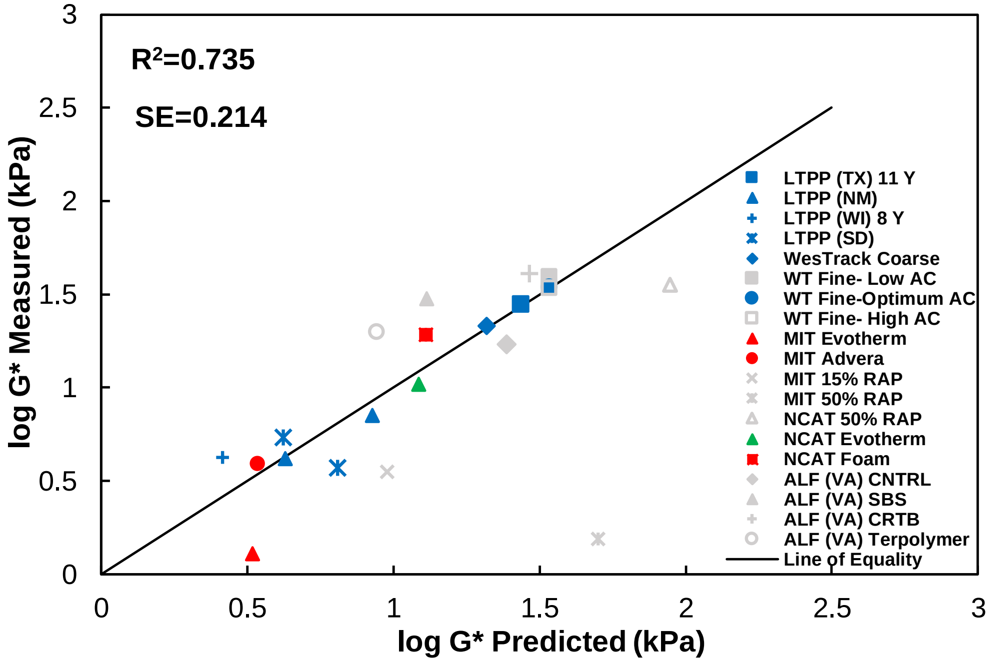

Figure 69. Smoothed Field Core Measurements versus Field Calibrated Kinetics Model Predictions at a Depth of 4.2 cm

Figure 70 shows the comparison between smoothed field core measurements and field calibrated pavement aging model predictions of log *G** with delineation of depth. Sections that were not used in the field calibration are now included in Figure 70. The results do not reveal a bias in the pavement aging model predictions with depth, suggesting the depth-dependent calibration function used is appropriate. The overall R^2 of 0.7 corresponding to the aggregated data suggests promising prediction accuracy given all of the variables that impact field aging that are not directly accounted for in the pavement aging model (morphology, UV, etc.).

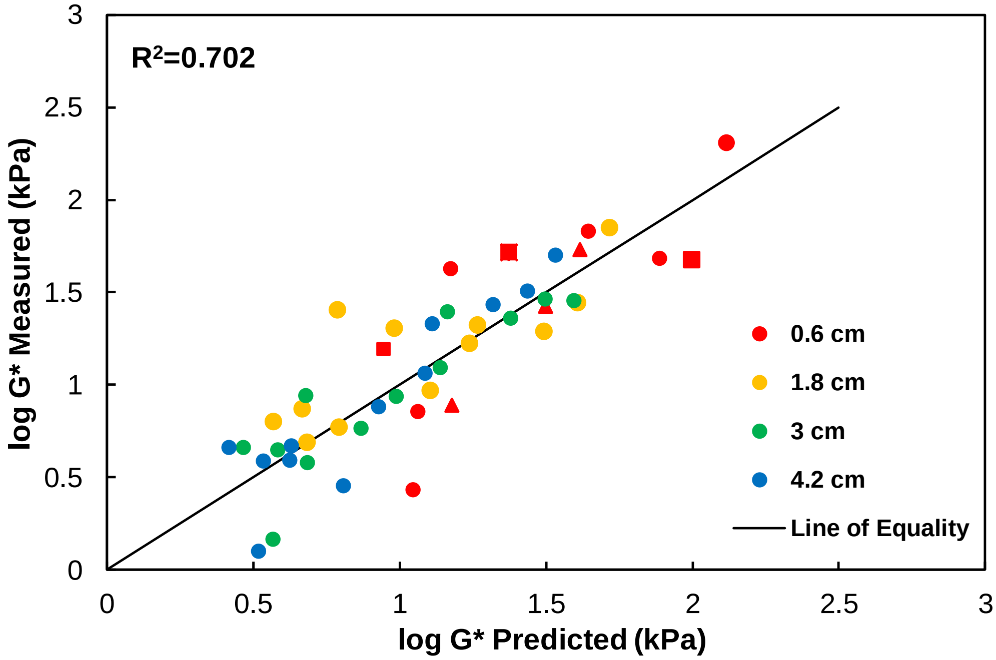

Figure 70. Field Calibration Delineation by Depth (Outlier Sections Removed)

Comparison between Field Core Measurements and Calibrated Pavement Aging Model Predictions

The comparison between field core measurements of log G^* and those predicted by the calibrated kinetics model for each project are shown in Figure 71 through Figure 75. In some cases, the error in the prediction is quite high while in other instances, the model prediction is quite good.

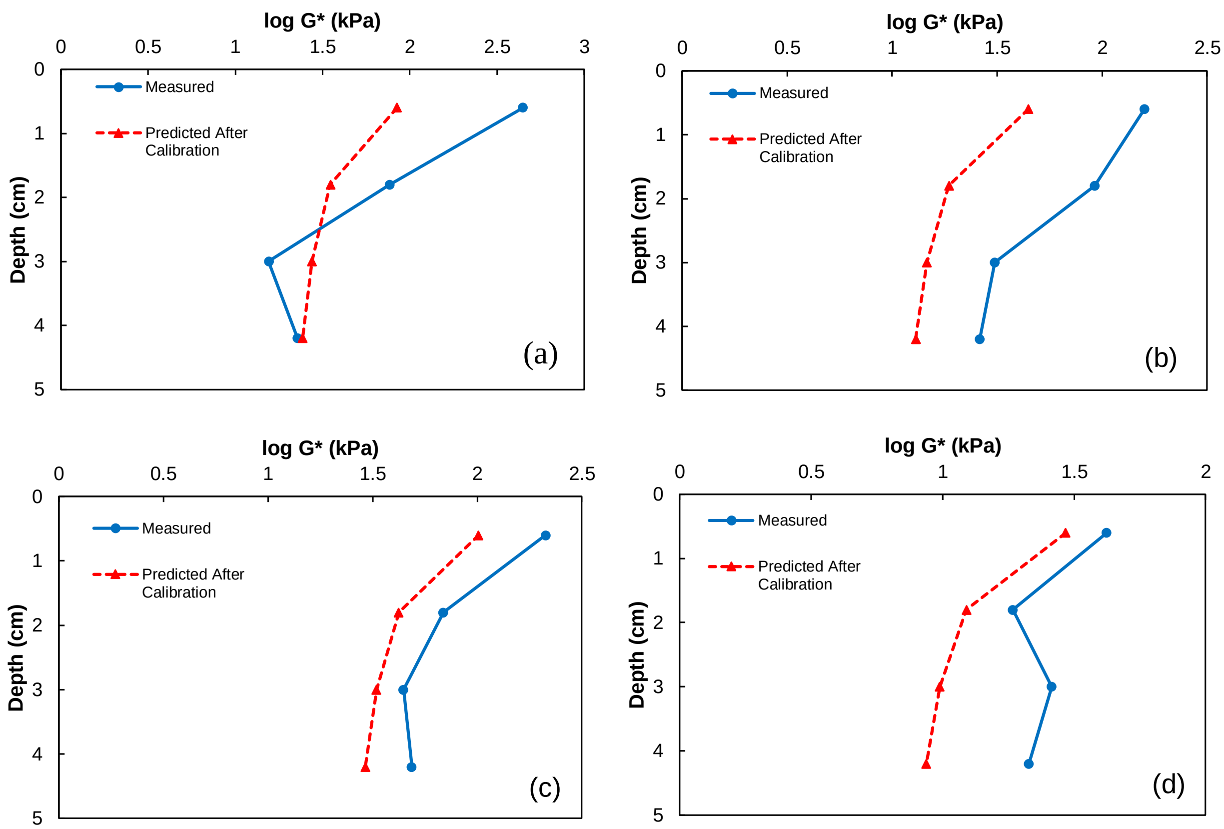

Figure 71. Comparison between Field Calibrated Pavement Aging Model Predictions and Field Core Measurements for (a) ALF CTRL (b) ALF SBS (c) ALF CRTB and (d) ALF Terpolymer

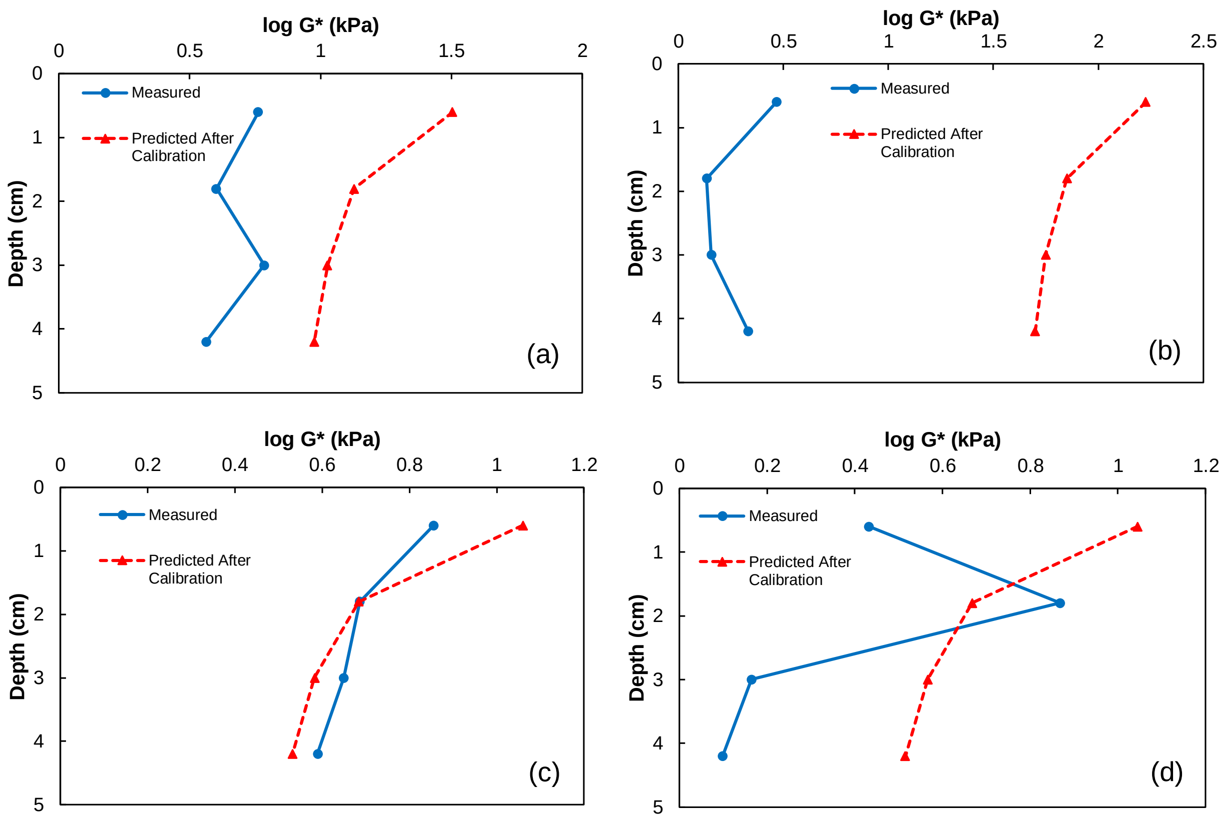

Figure 72. **Comparison between Field Calibrated Pavement Aging Model Predictions and Field Core Measurements for (a) MIT 15% RAP (b) MIT 50% RAP (c) MIT Advera and (d) MIT Evotherm**

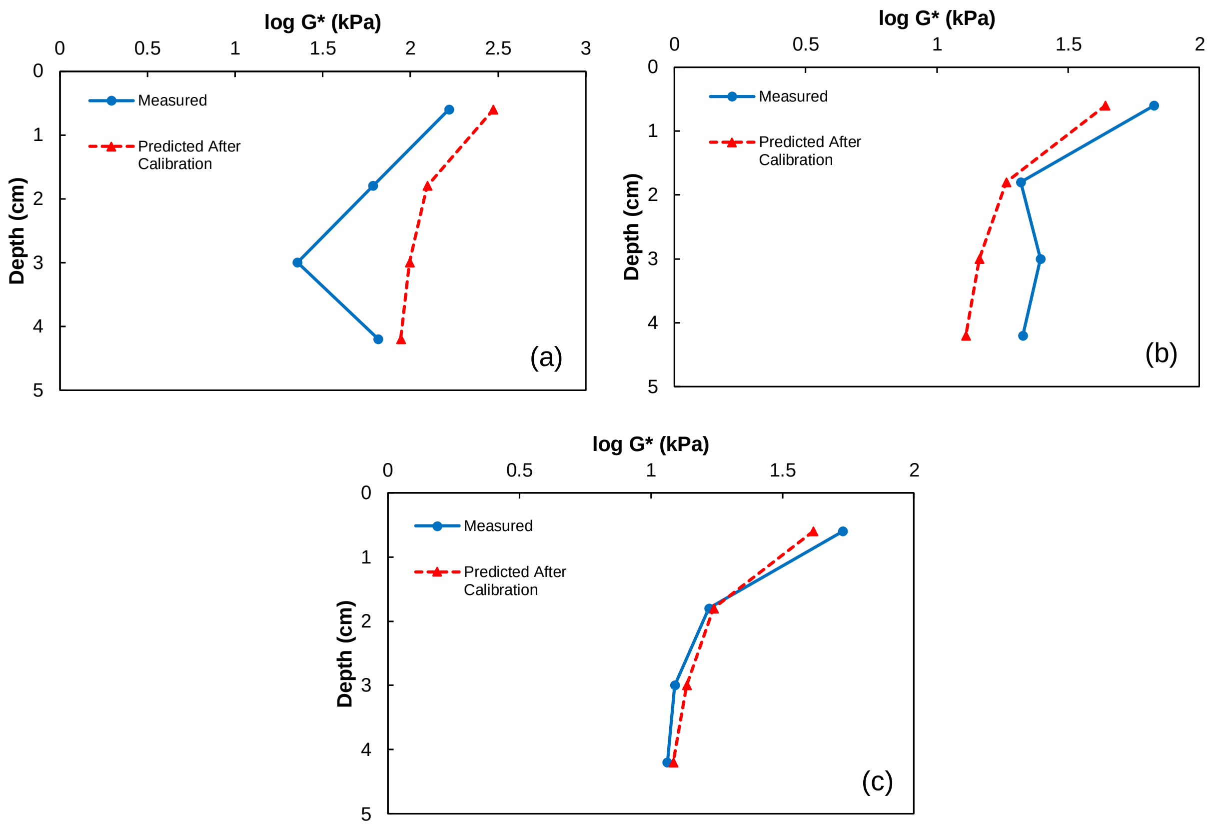

Figure 73. Comparison between Field Calibrated Pavement Aging Model Predictions and Field Core Measurements for (a) NCAT 50% RAP (b) NCAT Foam and (c) NCAT Evotherm

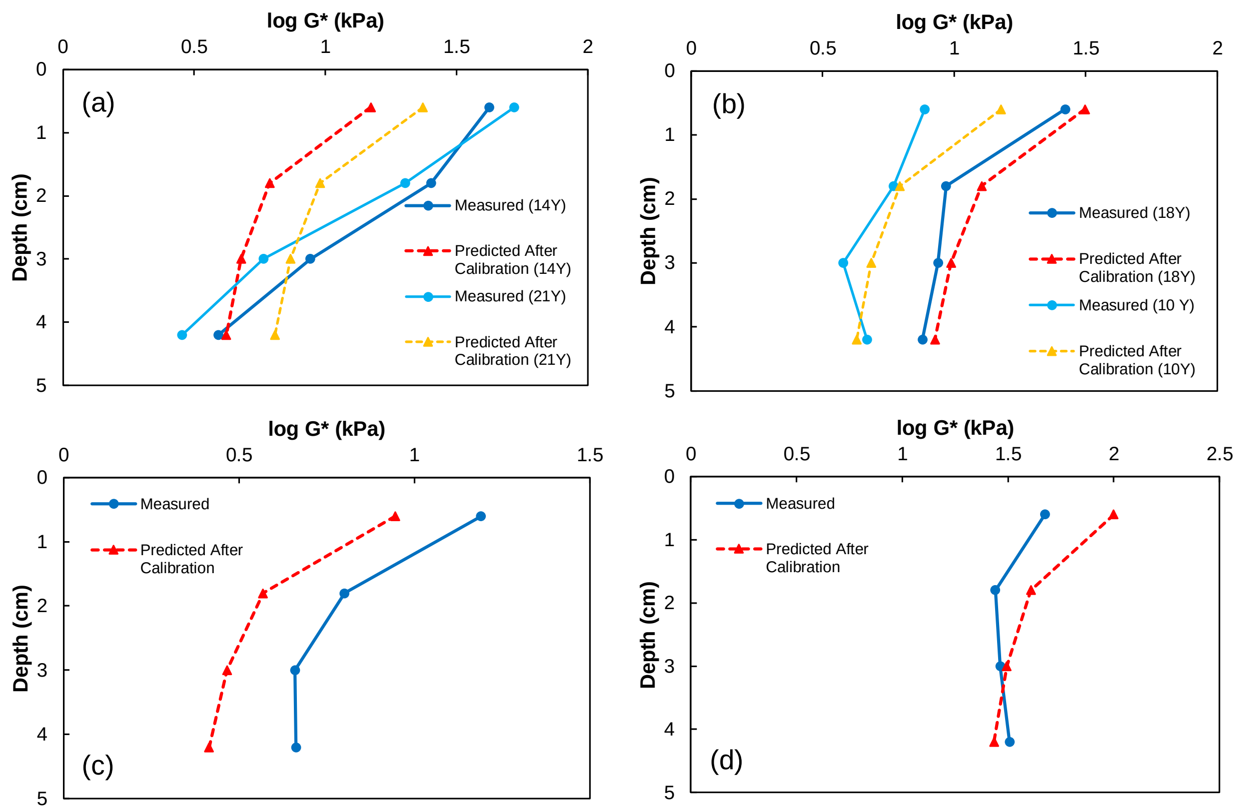

Figure 74. Comparison between Field Calibrated Pavement Aging Model Predictions and Field Core Measurements for (a) South Dakota (b) New Mexico (c) Wisconsin and (d) Texas

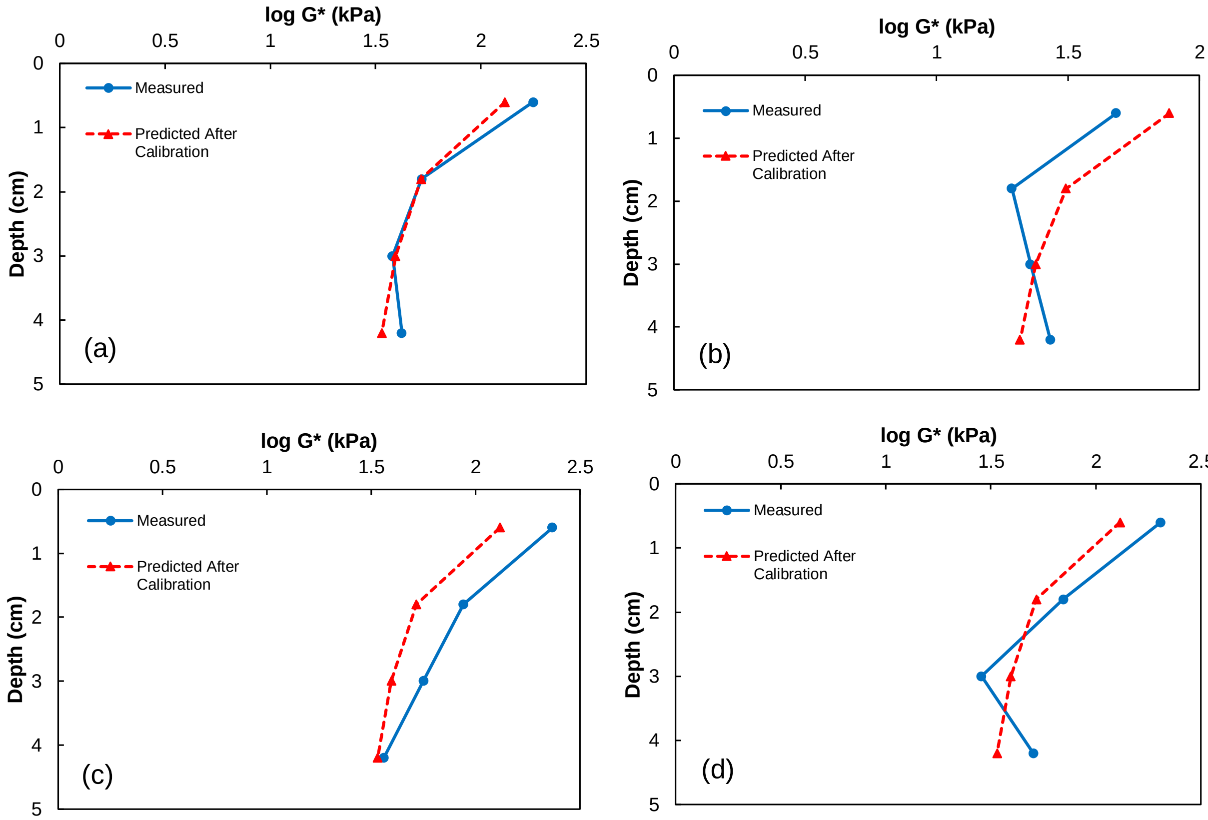

Figure 75. Comparison between Field Calibrated Pavement Aging Model Predictions and Field Core Measurements for (a) WT-Fine (High AC) (b) WT-Coarse (c) WT- Fine (Low AC) and (d) WT- Fine (Optimum AC)

Field Calibration Adjustment Factor for Deviations from the Optimum Asphalt Content

Because the results of the statistical analysis of the Brazil and WesTrack field cores show that asphalt content has a significant effect on field aging, the WesTrack sections used in the systematic study of mixture morphology were analyzed in order to calibrate an adjustment to the pavement aging model predictions as a function of deviation from the Superpave optimum asphalt content. Because air void content was found to have an insignificant effect on field aging through the analysis of Brazil and WesTrack field cores, an adjustment for air void content was not established.

The smoothed field core measurements of the WesTrack sections corresponding to the medium air void content were used to establish the asphalt content adjustment function. The relationship between the ratio of the log *G** value corresponding to the asphalt content of interest divided by the log *G** value corresponding to the optimum asphalt content (i.e., log *G** (opt)) and asphalt content and depth was investigated. The corresponding summary graph of the results is shown in Figure 76. Note that the WesTrack section low and high asphalt contents correspond to -0.7 percent and +0.7 percent from the optimum asphalt content. A linear trend line was fit to the relationship between the log *G** ratio and the deviation from the optimum asphalt content for each depth as shown in Figure 76. The slopes of these lines were then plotted against the depth and a function was fit to best characterize the relationship between slope and depth as shown in Figure 77. The equation shown in Figure 77 was then used as an adjustment function to account for deviations from the optimum asphalt content in pavement aging model predictions as a function of depth as shown in Equation 23.

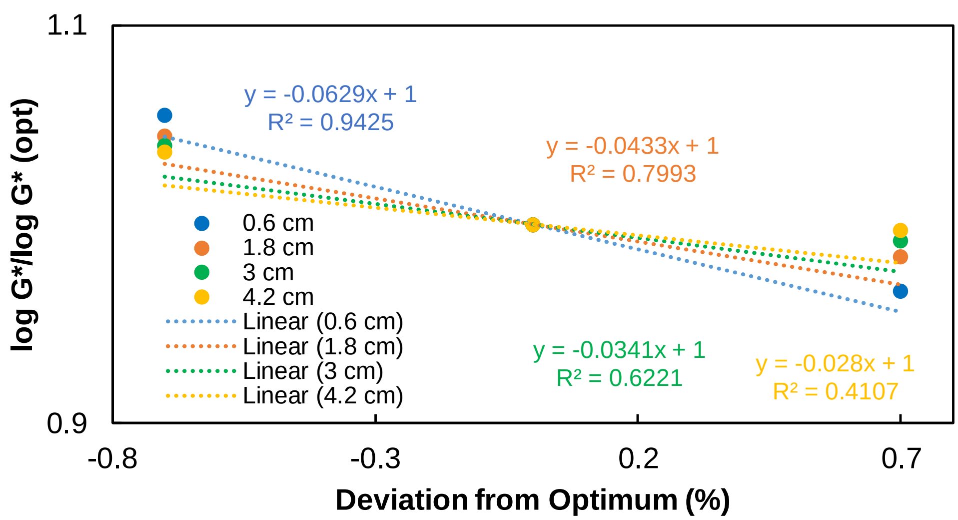

Figure 76. Relationship Between log *G ratio and Deviation from Optimum Asphalt Content for WesTrack Fine Materials at the Medium Air Void Content**

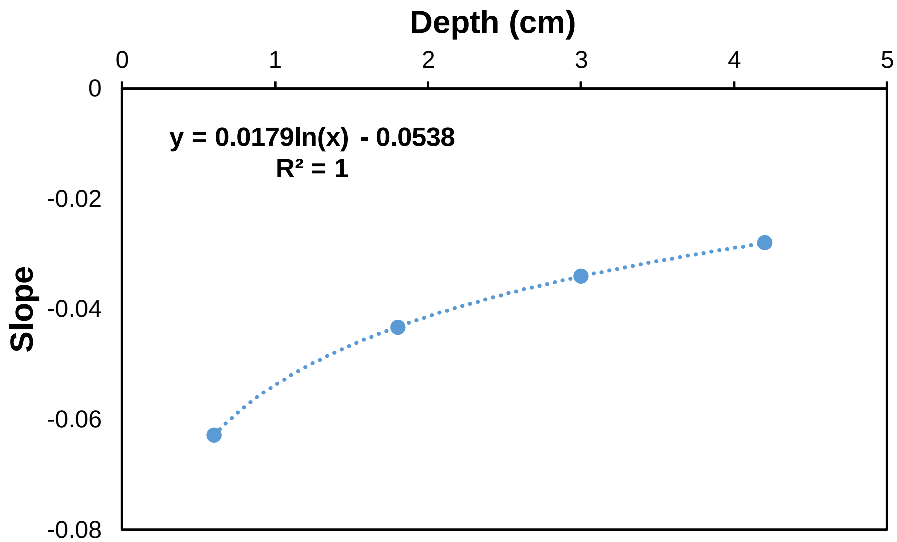

Figure 77. Relationship Between Slope and Depth

$$\log G^*_{field,adj} = \log G^*_{\text{field}} \cdot (1 + \%AC_{dev} \cdot (0.0179 \cdot \ln(d) - 0.0538)) \tag{23}$$

Where $\%AC_{dev}$ = the deviation from the optimum asphalt content (in percent).

To demonstrate how Equation 23 affects pavement aging model predictions, the comparison between field core measurements, calibrated pavement aging model predictions (i.e., Equation 22), and the calibrated pavement aging model predictions with the asphalt content adjustment were compared for the WesTrack sections. The results are shown in Figure 78 and Figure 79. As the asphalt content deviates from the optimum, the values predicted by the field calibrated pavement aging model, displayed in green on the graphs, deviate from the true measured values but the adjustment is relatively small, suggesting asphalt content does not have that significant of an effect on pavement aging predictions, especially given the uncertainty in pavement aging model predictions. Limited data was used to generate the adjustment for asphalt content and therefore, the effect of asphalt content merits additional consideration in future research.

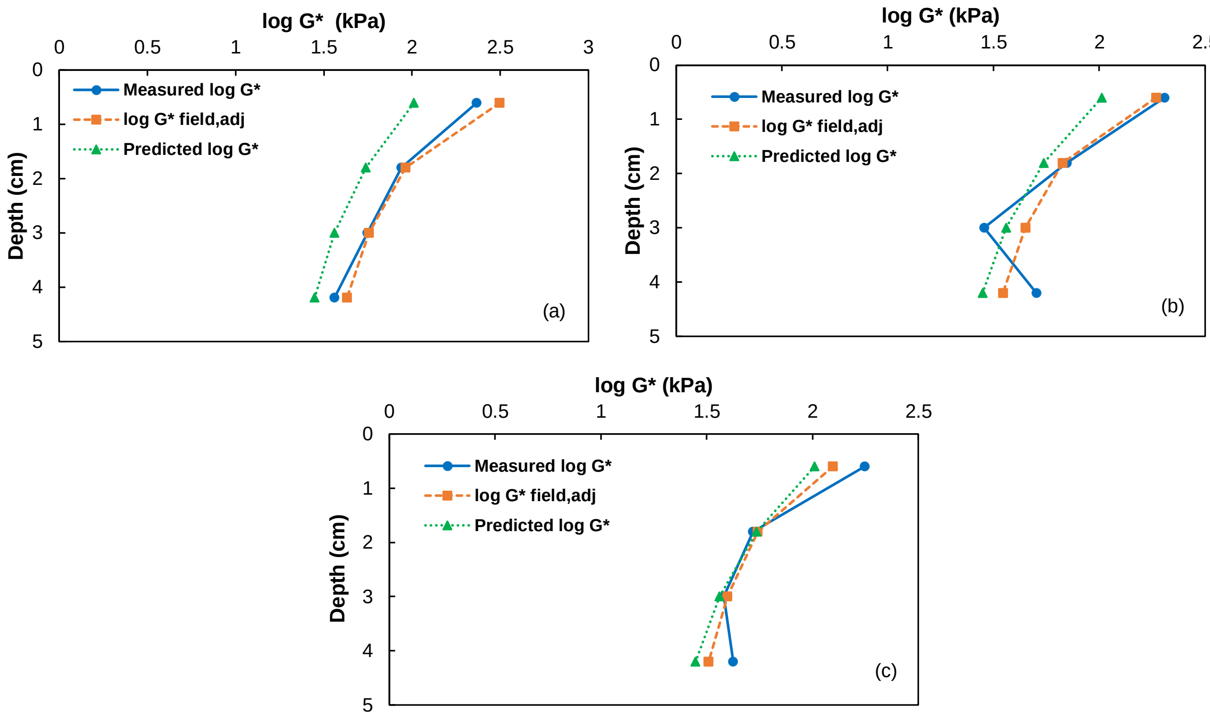

Figure 78. Depth versus log *G (Measured, Field Calibrated Pavement Aging Model Predicted, and Adjusted) for (a) WesTrack Fine- Low AC, Medium AV (b) WesTrack Fine- Optimum AC, Medium AV and (c) WesTrack Fine- High AC, Medium AV**

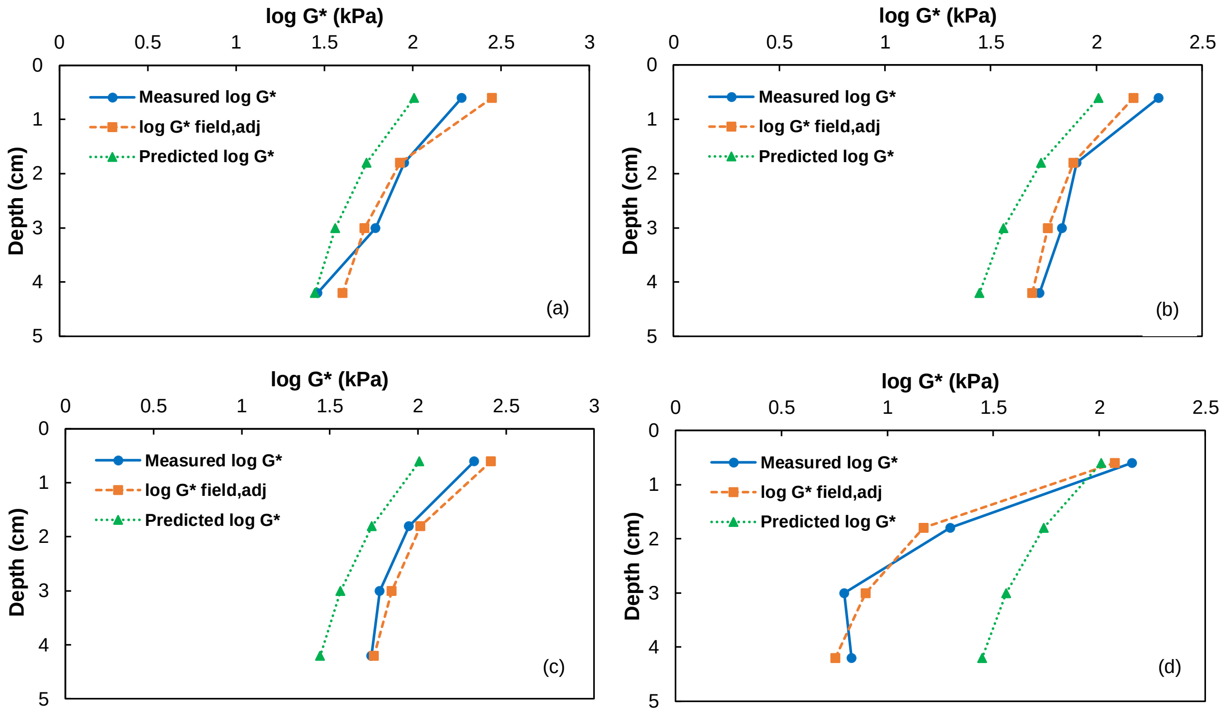

Figure 79. Depth versus log G* (Measured, Field Calibrated Pavement Aging Model Predicted, and Adjusted) for (a) WesTrack Fine- Optimum AC, Low AV (b) WesTrack Fine- Optimum AC, High AV (c) WesTrack Fine- Low AC, High AV and (d) WesTrack Fine- High AC, Low AV

Summary

In this section, the kinetics model proposed by Kim et al. (2018) was calibrated using field core measurements at varying depths. The calibrated pavement aging model can be used to predict the log G^* value of asphalt binder at 64°C and 10 rad/s as a function of hourly pavement temperature history and depth using mixture-specific kinetics. The model predicts aging of the unmodified HMA, WMA, and PMA materials studied reasonably well. The accuracy of model predictions is relatively poor near the pavement surface (i.e., 0.6 cm) but relatively good for depths between 1.8 cm and 4.2 cm. The limited RAP sections analyzed suggest that a separate calibration of the pavement aging model may be required for asphalt mixtures containing reclaimed materials. It was found through a systematic study of the effect of asphalt morphology on field aging that the asphalt content can have a significant effect on long-term oxidation. An adjustment to pavement aging model predictions as a function of deviations from the optimum asphalt content was established using limited data available from WesTrack sections. The adjustment shows that asphalt content has a relatively minor impact on pavement aging model predictions given the uncertainty in the model predictions.

CONCLUSIONS AND RECOMMENDATIONS

The following conclusions and recommendations are drawn from the results of this study:

1. A climatic aging index (CAI) proposed by Kim et al. (2018) was simplified and calibrated using a broad range of conventional and unconventional asphalt mixtures and climates to yield the required laboratory aging duration as a function of hourly pavement temperature history and depth that yields reasonable accuracy to matching field age levels ($R^2 = 0.78$).
2. The kinetics model proposed by Kim et al. (2018) was calibrated using field core measurements at varying depths using a broad range of asphalt mixtures and climates that can be used to predict the log G* value of asphalt binder at 64°C and 10 rad/s as a function of hourly pavement temperature history and depth with moderate accuracy ($R^2 = 0.70$).
3. Future research should be conducted to evaluate the relative accuracy and precision of the Global Aging System (GAS) Model versus the field calibrated pavement aging model presented herein.
4. A systematic analysis of the effect of asphalt morphology on field aging indicates that asphalt content can have a significant effect on long-term oxidation but that air void content has an insignificant effect. Using the limited results of this study, a calibration function to predict changes in the log *G** value of asphalt binder at 64°C and 10 rad/s with deviations from the Superpave optimum asphalt content within the pavement aging model was developed.

5. Based on the limited sections containing RAP evaluated in this study, the relationship between laboratory and field aging may be impacted by RAP. Therefore, the effect of RAP on CAI and the pavement aging model field calibration merits future investigation.
6. Due to the unrealistic thermal history of the PMA field projects evaluated herein, PMA sections were not included in the calibration of CAI or the pavement aging model. However, the results suggest reasonable prediction of laboratory aging durations and pavement aging using the established CAI and kinetics model field calibration established herein in many instances. These results suggest that the CAI and pavement aging model developed may be applicable to PMA materials. However, future research should further investigate the relationship between laboratory and field aging of PMA materials using field projects with realistic thermal histories.
7. In some instances, the short-term aging procedure in AASHTO R 30 exceeded the level of aging in four year old field cores. Therefore, refinement of the short-term aging procedure to better mimic aging that occurs during production and placement should be considered.
8. The results of the recalibration do not show a notable difference in the WMA sections compared to HMA. However, the WMA field cores available corresponding to limited field aging (4 years). Future research should further investigate WMA materials in more accurately predicting laboratory aging durations to match field pavement aging.

REFERENCES

1. Bell, C. *Summary Report on Aging of Asphalt-Aggregate Systems.* Strategic Highway Research Program (SHRP), 1989

2. Kim, Y., et al. *Long-Term Aging of Asphalt Mixtures for Performance Testing and Prediction.* Washington, DC, Publication National Cooperative Highway Research Program, 2018.

3. AASHTO R30. Standard Practice for Mixture Conditioning of Hot Mix Asphalt (HMA). AASHTO Provisional Standards, American Association of State Highway and Transportation Officials, Washington, D.C, 2002.

4. Airey, G.D. State of the Art Report on Ageing Test Methods for Bituminous Pavement Materials. *The International Journal of Pavement Engineering*, Vol. 4, 2003, pp. 165–176.

5. ASTM Standard D1754/D1754M − 09, Standard Test Method for Effects of Heat and Air on Asphaltic Materials (Thin-Film Oven Test), ASTM International, West Conshohocken, PA, 2014.

6. ASTM Standard D2872 − 12, Standard Test Method for Effect of Heat and Air on a Moving Film of Asphalt (Rolling Thin-Film Oven Test), ASTM International, West Conshohocken, PA, 2013.

7. ASTM Standard D6521-18, Standard Practice for Accelerated Aging of Asphalt Binder Using a Pressurized Aging Vessel (PAV), ASTM International, West Conshohocken, PA, 2000.

8. Bishara, S.W., Robertson, R.E. and Mahoney, D. Rapid oxidative ageing of binder using microwave energy. An improved method. *Proc. 2nd Eurasphalt & Eurobitume Congress, Session 2: Development in Bituminous Products and Techniques*, 2000, pp 27–36.

9. Traxler, R.N. Durability of asphalt cements. *Proc. Assn. Asphalt Paving Technol*. Vol. 32, 1963, pp. 44–58.

10. Mirza, M. W. and Witczak, M. W. Development of Global Aging System for Short and Long Term Aging of Asphalt Cements. *Journal of the Association of Asphalt Paving Technologists,* Vol. 64, 1995, pp. 393-430.

11. Elwardany, M. *Phenomenological Modeling and Laboratory Simulation of Long-Term Aging of Asphalt Mixtures*, Ph.D. Dissertation, North Carolina State University, Raleigh, North Carolina, 2017.

12. Van Oort, W. P. Durability of Asphalt – It's Aging in the Dark. *Journal of Industrial and Engineering Chemistry.* 1956, pp. 1196-1201.

13. Luo, X., Gu, F., and Lytton, R. Prediction of Field Aging Gradient in Asphalt Pavements. In *Transportation Research Record: Journal of the Transportation Research Board.* No. 2507, Transportation Research Board of the National Academies, Washington, D.C., 2015, pp. 19-28.

14. Woo, W., Chowdhury, A., and Glover, C. Field Aging of Unmodified Asphalt Binder in Three Texas Long-Term Performance Pavements. In *Transportation Research Record: Journal of the Transportation Research Board.* No. 2051, Transportation Research Board of the National Academies, Washington, D.C., 2008, pp. 15-22.

15. Kandhal, P., and Chakraborty, S. Effect of Asphalt Film Thickness on Short-and Long-Term Aging of Asphalt Paving Mixtures. In *Transportation Research Record: Journal of the Transportation Research Board.* No. 1535, Transportation Research Board of the National Academies, Washington, D.C., 1996, pp. 83-90.

16. Banerjee, A., Smit, A., and Prozzi, J. The effect of long-term aging on the rheology of warm mix asphalt binders. *Fuel.* Vol. 97, 2012, pp. 603-611.

17. Souza, F., and Castro, L. Effect of temperature on the mechanical response of thermo-viscoelastic asphalt pavements. *Construction and Building Materials.* Vol. 30, 2012, pp. 574-582.

18. Hachiya, Y., Nomura, K., and Shen, J. Accelerated Aging Test for Asphalt Concretes. *Zurich: 6th RILEM Symposium PTEBM*, 2003.

19. Schwartz, C.W., et al. Evaluation of Long-Term Pavement Performance (LTTP) Climatic Data for Use in Mechanistic-Empirical Pavement Design Guide(MEPDG) Calibration and Other Pavement Analysis *U.S. Department of Transportation Federal Highway Administration*, 2015. Report No. FHWA-HRT-15-019.

20. Gelaro, R., et al. The Modern-Era Retrospective Analysis for Research and Applications, Version 2 (MERRA-2). *Journal of Climate*, Vol. 30, 2017, pp 5419–5454.

21. ARA, Inc., ERES Division. Guide for Mechanistic-Empirical Design of New and Rehabilitated Pavement Structures. *National Cooperative Highway Research Program.* 2000.

22. Newcomb, D., et al. *Short-Term Laboratory Conditioning of Asphalt Mixtures.* Washington, DC, Publication National Cooperative Highway Research Program, 2015.

23. Gibson, N. et al. Performance Testing for Superpave and Structural Validation. *National Cooperative Highway Research Program.* 2012.